ANALYTICAL AND EXPERIMENTAL INVESTIGATION OF TEMPORAL VARIATION OF CLEAR WATER SCOUR DEPTH AT BRIDGE ABUTMENTS

A THESIS SUBMITTED TO
THE GRADUATE SCHOOL OF NATURAL AND APPLIED SCIENCES
OF
MIDDLE EAST TECHNICAL UNIVERSITY

BY

ÖMER KÖSE

IN PARTIAL FULFILLMENT OF THE REQUIREMENTS
FOR
THE DEGREE OF DOCTOR OF PHILOSOPHY
IN
CIVIL ENGINEERING

MAY 2007

Approval of the Graduate School of Natural and Applied Sciences

Prof. Dr. Canan Özgen
Director

I certify that this thesis satisfies all the requirements as a thesis for the degree of Doctor of Philosophy.

Prof. Dr. Güney Özcebe
Head of Department

This is to certify that we have read this thesis and that in our opinion it is fully adequate, in scope and quality, as a thesis for the degree of Doctor of Philosophy.

Prof. Dr. A. Melih Yanmaz
Supervisor

Examining Committee Members

Prof. Dr. Tülay Özbek	(Gazi Unv., CE)	
Prof. Dr. A.Melih Yanmaz	(METU, CE)	
Prof. Dr. İbrahim Gürer	(Gazi Unv., CE)	
Prof.Dr. Mustafa Göğüş	(METU, CE)	
Assoc. Prof. Dr. Nuri Merzi	(METU, CE)	

I hereby declare that all information in this document has been obtained and presented in accordance with academic rules and ethical conduct. I also declare that, as required by these rules and conduct, I have fully cited and referenced all material and results that are not original to this work.

Name, Last Name : Ömer Köse

Signature :

ABSTRACT

ANALYTICAL AND EXPERIMENTAL INVESTIGATION OF TEMPORAL VARIATION OF CLEAR WATER SCOUR DEPTH AT BRIDGE ABUTMENTS

Köse, Ömer
Ph.D., Department of Civil Engineering
Supervisor : Prof. Dr. A. Melih Yanmaz
May 2007, 124 pages

Computation of temporal variation of clear water scour is important for the design of bridge foundations. Previous studies conducted for determining equilibrium scour depth at bridge abutments indicated that very long flow duration was needed to achieve equilibrium scouring situations. However, the corresponding durations in the prototype conditions may yield considerably greater values than time to peak of the design flood. Therefore, there is a need to estimate the temporal variation of scour depth. An experimental study was carried out to observe temporal variation of scour depth and contours around vertical-wall and wing-wall abutments. The results of the experiments have been interpreted. A semi-empirical model has been developed for determining time-dependent variation of clear water scour depth at vertical-wall abutments. This approach is based on the application of sediment continuity equation to the scour hole around the vertical-wall abutment. To this end, time-dependent geometric features of the scour hole were investigated and a recent sediment pickup function was used to formulate the rate of sediment transport out of the scour hole. The results of the proposed model were compared with those of some empirical models. The findings of the model agree well with the experimental results.

Key words: abutment, scour, clear water, sediment transport.

ÖZ

KÖPRÜ KENAR AYAKLARI ETRAFINDAKİ TEMİZ SU OYULMA DERİNLİĞİNİN ZAMANA BAĞLI DEĞİŞİMİNİN ANALİTİK VE DENEYSEL OLARAK İNCELENMESİ

Köse, Ömer
Doktora, İnşaat Mühendisliği Bölümü
Tez Yöneticisi : Prof. Dr. A. Melih Yanmaz
Mayıs 2007, 124 sayfa

Köprü temellerinin projelendirilebilmesi için temiz su oyulmasının zamana bağlı değişiminin bilinmesi büyük önem taşımaktadır. Oyulma derinliğinin maksimum değerinin tespiti konusunda daha önce yapılan çalışmalar, oyulma derinliğinin maksimum değere ulaşması için çok uzun süreler gerektiğini göstermiştir. Aynı şekilde prototip şartlarında maksimum oyulmaya ulaşmak için gereken süre tasarım taşkın hidrograflarının pik debiye erişme süresini fazlasıyla aşmaktadır. Bu nedenle oyulma derinliğinin zamana bağlı değişiminin bilinmesi gerekmektedir. Dik ve kanat duvar kenar ayakları etrafındaki oyulma derinliği ile oyulma hacmi eş yükselti eğrilerinin zamana bağlı değişimini gözlemek amacıyla bir deney programı yürütülmüştür. Deneysel çalışmalardan elde edilen sonuçlar ayrıca yorumlanmıştır. Bu çalışma, dik köprü kenar ayaklarında zamana bağlı oyulmanın tespiti için yarı amprik bir modelin geliştirilmesini sunmaktadır. Bu yaklaşım katı madde süreklilik ifadesinin kenar ayak etrafında oluşan oyulma çukuruna uygulanmasını esas almaktadır. Bu amaçla, oyulma çukurunun zamana bağlı olarak değişen geometrik özellikleri incelenmiş ve oyulma çukurundan çıkan katı madde miktarını ifade etmek için bir sürüntü yükü sıçrama fonksiyonu kullanılmıştır. Önerilen modelin sonuçları literatürdeki bazı amprik modellerle de karşılaştırılmıştır. Model bulguları ve deney sonuçlarının iyi bir uyum gösterdikleri görülmüştür.

Anahtar Kelimeler: Kenar ayak, oyulma, temiz su, katı madde taşınımı.

TO MY PARENTS

ACKNOWLEDGMENTS

The author would like to express his deepest gratitude and sincere thanks to his advisor Prof. Dr. A. Melih Yanmaz for his continuous support and encouragement throughout the course of this study, without which it would have been very difficult to complete this thesis.

Special thanks are extended to Dr. Vehbi Özaydın of Technical Investigation and Quality Control Department of the State Hydraulic Works and the laboratory technicians of this department for their help during the preparation of the laboratory flume and abutment models.

Finally, the author would convey his thanks to his family members for their support which enabled him to concentrate on this research.

TABLE OF CONTENTS

LIST OF TABLES

TABLE

LIST OF FIGURES

FIGURE

LIST OF SYMBOLS

A coefficient used in scour hole volume expression

A_b parameter reflecting combined effects of flow, sediment, and abutment properties

A^* dimensionless surface area of scour hole

A_p unit area defined for sediment pickup

a half width of abutment;

a_d distance of the outer edge of abutment to the origin

B coefficient used in scour hole volume expression

B_c channel width

B' surface width element of the scour hole

b_s an analogous pier size

C coefficient used in scour hole volume expression

c a constant for given flow, sediment, and abutment properties

c_0 coefficient used in Equation (5.13)

c_1 power used in Equation (5.13)

c_2 power used in Equation (5.13)

D coefficient used in scour hole volume expression

D_{50} median sediment size

D_* dimensionless sediment size

d_s instantaneous maximum depth of scour at an abutment

d_{se} equilibrium depth of scour at an abutment

E sediment pickup rate in mass per unit area and time

F_r Froude number

F_d densimetric particle Froude number

F_e excess abutment Froude number

f coefficient of proportionality

f_c computed f values

f_p predicted f values

G parameter

g gravitational acceleration

h function

K_d factor to account for the effect of sediment size and abutment length

K_I factor to account for the effect of flow intensity

K_G factor to account for approach channel geometry

K_{yL} factor to account for the effect of abutment length and flow depth

K_s factor to account for the abutment shape

$K_{\theta a}$ adjustment factor for abutment inclination with the approach flow

k_s equivalent roughness height

L abutment length

L^* width of the floodplain

L_c contraction length

L_e expansion length

L_R combined abutment length and flow depth parameter

M parameter defining coordinates of the points between boundaries of the top and bottom surfaces of the volume element

M' parameter defining coordinates of the points between upper and lower surface areas

m a parameter for given flow, sediment, and abutment properties

m_c parameter

m_k parameter determines combined effect of relative approach flow depth and flow intensity

N densimetric particle Froude number based on shear velocity of approach flow

n Manning's roughness coefficient

n^* Manning's roughness coefficient in floodplain

n_p porosity

P parameter defining coordinates of the points on the boundary of the bottom surface of the volume element

P' parameter defining coordinates of the points in the area of the bottom surface of the volume element

Q parameter defining coordinates of the points on the boundary of the top surface of the volume element

Q' parameter defining coordinates of the points in the area of the top surface of the volume element

Q_f discharge

Q_{si} rate of sediment transport into the scour hole

Q_{so} rate of sediment transport from the scour hole

R prediction factor

R_h hydraulic radius

R^2 coefficients of determination

R_e Reynolds number

R_m prediction level factor

S dimensionless scour depth

S_e standard error of estimate

S_o slope of the channel bed

T transport stage parameter

T_b time corresponding to d_s=0.632 d_{se}

T_d dimensionless time term

T_s dimensionless time in the proposed method

t time

t_m maximum duration of the experiment

t_R time term

t_d dimensionless time

t_e time to reach equilibrium scouring condition

t_{max} maximum duration of experiment

u mean approach flow velocity

u_c mean threshold velocity of approach flow

u_* shear velocity

u_{*c} critical shear velocity

V volume of scour hole around a bridge abutment

V^* dimensionless scour hole volume

V_1 volume element of scour hole

V_2 volume element of scour hole

V_m volume of scour hole obtained from the model

V_p volume of the scour hole obtained from the program

W abutment width

X_t' time dependent X' coordinate of the scour hole

X'_{tmax} X' coordinate of maximum scour hole at time t_{max}

x_t' time dependent x' coordinate of the scour hole

x'_{tmax} x' coordinate of maximum scour hole at time t_{max}

y approach flow depth

y^* depth of flow in flood plain

y_t' time dependent y' coordinate of the scour hole

y'_{tmax} maximum scour hole y' coordinate at time t_{max}

z_t' time dependent z' coordinate of the scour hole

z'_{tmax} maximum scour hole z' coordinate at time t_{max}

α abutment width to length ratio

α_b empirical coefficient

ρ density of water

ρ_s density of sediment

γ specific weight of water

γ_s specific weight of sediment

υ kinematic viscosity of water

Δ relative density

Δt time interval

σ_g	geometric standard deviation of particle size distribution
ψ	factor accounting for turbulent fluctuations and vortex oscillations in the scour hole
ϕ	angular coordinate of a point on the base of the scour hole
ϕ_b	average upstream slope of the scour hole
ϕ_p	sediment pick-up function
θ	angle of repose of sediment
θ_a	angle between the abutment axis and approach flow
θ_w	acute angle of wing-wall abutment
η	parameter used to define the coordinates of the volume of the scour hole
ξ	parameter used to define the coordinates of the volume of the scour hole
ξ_c	empirical coefficient
ε	abutment geometric factor
τ_b	bed shear stress on flat bed
λ_p	characteristic abutment length scale
β_g	empirical coefficient
β_b	empirical coefficient
τ_{bc}	critical bed shear stress on sloping bed
τ_{cr}	critical bed shear stress on flat bed

CHAPTER 1

INTRODUCTION

1.1 . General

Bridges crossing wide rivers are subject to various external impacts, such as development of adverse hydraulic conditions during severe floods, disastrous earthquakes, etc., most of which lead to complete failure. Statistical analysis of bridge failures indicate that most frequent cause of bridge failures is attributable to excessive scouring during floods (Shirhole and Holt (1991), Lagasse et al. (2001), and Wardhana and Hadiprioni (2003)). Other reasons of failure include overloading, collision, and deficiencies in design, construction, material, lack of repair and maintenance, etc. Bridge failures can lead to loss of several lives and properties, traffic disruption, and deficiencies in various socio-economic conditions. If the reason of bridge failure is not concerned with the structural design and materials, it may originate from lack of hydraulic evaluations, which may also lead to pronounced uncertainty in view of bridge stability (Yanmaz and Çiçekdağ, 2001). New bridges need to be designed to withstand extreme conditions that are likely to occur in the light of lessons learned from past events. On the other hand, existing structures should be monitored periodically on behalf of decision-making for the degree of necessary protective works to be implemented to increase the safety (Caner et al., 2006).

The phenomenon of bridge scouring has attracted the attention of many researchers since the middle of the 20^{th} century because of repeated examples of bridge failures induced by excessive scouring at bridge sites. In spite of achievement of significant advances in this phenomenon, however, there are still several aspects that need to be clarified. This thesis specifically deals with the experimental investigation of scour evolution around bridge abutments of vertical-wall and wing-wall types and development of a semi-empirical model for determining the temporal variation of clear water scouring at vertical abutments.

1.2. Statement of the Problem

Majority of the previously reported empirical clear water scour equations are based on equilibrium conditions, which are achieved under very long flow durations. The design of bridge foundations on the basis of equilibrium clear water scour depths may yield considerably greater values than may occur if the flow is of short duration. For a known time-to-peak value of design flood hydrograph, smaller scour depths may be obtained, which reduce the total cost of construction (Yanmaz and Altınbilek, 1991). Therefore, investigation of temporal variation of clear water scour at bridge elements is of importance to estimate the possible extension of the scour hole, which would provide relevant information for safe design of footing and selection of particular type of scour countermeasure.

Time variation of scour depth at bridge abutments has been studied by several investigators, such as Wong (1982), Tey (1984), Cardoso and Bettess (1999), Ballio and Orsi (2000), Oliveto and Hager (2002), Coleman et al. (2003), Dey and Barbhuiya (2005), and Oliveto and Hager (2005). In spite of availability of these methods, however, there is no single analytically derived scour-prediction equation, which is valid for wide ranges of flow conditions, channel bed and material properties, and abutment shape configurations. Accurate modeling of the scouring phenomenon in a laboratory medium is relatively difficult due to the combined effects of complex turbulent boundary layer, scale effects, time-dependent flow pattern, and sediment transport mechanism in the scour hole. On the other hand, relevant field data are scarce and subject to high degrees of uncertainty. Therefore, calibration of models using limited prototype information is also subject to modeling uncertainty.

Wide ranges of experiments were carried out to observe the erosion patterns around vertical-wall and wing-wall abutment models. A semi-empirical model is developed for vertical-wall abutments. The model is based on the application of sediment continuity equation to the scour hole around the vertical-wall abutment. The rate of sediment transport out of the scour hole is formulated using a sediment pickup function proposed by Dey and Debnath (2001) and the experimental results of scour measurements. The findings of the present study are compared with those of some recently proposed models.

Chapter 2 gives fundamentals of the phenomenon of scouring with special reference to the clear-water abutment scouring. The experimental setup and details of the experimental procedures are described in Chapter 3. Chapter 4 gives the results of the analysis of experiments with special emphasis to the scour patterns at abutment models. The calibration data that will form the basis of the semi-empirical model are also presented in this chapter. Chapter 5 is devoted to the derivation of the aforementioned semi-empirical model. In the semi-empirical model, two different approaches are considered for the formulation of the volume of the scour hole around the vertical-wall abutment. The first approach uses intensive mathematical formulations for this volume expression. The second approach is based on definition of a dimensionless volume expression using the experimental values of scour contours. The results of the semi-empirical model are compared with the experimental values and with the findings of some empirical methods. Finally, Chapter 6 presents a brief discussion on this research, gives conclusions extracted from the thesis and recommendations for future studies.

CHAPTER 2

LOCAL SCOUR AT BRIDGE ABUTMENTS

2.1. Introduction

Accurate estimation of maximum possible depth of scour at infrastructural elements of bridges is of importance for safe design. Although numerous studies have been carried out to examine various aspects of bridge scouring, there are still limited investigations on the subject of abutment scouring. This chapter deals with the analysis of characteristic trends of clear water scouring at bridge abutments with reference to laboratory observations. Based on the review of the phenomenon, the dimensionless scour depth at an abutment is found to depend on some governing dimensionless terms, such as the flow intensity, Froude number, relative approach flow depth, sediment grading, relative sediment size, time parameter, geometric features of the abutment, foundation, and approach channel. Relative importance and effects of these parameters on the development of scouring are discussed. Furthermore, scale effects inherent to laboratory measurements are also interpreted.

2.2. General Remarks on Scour Mechanism at Bridge Sites

Scour occurs at alluvial riverbeds whenever the rate of sediment transport is accelerated due to the contraction of the flow area, such as at channel constrictions, around bridge piers and abutments, or due to impinging effect of jets leaving outlet facilities. The sediment continuity equation for the riverbed is

$$\frac{dV}{dt} = Q_{si} - Q_{so} \tag{2.1}$$

in which V is the volume of the control element at the loose bed, t is the time, Q_{si} and Q_{so} are the rates of sediment transport into and out of the control volume. A localized contraction, such as a bridge opening, would lead to an increase in the local sediment transport capacity due to flow acceleration. Since the upstream transport rate is normally smaller than that of the contracted section, Q_{so} will be greater than Q_{si} that would lead to a decrease in the volume of the control element. It means that the bed level is lowering with respect to time. This phenomenon is named as scouring. If it takes place around an object like a pier or abutment, it is known as local scour around that obstacle. If scouring takes place at a constriction having an alluvial bed, the phenomenon is termed as the localized or contraction scour. The general or degradation scour is that phenomenon, which occurs irrespective of the presence of any human interference, such as implementation of various types of hydraulic structures, use of rivers, etc. The general scour, which may take place over a geologic time scale, is influenced by the fluvial characteristics of the river. Due to the slow process of lowering of the entire riverbed elevation, the general scour is unlikely to be of significance to the engineer assessing a bridge site with respect to total potential scour. Therefore, only the mechanisms of local and contraction scours will be discussed in this chapter.

Two types of scour develop at loose boundaries, i.e. clear water scour and live-bed scour, depending on whether or not there is bed load transportation at the upstream. In case of clear water scour, the flow inertia is relatively low that the bed shear stress is smaller than the threshold value defined for the given bed material. Scour occurs in the contracted section due to the local acceleration of the flow and continues until the scour hole becomes stable. Rate of change of scour is a function of the erosive capacity of the flow in the scour hole. Local scour at the downstream of a dam due to the impinging effect of the jet is a typical example for clear water scour. When the bed shear stress exceeds a threshold value, there is bed load transportation at the upstream, which interferes with the local sediment transport rate in the scour hole. The rate of scour is a function of the relative transport capacity of the approach flow and the flow in the scour hole that is influenced by the flow intensity as well as the geometric characteristics of the abutment. For live bed scour, sediment is transported through the scour hole by means of an excess shear stress. However, in case of clear water conditions, particles on the surface of the scour hole may be occasionally moved but are not carried away.

A bridge crossing a wide river is subject to two different flow conditions; namely the flow in the main channel and in the floodplains which are only occupied by the flow during floods. Under low flow conditions, floodplains are normally utilized for agricultural activities. Therefore, floodplains may sometimes be spanned by long embankments to reduce the total length of the bridge. Such an application is shown in Figure 2.1 for which the level of hydraulic and structural interaction depends on the degree of constriction and the geometric features of the structural elements of the bridge opening.

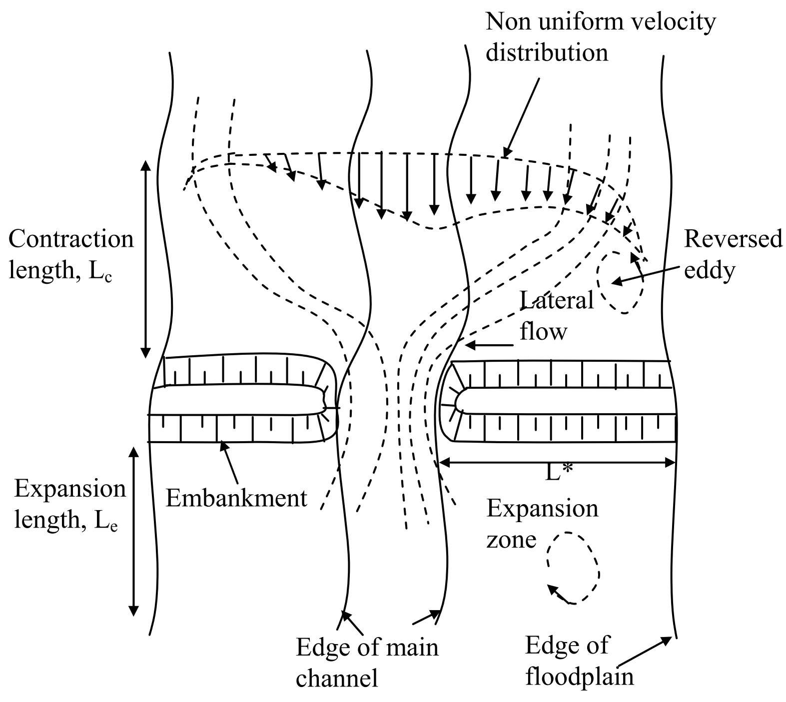

Figure 2.1. Flow conditions around a bridge in a wide river (Yanmaz and Caner, 2006).

The upstream of the bridge opening is subject to strong curvature of the flow lines towards the main channel, where flow accelerates. Towards the edges of the floodplains, slowly moving eddy creates ineffective flow conditions. Details of the flow conditions in contraction and expansion zones will be discussed in the subsequent sections.

2.3. Local Scour at Bridge Abutments

Placement of infrastructural elements of bridges in flow section contracts the bridge opening and would lead to flow acceleration. When the local flow field in bridge opening is strong enough, the bed material is removed. The phenomenon of local scour around bridge piers and abutments has been investigated because of repeated examples of bridge failures, most of which are attributable to this problem. Although a number of abutment scour-prediction equations have been reported in the literature, however, there is no single analytically derived equation, which is valid for wide ranges of flow conditions, bed material properties, and abutment shape configurations because of difficulties of modeling the phenomenon in a laboratory medium. The bridge scouring phenomenon is relatively complex mainly due to the combined effects of turbulent boundary layer, scale effects, time-dependent flow pattern, and sediment transport mechanism in the scour hole (Yanmaz and Altınbilek, 1991). Lack of understanding of complex flow phenomenon leads to pronounced uncertainty due to insufficient modeling (Yanmaz and Çiçekdağ, 2001; Yanmaz and Çelebi, 2004). On the other hand, reliable field data are scarce leading to calibration problems. Therefore, engineering solutions concerning determination of safe depth of burial of footing and selection of scour countermeasures are subject to uncertainty. That is why additional experimental studies need to be conducted.

The close upstream of a bridge abutment is subject to a strong pressure field, leading to the separation of flow, formation of downflow, and primary vortices, which migrate downstream past the abutment. During heavy floods, the downflow may also be supplemented with the flow, which is intercepted from the channel sides and the scouring action is pronounced. Hence, primary vortices and wake vortices scour the loose bed yielding the development of a scour hole around the abutment. The degree of severity of the problem is dictated by the magnitude of this scour hole. Figure 2.2 illustrates the vortex systems developed around a bridge abutment. Excessive local scour at the bridge abutment may cause undermining of the abutment foundation causing the bridge to fail. An accurate prediction of the scour depth and pattern around bridge abutments is essential for a safe and economic design of bridge foundation. Overestimation of the local scour leads to uneconomic solution, whereas underestimation of this phenomenon leads to unsafe design. The local flow field around bridge abutment is complex since it is three-dimensional separated vorticial turbulent flow. The complexity of the flow field increases during floods because of the unsteadiness and the possibility of flow reversal at the bridge site. The flow field interacts dynamically with the erodible bed during the development of the scour hole. The local scour pattern around abutments depends on the local flow structure as well as the type and properties of the erodible bed (Raudkivi and Ettema, 1983). At abutments the obstruction of the flow forms a horizontal vortex starting at the upstream end of the abutment and running along the toe of the abutment and forms a vertical wake vortex at the downstream end of the abutment.

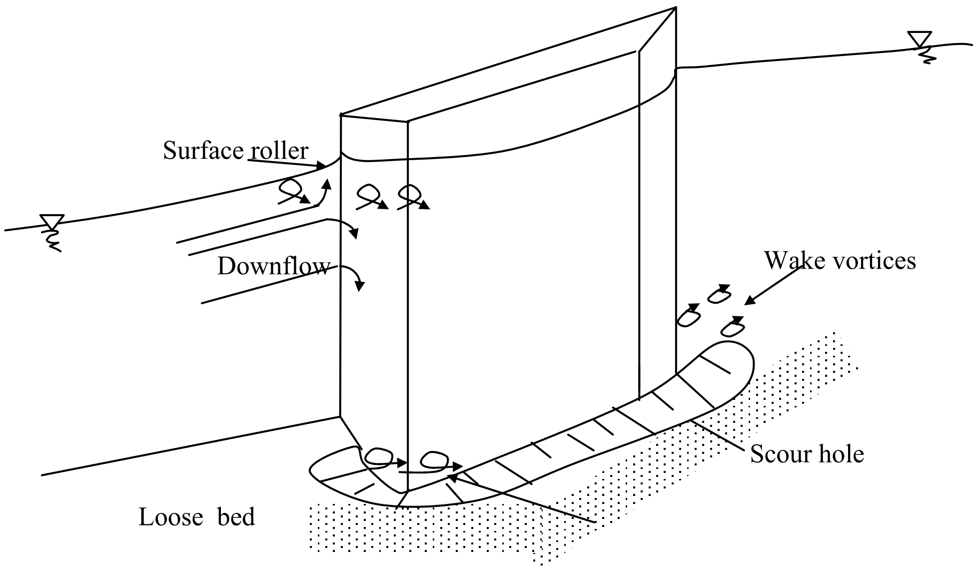

Figure 2.2. Definition sketch for scouring at an abutment (Yanmaz, 2002).

Characteristic trends of governing variables affecting the abutment scouring need to be interpreted to achieve some design guidelines. The depth of scour (d_s) at an abutment is influenced by the abutment length perpendicular to the flow direction (L), the mean approach flow velocity (u), water density (ρ), sediment density (ρ_s), kinematic viscosity of water (υ), mean approach threshold velocity (u_c), gravitational acceleration (g), approach water depth (y), median sediment size (D_{50}), geometric standard deviation of particle size distribution (σ_g), abutment shape (K_s), approach channel geometry (K_G), and time (t). Dimensionless parameters can be generated using Buckingum's- π theorem. After modifying the dimensionless parameters to end up with more practical results, one obtains

$$\frac{d_s}{L} = f\left(R_e, F_{rL}, \Delta, \frac{u}{u_c}, \frac{y}{L}, \frac{L}{D_{50}}, \sigma_g, K_s, K_G, T_s\right) \tag{2.2}$$

where R_e is the Reynolds number, uy/υ, F_{rL} is the abutment Froude number, $u/(gL)^{0.5}$, $\Delta=(\rho_s-\rho)/\rho_s$, ρ_s is the sediment density, ρ is the water density, and $T_s=tD_{50}(\Delta g D_{50})^{0.5}/L^2$ is the dimensionless time. For fully developed turbulent flow, effect of Reynolds number is negligible. The term u/u_c, also known as flow intensity, would imply the stage of sediment transport on the approach flow bed. The relative approach flow depth, y/L, reflects the effect of flow shallowness. Alternatively, the flow Froude number, $F_r=u/(gy)^{0.5}$ can also be used to account for the effect of state of flow, i.e. subcritical or supercritical (Yanmaz and Caner, 2006). Shape effect of abutments is dictated by their types, i.e. vertical-wall, wing-wall, and spill-through abutments. Although selection of a particular type of abutment is normally governed by magnitudes of support reactions and lateral earth pressure and foundation properties, a spill-through abutment produces smallest scour depth compared to other types of abutment (Yanmaz, 2002). So, for a given type of abutment under clear water conditions with uniform bed material, Equation (2.2) reduces to

$$\frac{d_S}{L} = f\left(F_{rL}, \frac{u}{u_c}, \frac{y}{L}, \frac{L}{D_{50}}, K_G, T_s\right) \tag{2.3}$$

In this study, the effects of other parameters, e.g. interaction of an abutment with a close pier, irregularity of the channel cross-section, submergence of the superstructure, alignment of abutment axis with respect to approach flow, etc., are ignored. The effects of governing parameters listed in Equation (2.3) will be further discussed with special reference to some clear water flume data. To this end, clear water scour data with uniform bed material compiled from Gill (1972), Rajaratnam and Nwachukwu (1983), Kwan (1984), Tey (1984), Dongol (1994), Lim (1997), Lauchlan and Melville (2001) and from the author are used. The experimental procedure of this study is presented in detail in Chapter 3.

2.3.1 Effect of Abutment Froude Number and Scaling

The scale effect for pier experiments has been discussed by Ettema et al. (1998). A similar discussion also applies to abutments placed in main channels. In this study, abutment Froude number is used specifically to account for the effect local energy gradients for flow around abutments. The velocity head at the upstream face of an abutment, $u^2/2g$, can be made dimensionless by dividing it by the abutment size to obtain the form of the square of the abutment Froude number, u^2/gL. The study carried out by Ettema et al. (1998) indicated that the scour depth at piers did not scale linearly with pier width unless there was complete geometric similitude of pier, flow, and sediment particles forming the bed. Similitude of scour depth data from the flume to the field requires the constancy of F_r, u/u_c, and y/L. Flume experiments, however, are normally forced to use bed materials, which have comparable sizes as the prototype since very fine particles in a laboratory medium would be subject to suspension. Therefore, to maintain similar modes of sediment transportation, the term reflecting the effect of sediment coarseness, L/D_{50}, cannot satisfy the length scale selected according to the other geometric variables, such as abutment length, flow depth, etc. So, the constancy of L/D_{50} cannot be maintained. To attain a desired particle mobility level, the value of u/u_c should be the same in the laboratory and the field. This implies that greater values of u than required in Froude number simulation are needed in a laboratory medium. Hence, the Froude number used in laboratory experiments may be greater than that for the corresponding field conditions. On the other hand, as can be seen in Figure 2.3, relative scour depth, d_s/L, increases with increasing Froude number in the range of the available data, i.e. $F_{rL}<0.4$. However, to formulate the effect of the Froude number, a wider range of data is needed. Therefore, clear water conditions in a laboratory medium can cause deeper scour holes, relative to the abutment length, than any likely to occur at bridge abutments in rivers. As a concluding remark, scour-prediction equations derived using laboratory data overestimate the scour depths. Therefore, the design of abutment footing on the basis of such equations gives conservative values.

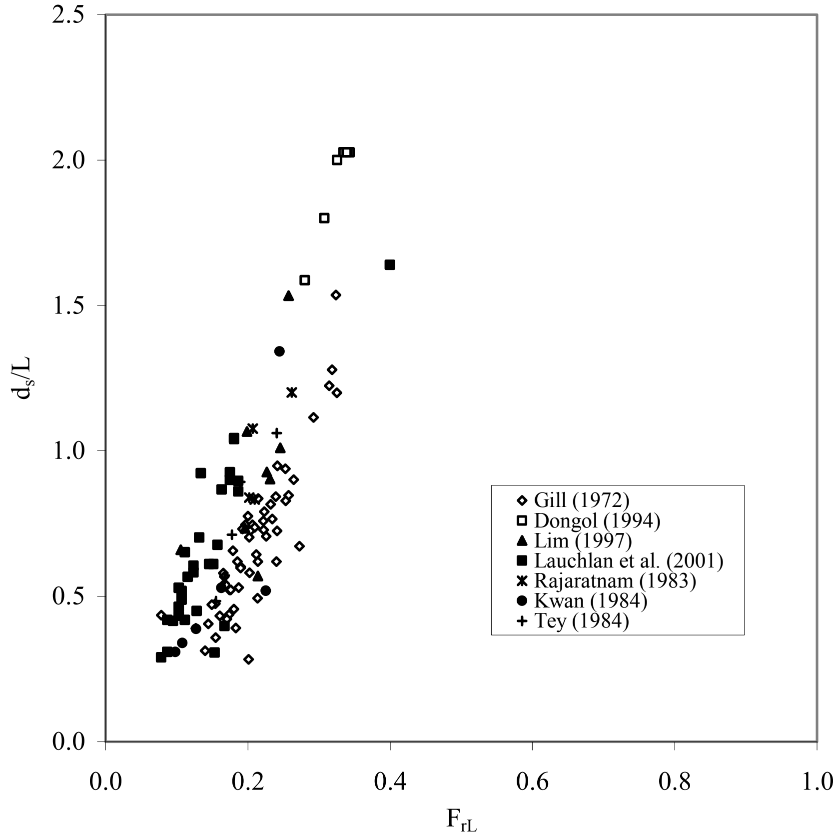

Figure 2.3. Variation of d_s/L against F_{rL} (Yanmaz and Köse, 2006)

2.3.2. Effects of Flow Intensity and Flow Shallowness

As stated before, the flow intensity, u/u_c, reflects the type of bed regime. On the other hand, for a given sediment size, the flow depth, y, also influences the mean threshold velocity, u_c, i.e. the greater the flow depth, the higher the mean threshold velocity. That is why the combined effect of relative approach flow depth and flow intensity under clear water conditions, i.e. $m_k=(y/L)(u/u_c)$ is investigated using the available data (See Figure 2.4).

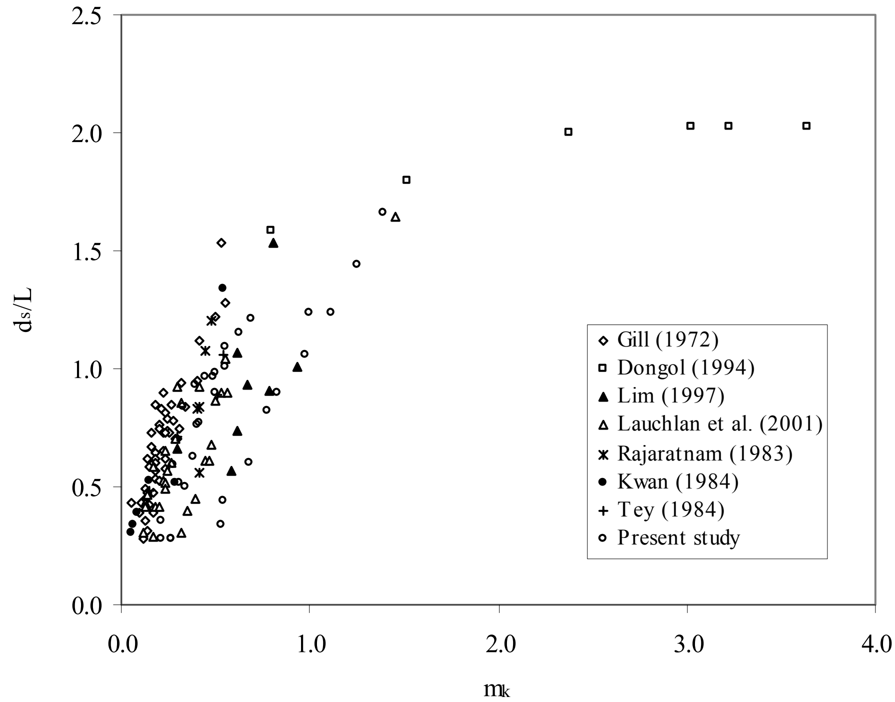

Figure 2.4. Correlation between m_k and d_s/L (Yanmaz and Köse, 2006)

For m_k <1.0, the relative scour depth for all data sets increases almost linearly, whereas it tends to approximately 2.0 in the range, $m_k \geq 1.0$. A linear multiple regression analysis is carried out for the data presented in Figure 2.4 and the following equation is obtained (Yanmaz and Köse, 2006).

$$\frac{d_s}{L} = 1.36\left(\frac{y}{L}\right)^{0.46}\left(\frac{u}{u_c}\right)^{0.94} \tag{2.4}$$

for which the coefficient of determination is 0.88. For live bed conditions, the effect of flow intensity is negligible since the relative scour depth fluctuates around a mean value due to random sediment supply from the upstream and progressive changes in bed resistance.

The effect of flow depth relative to the abutment length needs further interpretation. Implementation of an abutment into a flow section would lead to development of a surface roller, which has an opposite sense of rotation as the principal vortex at the bed level (See Figure 2.2). For shallow flows, the surface roller tends to retard the downflow. Therefore, it results in reduction of scour depth. Melville and Coleman (2000) classify the abutments as short, intermediate length, and long with respect to y/L ratio using the following limiting values. For deep flows and short abutments ($y/L>1.0$), the scour depth is independent of flow depth but depends on L. Conversely, for shallow flows with greater abutment lengths ($y/L\leq0.04$), the scour depth is independent of L but varies linearly with y. For long abutments only a portion of abutment, close to the bridge opening yield the deepest scour hole. Towards the banks, however, the slowly moving reversed eddy as shown in Figure 2.1 is not capable of producing scour along the upstream face of the abutment. Therefore, for long abutments, the scour depth is found to be independent of the abutment length. For intermediary ranges, i.e. $0.04<y/L\leq1.0$, the scour depth is proportional to the square root of the product of y and L. When the available clear water data are plotted as relative scour depth, d_s/L, versus relative approach flow depth, y/L, it is observed that the design curves suggested by Melville and Coleman (2000) bound the available clear water scour data (See Figure 2.5). Moreover, the studies of Melville and Coleman (2000) show that the live bed data are also bounded by these limiting curves. Therefore, these limits may be used for design applications.

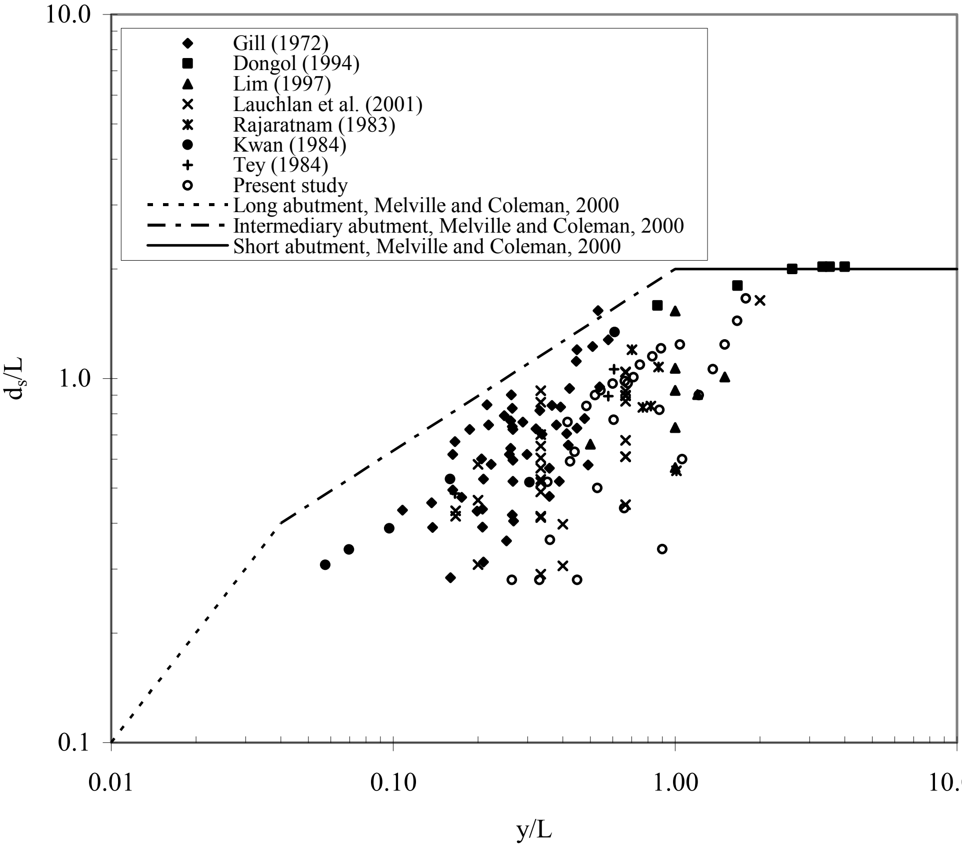

Figure 2.5. Variation of d_s/L with respect to y/L (Yanmaz and Köse, 2006)

2.3.3 Effects of Sediment Coarseness and Bed Material Gradation

The effect of L/D_{50} term on the scour development diminishes for $L/D_{50}>50$, which reflects most of the actual prototype conditions. For grain sizes with $L/D_{50}<50$, the grains are large enough relative to the width of the groove excavated by downflow which impedes the scouring process (Melville and Coleman, 2000).

The studies conducted on the effect of bed material gradation and effect of cohesion on bridge scouring, especially for live bed conditions are limited. The depth of scour around any infrastructural bridge element generally tends to decrease with increasing value of σ_g because of armoring effect at the bed level.

2.3.4. Effect of Approach Channel Geometry

Many of the equations dealing with abutment scouring reported in the literature use the total length of an abutment projected normal to flow as an independent variable. This approach is normally applicable to short abutments upstream of which may be subject to one dimensional flow conditions. However, for long approach embankments as shown in Figure 2.1, the approach flow has a non-uniform velocity distribution across the cross-section. For wide and shallow floodplains there exist ineffective flow areas with relatively small velocities and flow depths. Therefore, only a certain portion of the embankment, which is subject to active flow conditions, should be considered in the computation of the scour depth around the abutment. The length of embankment blocking live flow can be determined from a graph of conveyance versus distance measured along the upstream face of the embankment. Such information can be obtained from the execution of HEC-RAS program (USACE, 2002). In a different approach, Sturm (1999) considered the distribution of flow rate in the overall cross-section rather than defining an effective abutment length. Melville and Coleman (2000) defined a coefficient K_G as included in Equations (2.2) and (2.3) to account for the effect of embankment length and approach channel characteristics. This coefficient is expressed by

$$K_G = \sqrt{1 - \left(\frac{L^*}{L}\right)\left[1 - \left(\frac{y^*}{y}\right)^{5/3}\left(\frac{n}{n^*}\right)\right]} \tag{2.5}$$

where L^* is the width of floodplain, y* is the average depth of flow in floodplain, y is the depth of flow in main channel, n and n* are Manning's roughness coefficients in main channel and floodplain, respectively. For given values of y, y*, n and n*, as relative length of projecting embankment into main channel, L*/L, increases, the value of K_G or the depth of scour at the abutment decreases since part of the approach flow is deflected by the lateral flow parallel to the upstream face of the abutment (See Figure 2.1), which tends to diminish the effect of downflow, and hence the depth of scour.

2.3.5. Effect of Time

Most of the previous studies were carried out for equilibrium conditions for which the effect of T_s is neglected (Yanmaz, 2002). Equilibrium scouring situation for clear water conditions is achieved under very long flow duration, which may be of the order of several days in a laboratory medium. For example, Lim (1997) reported that the required time to reach the equilibrium scour at abutments in clear water scour is 3-8 days, depending on the flow and sediment conditions. Melville and Chiew (1999) defined the time to reach equilibrium conditions such that the rate of increase of scour depth does not exceed 5% of the pier diameter in the succeeding 24 h period. Besides, Yanmaz and Altınbilek (1991) and Mia and Nago (2003) presented semi-empirical models for temporal variation of clear water scour at cylindrical piers. The latter two models require also very long duration for equilibrium situations. The design of bridge foundations on the basis of equilibrium clear water scour depths may yield considerably greater values than may occur if the flow is of short duration. For a known time-to-peak value of design flood hydrograph, smaller scour depths may be obtained, which reduce the total cost of construction (Yanmaz and Altınbilek, 1991). Therefore, investigation of temporal variation of clear water scour at bridge elements is of importance to estimate the possible extension of the scour hole. Coleman et al. (2003) proposed the following equation for temporal variation of clear water scour at vertical-wall abutments.

$$\frac{d_s}{d_{se}} = \exp\left[-0.07\left(\frac{u}{u_c}\right)^{-1}\left|\ln\left(\frac{t}{t_e}\right)\right|^{1.5}\right] \tag{2.6}$$

where d_{se} is the equilibrium scour depth at a vertical-wall abutment and t_e is the time to develop equilibrium scour depth. The equilibrium depth of scour, d_{se}, at a vertical-wall abutment mounted in a main channel composed of uniform bed material can be determined from (Melville and Coleman, 2000)

$$d_{se} = K_{yL} K_I K_d \tag{2.7}$$

where K_{yL} is a factor accounting for the effects of flow depth and abutment length, K_I is the flow intensity factor which can be taken as u/u_c for clear water conditions in uniform bed material, and K_d is a factor reflecting the effects of abutment length and particle size. The values of K_{yL} can be taken as 2L, $2(yL)^{0.5}$, and 10y for y/L>1.0, 0.04<y/L≤1.0, and y/L≤0.04, respectively. The adjustment factor K_d is unity for $L/D_{50}>25$, which reflects most of the actual prototype conditions. The flow intensity factor is modified to take into account the bed armoring effect due to sediment gradation. For $L/D_{50}>60$, the value of t_e in seconds is determined from (Coleman et al., 2003)

$$t_e = 10^6 \left(\frac{u}{u_c}\right)^3 \left(\frac{y}{u}\right) \left\{3 - \left[1.2\left(\frac{y}{L}\right)\right]\right\} \qquad \text{for } y/L<1 \tag{2.8}$$

$$t_e = 1.8 * 10^6 \left(\frac{L}{u}\right)\left(\frac{u}{u_c}\right)^3 \qquad \text{for } y/L \geq 1 \tag{2.9}$$

Oliveto and Hager (2002) derived the following equation for time-dependent scour depth at vertical-wall abutments under clear water conditions

$$\frac{d_s}{L_R} = 0.085 \sigma_g^{-0.5} F_d^{1.5} \log T_d \tag{2.10}$$

where $L_R = L^{2/3} y^{1/3}$, F_d is densimetric particle Froude number, $u/(\Delta g D_{50})^{0.5}$, Δ is relative density, $T_d = t/t_R$, and $t_R = L_R/(\Delta g D_{50})^{0.5}$. Contrary to the Coleman et al. (2003) approach, Equation (2.10) does not require equilibrium scouring parameters. The results obtained from different equations giving equilibrium scour depth may differ widely from each other, which restrict to reach concrete universal conclusions (Yanmaz, 2002). Therefore, precision of time-dependent scour depths given by Equation (2.6) is influenced by the accuracy of equilibrium parameters.

2.3.6. Effect of Abutment Shape and Alignment

Three types of abutments are commonly used in practice, which are vertical-wall abutments, spill-through abutments, and wing-wall abutments as shown in Figure 2.6 in which θ_w is the acute angle of the wing-wall abutment. A well streamlined body, such as spill-through abutment or wing-wall abutment produces a vortex of low strength while a sharp obstruction e.g. a vertical-wall abutment is capable of producing a strong vortex field. Therefore, greater scour depths occur in the case of a vertical-wall abutment compared with a streamlined body. In the case of spill-through and wing-wall abutments, the energy of the diverted flow is dissipated on the sloping sides of the abutments which reduce the strength of the vortex. The reduction in the strength of the vortex is higher in spill-through abutments than in wing-wall abutments. As a result, the scour depths at spill- through abutments will be smaller in comparison with the scour depths at wing-wall abutments. According to HEC-18 procedure (Richardson, and Davis, 1995) the shape of the abutment can influence the maximum scour depth by 20% and vertical-wall abutments will produce scour depths about the double of that of spill-through abutments.

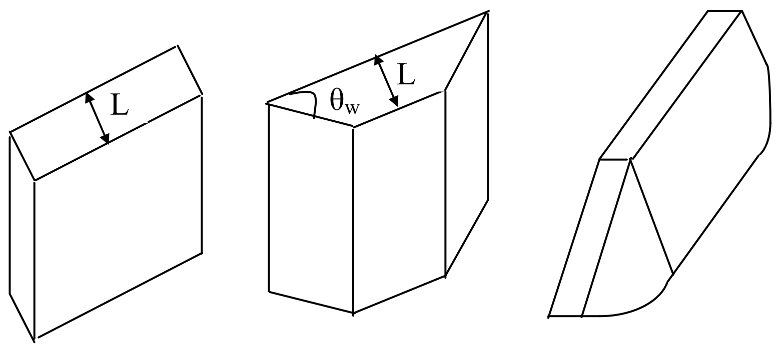

Vertical-wall abutment   Wing-wall abutment   Spill-through abutment

Figure 2.6. Various abutment types

The influence of the abutment shape on local scour depth is more important for shorter abutments. The effect of shape is expressed using the shape factor K_s whose values are presented in Table 2.1. The abutment alignment is dictated by the inclination angle, θ_a, of the abutment axis with the approach flow as shown in Figure 2.7. It has been generally found that the scour depth increases with an increase in θ_a (See Table 2.2). Using the perpendicularly aligned abutment (θ_a=90^o) as a reference, abutments pointed upstream are found to produce greater scour depths since the vortices developed along the upstream face of the abutment are confined in the dead flow zone. As seen in Table 2.1, H and V stand for the horizontal and vertical values of slope.

Table 2.1. Shape factors for abutments (Melville, 1997)

Abutment Shape	K_s
Vertical-wall	1.00
Wing-wall	0.75
Spill-through (0.5H:1V)	0.60
Spill-through (1H:1V)	0.50
Spill-through (1.5H:1V)	0.45

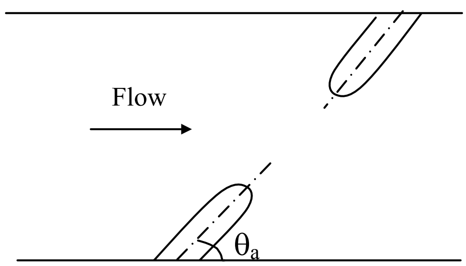

Figure 2.7. Definition sketch for abutment inclination

Table 2.2. $K_{\theta a}$ coefficient for abutments (Melville and Coleman, 2000)

θ_a (°)	30	45	60	90	120	135	150
$K_{\theta a}$	0.90	0.95	0.98	1.0	1.05	1.07	1.08

2.3.7. Effect of Flow Unsteadiness

Most of the existing scour prediction equations are developed based on experimental work under steady flow conditions. The flow in a river during a flood is unsteady and discharge changes may be quite rapid. The estimated scour depth for the maximum flood discharge using relations for steady flow is normally conservative since the maximum flood discharge does not generally last long enough for scour to develop to its full potential i.e. equilibrium condition (Kothyari et al., 1992). Additional elaborative and extensive laboratory investigations need to be conducted to observe the effects of various hydrograph parameters, such as hydrograph shape and duration.

The next section gives a number of scour-prediction equations for abutments. Although numerous methods have been reported in the literature, the results of these methods, when applied to a specific case, differ widely from each other because of differences in their derivational conditions. Therefore, care should be taken when a particular equation is used. Derivational conditions must reflect similar situations as of the case to be applied.

2.4. Abutment Scour Prediction Models

Liu et al., Approach (1961)

Liu et al. (1961) derived the following equation for clear water scouring at vertical-wall abutments:

$$\frac{d_s}{y} = 2.15\left(\frac{L}{y}\right)^{0.40} F_r^{0.33} + 0.30 \tag{2.11}$$

in which d_s is the terminal scour depth measured at the end of the experiment, F_r is Froude number of approach flow and other terms are the same as previously defined.

Laursen's Approach (1963)

Laursen (1963) derived the following relationship for clear water scour at a vertical-wall abutment:

$$\frac{L}{y} = 2.75\frac{d_s}{y}\left[\frac{\left(0.09\frac{d_s}{y}+1\right)^{1.17}}{\frac{\tau_o}{\tau_c}} - 1\right] \tag{2.12}$$

where τ_o= bed shear stress on the approach section and τ_c = critical shear stress for initiation of bed motion.

Gill's Approach (1972)

Gill (1972) developed the following equation for the maximum scour depth at a vertical-wall abutment:

$$\frac{d_s}{y} + 1 = \beta_g\left(\frac{B}{B-L}\right)^{(6/7)}\left[\frac{1}{\left(\frac{B}{B-L}\right)^{0.5}\left(1-\frac{\tau_c}{\tau_o}\right)+\frac{\tau_c}{\tau_o}}\right]^{(3/7)} \tag{2.13}$$

where β_g is an empirical coefficient depending on the flow depth and the size of the bed material, and B=channel width. Based on laboratory data, he obtained that $\beta_g=8.375(D_{50}/y)^{0.5}$. For maximum clear water conditions, $1-(\tau_c/\tau_o)=0$. For live bed conditions, i.e.$\tau_c/\tau_o \geq 1$, Equation (2.13) reduces to

$$\frac{d_s}{y} + 1 = \left(\frac{B}{B-L}\right)^{(6/7)}\left(\frac{\tau_o}{\tau_c}\right)^{(3/7)} \tag{2.14}$$

Froehlich's Approach (1989)

Froehlich (1989) compiled a total of 164 clear water measurements of the maximum depth of scour from eleven investigators. Multiple linear regression analysis was used to determine a relation between the depth of scour and a set of dimensionless independent variables. Froehlich's (1989) regression equation for clear water conditions is

$$\frac{d_s}{y} = 0.78\, K_s\, K_{\theta a} \left(\frac{L}{y}\right)^{0.63} F_r^{1.16} \left(\frac{y}{D_{50}}\right) \sigma_g^{-1.87} + 1 \tag{2.15}$$

where K_s= shape factor for abutment and embankment, $K_{\theta a}$ = embankment skewness factor, and the others are the same as previously defined. In Equation (2.15), +1.0 is considered as a safety factor for conservative estimation of the scour depth.

Lim's Approach (1997)

Lim (1997) proposed the following equation for maximum clear water scour at vertical-wall abutments.

$$\frac{d_s}{y} + 1 = 3.5 F_{ro}^{0.75} \left(\frac{L}{y}\right)^{0.29} \left(\frac{D_{50}}{y}\right)^{0.25} \tag{2.16}$$

where $F_{ro} = \rho u^2 / [(\rho_s - \rho) g D_{50}]$ is a measure of the ratio of the tractive force which acts on the sand grain to the submerged weight of the grain.

Cardoso and Bettess's Approach (1999)

Cardoso and Bettess (1999) conducted experiments imposing approximately the threshold velocity on the floodplain. They fitted various models to their experimental data and the model proposed by Whitehouse (1997) is modified to end up with the following equation.

$$\frac{d_s}{d_{se}} = 1 - \exp\left[-1.025\left(\frac{t}{T}\right)^{0.350}\right] \tag{2.17}$$

where d_{se}= equilibrium scour depth, t = time, T= time corresponding to $d_s = 0.632d_{se}$. Equilibrium scour depths were reported but a general method computing d_{se} values has not been proposed.

Kothyari and Ranga Raju's Approach (2001)

Kothyari and Ranga Raju (2001) defined an analogous pier having a size b_s (perpendicular to flow direction) that scour around it is the same as that around the given abutment conditions. The following equation is used for computation of b_s values from the known equilibrium scour depths.

$$\frac{d_{se}}{b_s} = 0.66\left(\frac{b_s}{D_{50}}\right)^{-0.25}\left(\frac{y}{D_{50}}\right)^{0.16}\left(\frac{u^2 - u_c^2}{\frac{\Delta\gamma_s}{\rho}D_{50}}\right)^{0.4} a^{-0.3} \tag{2.18}$$

where a_k=(B-b_s)/B, B=channel width, $\Delta\gamma_s$=γ_s-γ, γ_s=specific weight of sediment, γ= specific weight of water, and ρ= density of water.

Ballio and Orsi's Approach (2001)

Ballio and Orsi (2001) carried out observations on scour at vertical-wall abutments under clear water conditions. Using the durations changing from one hour to one month. In contrast to the majority of the literature studies, they stated that scour hole depth could not reach equilibrium. They tried to adapt some expressions reported in the literature, into their data and found out that Franzetti et al. (1994) formula matched to their data best. Making a small modification in the coefficients, they proposed the following formula:

$$\frac{d_s}{d_{se}} = 1 - e^{-\alpha_b\left(\frac{tu}{\lambda_p}\right)^{\beta_b}} \tag{2.19}$$

where d_{se}= equilibrium scour depth estimated by eye-fitting measured trends to the analytical expression, α_b=0.028, t=time, u=average approach flow velocity, $\lambda_p=(Ly)^{0.5}$, and β_b=0.33.

Kayatürk's Approach (2005)

Kayatürk (2005) investigated the effect of collars on abutment scour. As part of her doctoral research, Kayatürk (2005) derived the following empirical equation for clear water scour depth at vertical-wall abutments:

$$\frac{d_s}{y} = \left(\frac{L}{y}\right)^{1.4} (F_r)^{1.76} \left(\frac{L}{W}\right)^{0.12} \left(\frac{L}{B}\right)^{-0.66} \tag{2.20}$$

where W = abutment width, B= channel width, and L= projecting length of abutment perpendicular to the flow. This equation is subject to a limitation that scour depths were obtained at the end of six hours duration, i.e., not reflecting equilibrium conditions.

Dey and Barbhuiya's Approach (2005)

In Dey and Barbhuiya's (2005) method, clear water scour conditions were maintained for all runs adjusting the approaching flow condition to $u/u_c \approx 0.95$. A semi-empirical model is presented to compute the equilibrium scour depth in an evolving scour hole at short abutments, 45^0 wing-wall and semicircular abutments, in uniform and non uniform sediments under clear water conditions.

The following differential equation, which is based on conservation of mass with the consideration of the primary vortex system as the main agent of the scouring, is obtained:

$$\left(1-n_p\right)\left[\varepsilon\cos\phi_b\left(\frac{\varepsilon}{1-\varepsilon}S\cos\phi_b+2\frac{a_d}{L}\right)+\frac{(1+\varepsilon)S\cot\phi_b+2(1-\varepsilon)\frac{a_d}{L}}{\sin\phi_b}\right]\frac{dS}{dT_s}$$
$$=\varepsilon\cos\phi_b\left(\frac{\varepsilon}{1-\varepsilon}S\cos\phi_b+2\frac{a_d}{L}\right)\frac{L}{D_{50}}\phi_p \tag{2.21}$$

where n_p=porosity, ε = abutment geometric factor (0.08 for vertical-wall abutments), S = dimensionless scour depth, which is d_s/L, ϕ_b = average upstream slope of the scour hole, which is slightly greater than the natural angle of repose of sediment, a_d=distance of the outer edge of abutment to the origin defined by Dey and Barbhuiya (2005), and ϕ_p = sediment pickup function, which will be defined in Chapter 4.

Dey and Barbhuiya (2005) proposed the following equations for equilibrium clear water scour depths:

$$\frac{d_{se}}{L}=7.281\,F_e^{0.314}\left(\frac{y}{L}\right)^{0.128}\left(\frac{L}{D_{50}}\right)^{-0.167} \quad \text{for vertical-walls} \tag{2.22}$$

$$\frac{d_{se}}{L} = 8.319\, F_e^{0.312} \left(\frac{y}{L}\right)^{0.101} \left(\frac{L}{D_{50}}\right)^{-0.231} \quad \text{for } 45^o \text{ wing-walls} \tag{2.23}$$

$$\frac{d_{se}}{L} = 8.689 F_e^{0.192} \left(\frac{y}{L}\right)^{0.103} \left(\frac{L}{D_{50}}\right)^{-0.296} \quad \text{for semicircular abutment} \tag{2.24}$$

where F_e is called the excess abutment Froude number that is $F_e = u_e / (\Delta g L)^{0.5}$, $u_e = u - \xi_c u_c$, u=approach flow velocity, u_c is mean threshold velocity for bed particles, ξ_c is a coefficient, which is 0.5 for vertical wall abutments. The correlation coefficients between the experimentally obtained and the computed scour depths for vertical-wall, 45^o wing-wall and semicircular abutments were 0.991, 0.971, and 0.964 respectively.

CHAPTER 3

EXPERIMENTAL INVESTIGATION

3.1. Scope of Experiments

This section is devoted to the description of the experimental procedure, including setup, instrument used, and scope of the laboratory studies. Experiments were conducted in the Hydraulics Laboratory of the Technical Research and Quality Control Department of Turkish State Hydraulic Works in Ankara.

All experiments were conducted using a 30 m long, 1.25 m wide and 1 m deep circulating flume having a bed slope of 0.001. In the course of the experiments, two different bed materials composed of quartz sand were used to investigate the size effect of sediment on the scouring mechanism. The median sizes of the bed materials were 1.8 mm and 0.9 mm with a geometric standard deviation of approximately 1.40. Particle size distribution of the bed materials are shown in Figures 3.1 and 3.2. To investigate the effect of abutment size, plexiglas vertical-wall abutment models with lengths of 12.5 cm, 10 cm, and 5 cm having a constant width of 20 cm were tested. Furthermore, two different types of wing-walls having acute angles of 45^o and 60^o were also tested. The bottom and side walls of the flume, except the test section, are made of concrete. Water is pumped from a storage tank having a capacity of 60 m^3 by means of a pump through a 30 cm-diameter steel pipe to an overhead water tank. Volumetric flow rate is measured via a manometer mounted to the side of the water supply tank. Discharge is controlled at the overhead tank by a valve. There was a small pool between the supplier water tank and the entrance of the flume to reduce the turbulence. Besides, two rows of brick block having holes were placed across the width of the flume to further dampen the flow disturbances at the entrance of the flume. A steel gate hinged at the bottom with an adjustable inclination was installed at the downstream end of the flume to control the flow depth. The flow then passes through a concrete ramp and enters the flume. Three movable point gages were mounted along the flume to measure the water stage and flow depth. These gages were also capable of measuring the bed elevation both along and across the flume as shown in Figure 3.3. A 7 m long, 1.25 m wide, and 40 cm deep test section was constructed and served as a test reach. This reach starts at 15 m from the entrance of the flume where fully-developed flow conditions prevail. The abutment models were set at the mid-length of the test section. One side of test section was composed of a 190 cm long plexiglass for enabling visual observations. Figure 3.3 shows a schematic view of the test reach, whereas Figure 3.4 presents a general view of the flume. The profile of the flume with the characteristic dimensions is presented in Figure 3.5.

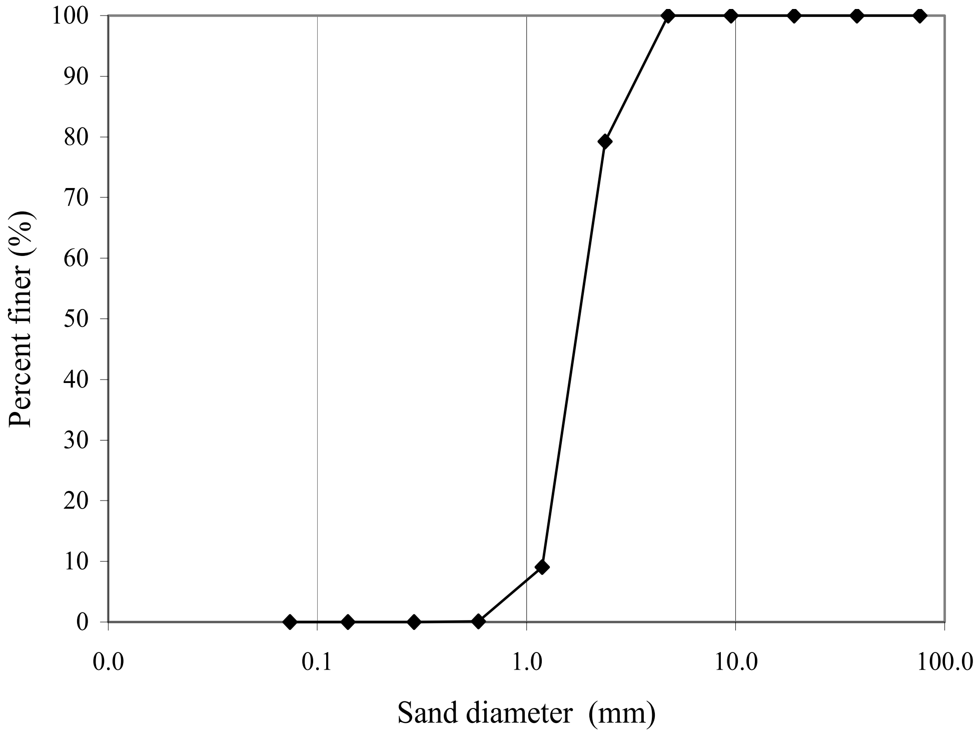

Figure 3.1. Particle size distribution of the first bed material

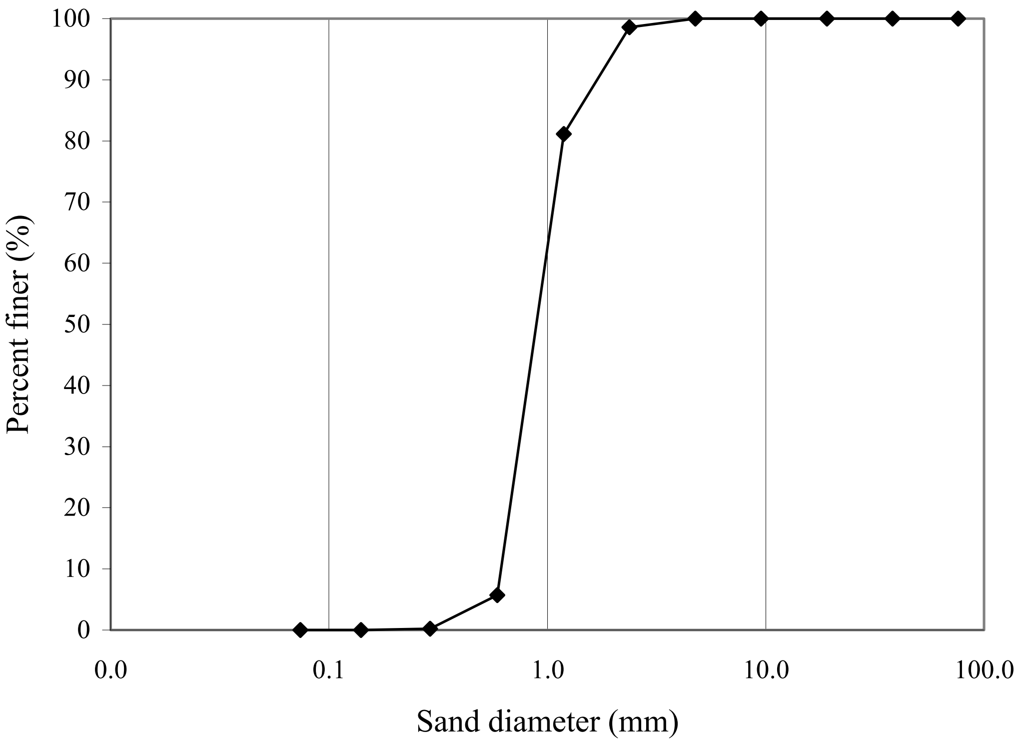

Figure 3.2. Particle size distribution of the second bed material

Figure 3.3. Measurement equipment for taking scour hole coordinates

Figure 3.4. A general view of the flume

As stated before, five types of abutments made of plexiglas were used in the experiments. Abutments were fixed to the side of the wall by a sliding mechanism. Top surfaces of the abutments were kept open to facilitate the necessary measurements from the interior of the model. Details of scour measurements will be given in the subsequent sections.

3.2. Preliminary Studies

An overhead water tank provided the necessary energy and water supply to the flume. Flow rate in the flume was measured by a pre-calibrated sharp-crested rectangular weir having a width of 100 cm. The static water column was measured by a vernier scale. Once the experiment was started, differential head was measured and the desired discharge was obtained by regulating the valve in the main pipeline. The maximum capacity of the system is 150 lt/s. However, only a certain range of this capacity was utilized to maintain clear water conditions in the flume.

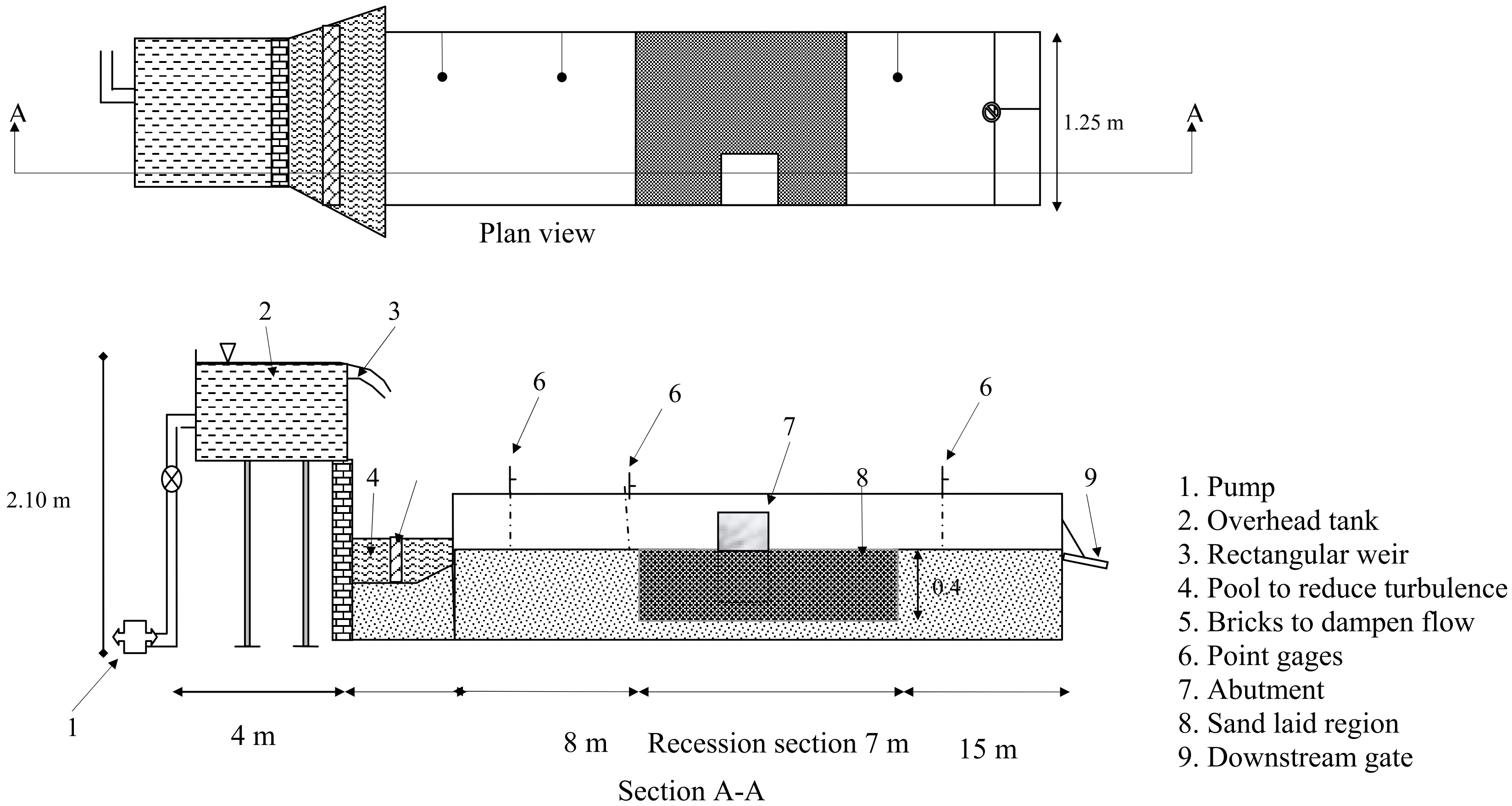

Figure 3. 5. Test flume (Not to scale)

3.2.1. Determination of Normal Depth

Studies concerning calibration of the channel and determination of the normal depth were carried out prior to the placement of the abutments in the test section. The elevations of the water surface above the channel bed level at each observation point were recorded. Along the channel, three vernier point gages were mounted to the side of the channel wall and the flow depths were measured. The normal depth for a particular discharge was computed by taking the mean of these readings. Tailwater gate was adjusted such that the readings of flow depths at the fixed locations of the point gages were almost the same with an error of approximately ±3 mm. Once the normal depths had been measured for different discharges, the roughness coefficient of the channel was determined by using Manning's formula, $n = (1/Q_f)AR_h^{2/3}S_o^{0.5}$, where n is Manning's roughness coefficient, Q_f is discharge in m^3/s, A is the cross-sectional area of the flow in m^2, R_h is the hydraulic radius in m, and S_o is the channel slope. Manning's roughness coefficient was then calculated as 0.014. The average Manning roughness coefficient for two bed materials was computed as 0.0138 using Strickler's equation. Therefore, n=0.014 is accepted to be the representative value for the flume. With the findings of this analysis, the rating curve of the flume was obtained as shown in Figure 3.6 in which y is the average normal depth in the flume.

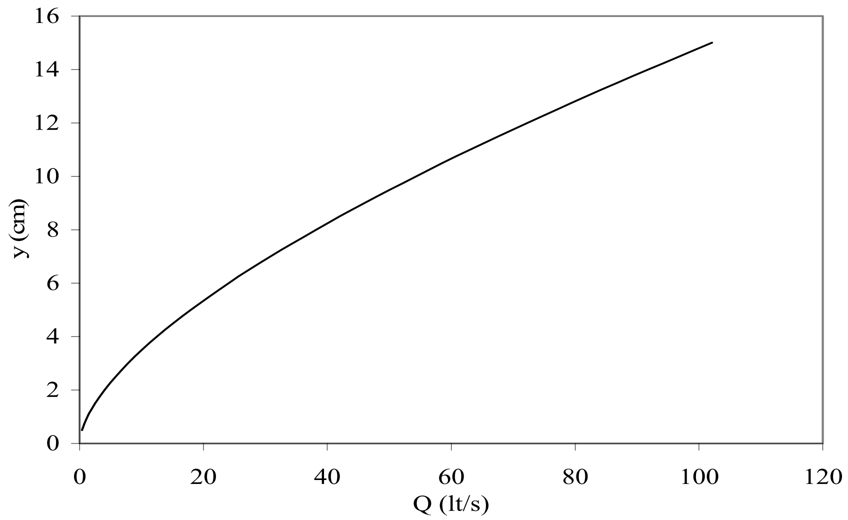

Figure 3.6. Rating curve of the channel

3.2.2. Measurement of Scour Depths and Contours

The scope of the experiments is presented in Table 3.1 in which u_* is the shear velocity of the approach flow, u_{*c} is the critical shear velocity for sediment threshold, F_r is the Froude number of the approach flow, F_d is the densimetric particle Froude number $(u/(\Delta g D_{50})^{0.5})$, and the other terms are the same as previously defined. Table 3.2 presents information on experiments carried out for scour contour measurements. Most of the experiments were carried out using the coarser bed material, i.e. D_{50}=1.8 mm to maintain clear water conditions for a wider range of flow depths. The geometric standard deviation of the bed materials, $\sigma_g=(D_{84}/D_{16})^{0.5}$, was relatively small, i.e. approximately 1.40. As mentioned before, the bed materials were placed as a 40 cm thick layer in the flume bed with a slope of 0.001. The bed material of the flume was flattened before each run and the flume was filled up with water issued gently from a hose at a low rate without causing any disturbance to the bed material. When the required depth of flow was achieved in the flume, the upstream valve of the flume and the tail gate were adjusted slowly to obtain the desired rate of flow.

The permissible upper limit of mean flow velocity was decided such that no sediment inflow was allowed from the upstream under clear water conditions. Since the bed materials used in the experiments were almost uniform, then Shields criterion was used to determine the critical shear velocities, u_{*c}. Visual observations on threshold conditions were also noted. The corresponding mean threshold velocities, u_c, are calculated using the logarithmic average velocity equation for a rough bed (Lauchlan and Melville, 2001; Dey and Barbhuiya, 2005)

$$\frac{u_c}{u_{*c}} = 5.75 \log \frac{y}{k_s} + 6.0 \tag{3.1}$$

where k_s is equivalent roughness height, which can be taken as $2D_{50}$ for plane bed under clear water conditions.

Table 3.1. Scope of Experiment

Exp.No:	D_{50}	L	Q_f	y	d_s	u_*	u_{*c}	u	F_r	u_c	u/u_c	F_d
	mm	cm	lt/s	cm	cm	m/s	m/s	m/s		m/s		
1	1.80	12.50	45	8.91	12.60	0.028	0.029	0.40	0.43	0.52	0.77	2.34
2	1.80	12.50	40	8.30	12.30	0.027	0.029	0.39	0.43	0.51	0.75	2.28
3	1.80	12.50	35	7.50	12.10	0.026	0.029	0.37	0.43	0.50	0.74	2.16
4	1.80	12.50	30	6.80	11.60	0.025	0.029	0.35	0.43	0.49	0.71	2.05
5	1.80	12.50	25	6.06	10.50	0.023	0.029	0.33	0.43	0.48	0.68	1.93
6	1.80	12.50	20	5.20	7.40	0.022	0.029	0.31	0.42	0.47	0.65	1.75
7	1.80	12.50	15	4.40	4.50	0.020	0.029	0.27	0.41	0.45	0.6	1.58
(8-12)	Measurements for contour lines of scour hole, L=12.5 cm, Vertical-wall											
13	1.80	10.00	45	8.91	12.10	0.028	0.029	0.40	0.43	0.52	0.77	2.34
14	1.80	10.00	40	8.30	11.50	0.027	0.029	0.39	0.43	0.51	0.75	2.28
15	1.80	10.00	35	7.50	10.90	0.026	0.029	0.37	0.43	0.50	0.74	2.16
16	1.80	10.00	30	6.80	9.70	0.025	0.029	0.35	0.43	0.49	0.71	2.05
17	1.80	10.00	25	6.06	7.70	0.023	0.029	0.33	0.43	0.48	0.68	1.93
18	1.80	10.00	20	5.20	5.00	0.022	0.029	0.31	0.42	0.47	0.65	1.75
19	1.80	10.00	15	4.40	2.80	0.020	0.029	0.27	0.41	0.45	0.6	1.58
(20-24)	Measurements for contour lines of scour hole, L= 10 cm, Vertical wall											
25	1.80	5.00	45	8.91	8.30	0.028	0.029	0.40	0.43	0.52	0.77	2.34
26	1.80	5.00	40	8.30	7.20	0.027	0.029	0.39	0.43	0.51	0.75	2.28
27	1.80	5.00	35	7.50	6.20	0.026	0.029	0.37	0.43	0.50	0.74	2.16
28	1.80	5.00	30	6.80	5.40	0.025	0.029	0.35	0.43	0.49	0.71	2.05
29	1.80	5.00	25	6.06	4.60	0.023	0.029	0.33	0.43	0.48	0.68	1.93
30	1.80	5.00	20	5.20	3.00	0.022	0.029	0.31	0.42	0.47	0.65	1.75
31	1.80	5.00	15	4.40	1.70	0.020	0.029	0.27	0.41	0.45	0.6	1.58
(32-36)	Measurements for contour lines of scour hole, L= 5 cm, Vertical wall											
37	1.80	5 (45^0)	45	8.91	4.50	0.028	0.029	0.40	0.43	0.52	0.77	2.34
38	1.80	5 (45^0)	40	8.30	3.30	0.027	0.029	0.39	0.43	0.51	0.75	2.28
39	1.80	5 (45^0)	35	7.50	2.10	0.026	0.029	0.37	0.43	0.50	0.74	2.16
40	1.80	5 (45^0)	30	6.80	1.70	0.025	0.029	0.35	0.43	0.49	0.71	2.05
41	1.80	5 (45^0)	25	6.06	0.80	0.023	0.029	0.33	0.43	0.48	0.68	1.93
42	1.80	5 (45^0)	20	5.20	0.40	0.022	0.029	0.31	0.42	0.47	0.65	1.75
43	1.80	5 (45^0)	15	4.40	0.20	0.020	0.029	0.27	0.41	0.45	0.6	1.58
(44-48)	Measurements for contour lines of scour hole, Wing-wall (45^o)											
49	1.80	8.6 (60^0)	45	8.91	9.30	0.028	0.029	0.40	0.43	0.52	0.77	2.34
50	1.80	8.6 (60^0)	40	8.30	7.60	0.027	0.029	0.39	0.43	0.51	0.75	2.28
51	1.80	8.6 (60^0)	35	7.50	6.10	0.026	0.029	0.37	0.43	0.50	0.74	2.16
52	1.80	8.6 (60^0)	30	6.80	4.10	0.025	0.029	0.35	0.43	0.49	0.71	2.05
53	1.80	8.6 (60^0)	25	6.06	3.20	0.023	0.029	0.33	0.43	0.48	0.68	1.93
54	1.80	8.6 (60^0)	20	5.20	2.30	0.022	0.029	0.31	0.42	0.47	0.65	1.75
55	1.80	8.6 (60^0)	15	4.40	1.90	0.020	0.029	0.27	0.41	0.45	0.6	1.58
(56-60)	Measurements for contour lines of scour hole, Wing-wall (60^o)											
61	0.90	12.50	20	5.20	9.50	0.022	0.019	0.31	0.43	0.32	0.98	3.56
62	0.90	12.50	15	4.40	6.50	0.020	0.019	0.27	0.42	0.30	0.89	3.39
63	0.90	12.50	10	3.30	3.50	0.018	0.019	0.24	0.42	0.29	0.84	2.40
64	0.90	10.00	20	5.20	9.00	0.022	0.019	0.31	0.43	0.32	0.98	3.56
65	0.90	10.00	15	4.40	6.29	0.020	0.019	0.27	0.42	0.30	0.89	3.39
66	0.90	10.00	10	3.30	2.80	0.018	0.019	0.24	0.42	0.29	0.84	2.40
67	0.90	5.00	20	5.20	6.20	0.022	0.019	0.31	0.43	0.32	0.98	3.56
68	0.90	5.00	15	4.40	4.10	0.020	0.019	0.27	0.42	0.30	0.89	3.39
69	0.90	5.00	10	3.30	2.20	0.018	0.019	0.24	0.42	0.29	0.84	2.40
70	0.90	5 (45^0)	20	5.20	2.40	0.022	0.019	0.31	0.43	0.32	0.98	3.56
71	0.90	5 (45^0)	15	4.40	1.80	0.020	0.019	0.27	0.42	0.30	0.89	3.39
72	0.90	5 (45^0)	10	3.30	1.30	0.018	0.019	0.24	0.42	0.29	0.84	2.40
(73-77)	Measurements for contour lines of scour hole, Wing-wall (45^o)											
78	0.90	8.6 (60^0)	20	5.20	4.80	0.022	0.019	0.31	0.43	0.32	0.98	3.56
79	0.90	8.6 (60^0)	15	4.40	2.60	0.020	0.019	0.27	0.42	0.30	0.89	3.39
80	0.90	8.6 (60^0)	10	3.30	2.30	0.018	0.019	0.24	0.42	0.29	0.84	2.40
(81-85)	Measurements for contour lines of scour hole, Wing-wall (60^o)											

Table.3.2. Scope of Experiments Carried out for Scour Contour Measurements

Experiment No	L (cm)	D_{50} (mm)	u/u_c	y (cm)	t_m (min)
8	12.5 (Vertical-wall)	1.8	0.777	8.9	5
9	12.5 (Vertical-wall)	1.8	0.777	8.9	20
10	12.5 (Vertical-wall)	1.8	0.777	8.9	60
11	12.5 (Vertical-wall)	1.8	0.777	8.9	100
12	12.5 (Vertical-wall)	1.8	0.777	8.9	150
20	10 (Vertical-wall)	1.8	0.777	8.9	5
21	10 (Vertical-wall)	1.8	0.777	8.9	20
22	10 (Vertical-wall)	1.8	0.777	8.9	60
23	10 (Vertical-wall)	1.8	0.777	8.9	100
24	10 (Vertical-wall)	1.8	0.777	8.9	150
32	5 (Vertical-wall)	1.8	0.777	8.9	5
33	5 (Vertical-wall)	1.8	0.777	8.9	20
34	5 (Vertical-wall)	1.8	0.777	8.9	60
35	5 (Vertical-wall)	1.8	0.777	8.9	100
36	5 (Vertical-wall)	1.8	0.777	8.9	150
44	5 (45^o Wing-wall)	1.8	0.777	8.9	5
45	5 (45^o Wing-wall)	1.8	0.777	8.9	20
46	5 (45^o Wing-wall)	1.8	0.777	8.9	60
47	5 (45^o Wing-wall)	1.8	0.777	8.9	100
48	5 (45^o Wing-wall)	1.8	0.777	8.9	150
56	8.6 (60^o Wing-wall)	1.8	0.777	8.9	5
57	8.6 (60^o Wing-wall)	1.8	0.777	8.9	20
58	8.6 (60^o Wing-wall)	1.8	0.777	8.9	60
59	8.6 (60^o Wing-wall)	1.8	0.777	8.9	100
60	8.6 (60^o Wing-wall)	1.8	0.777	8.9	150
73	5 (45^o Wing-wall)	0.9	0.985	5.2	5
74	5 (45^o Wing-wall)	0.9	0.985	5.2	20
75	5 (45^o Wing-wall)	0.9	0.985	5.2	60
76	5 (45^o Wing-wall)	0.9	0.985	5.2	100
77	5 (45^o Wing-wall)	0.9	0.985	5.2	150
81	8.6 (60^o Wing-wall)	0.9	0.985	5.2	5
82	8.6 (60^o Wing-wall)	0.9	0.985	5.2	20
83	8.6 (60^o Wing-wall)	0.9	0.985	5.2	60
84	8.6 (60^o Wing-wall)	0.9	0.985	5.2	100
85	8.6 (60^o Wing-wall)	0.9	0.985	5.2	150

In the experiments, the maximum scour depths around the abutments, d_s, were measured against time t, relative to the initial bed level using a number of vertical scales attached to the interior of the abutment with a stick having a small inclined mirror at its end. The measurements were conducted at various sections using these scales to collect information along the faces of the abutment. To overcome some visual observational difficulties, which may arise due to the mounding up of the sediment against the abutment wall, repeated measurements were performed. The measured data to be used in the model development are presented in dimensionless format in Figures 3.7 through 3.16 relating $S=d_s/L$ to t/t_m, where t is the time and t_m is the maximum duration of an experiment. During the course of the experiments, it was observed that the maximum scour depths occurred around the upstream corner of the abutment, whereas the rear face of the abutment was subject to accretion. It was also observed for small flow depths and small abutment lengths that equilibrium scour depths reached shortly.

As indicated before, a very long duration, t_e, is required to reach the equilibrium state under clear water conditions. The order of magnitude of t_e for the experimental data used in this study can be computed from Equations (2.8) and (2.9) for vertical-wall abutments. The results changed from 0.78 to 7.30 days. Considering a length scale of practical interest, e.g. 1:50 in Froude modeling, the corresponding prototype flood durations may range between 132 and 1239 hours, which are unrealistically long and, therefore, out of practical interest for most small to medium sized watersheds. Most prototype flood durations commonly confronted may normally be shorter than such durations needed to reach equilibrium under clear water conditions. On the other hand, live bed conditions are expected after a threshold value during the rising stage of hydrographs having relatively long base times. Hence conduction of laboratory experiments with relatively shorter durations than needed to reach equilibrium conditions may be considered sufficient. Considering physical limitations in laboratory conditions e.g. preparation of the experimental setup, operation of the pumps and appurtenant equipment as well as measurement of relevant data, the maximum test duration of an experiment, t_m, was limited by six hours during which the final equilibrium scour depths were not achieved although the rate of scour decelerated to smaller values for all experiments. This duration corresponds to 42 hours of flood duration according to the aforementioned length scale, i.e. 1:50.

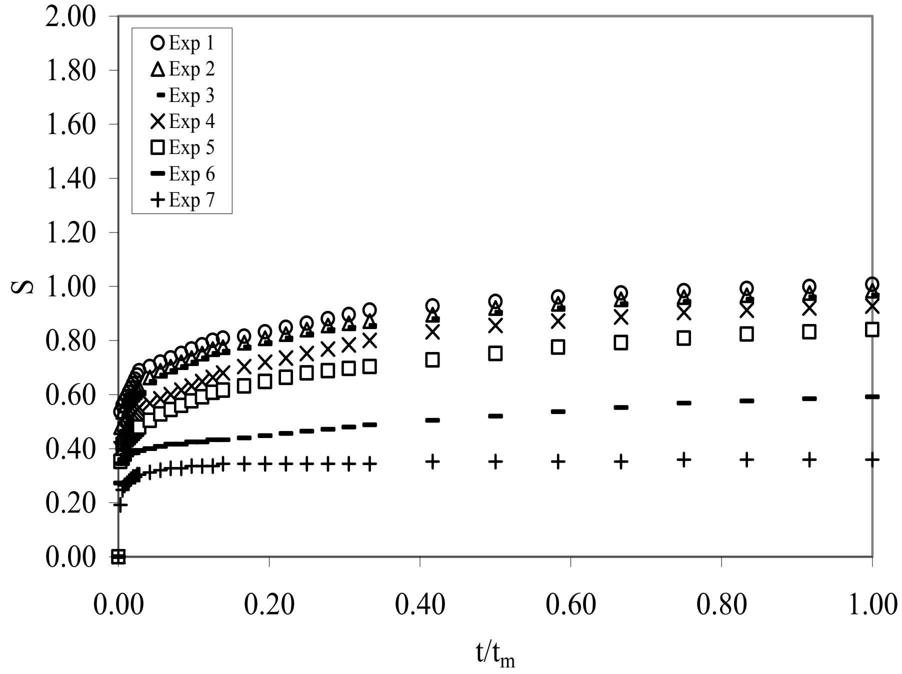

Figure 3.7. Temporal variation of scour depths for Experiments 1-7

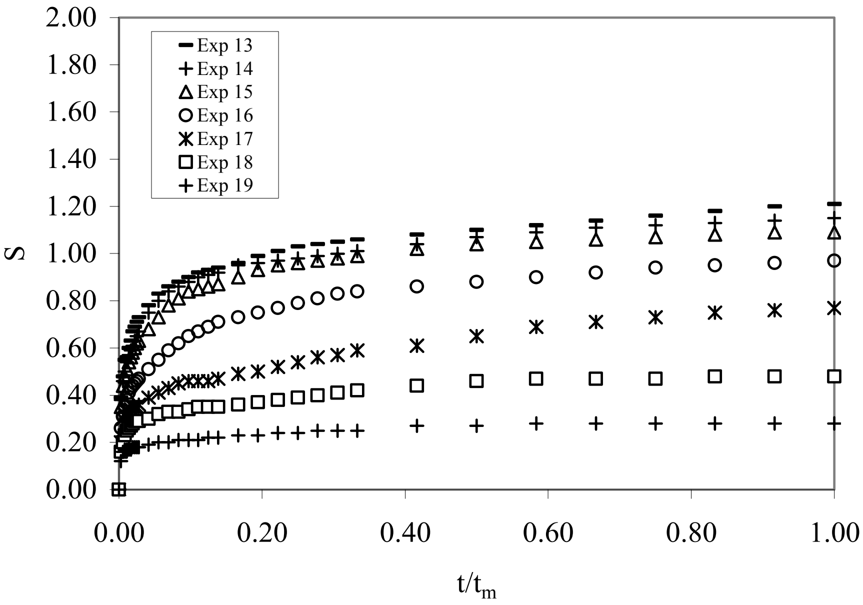

Figure 3.8. Temporal variation of scour depths for Experiments 13-19

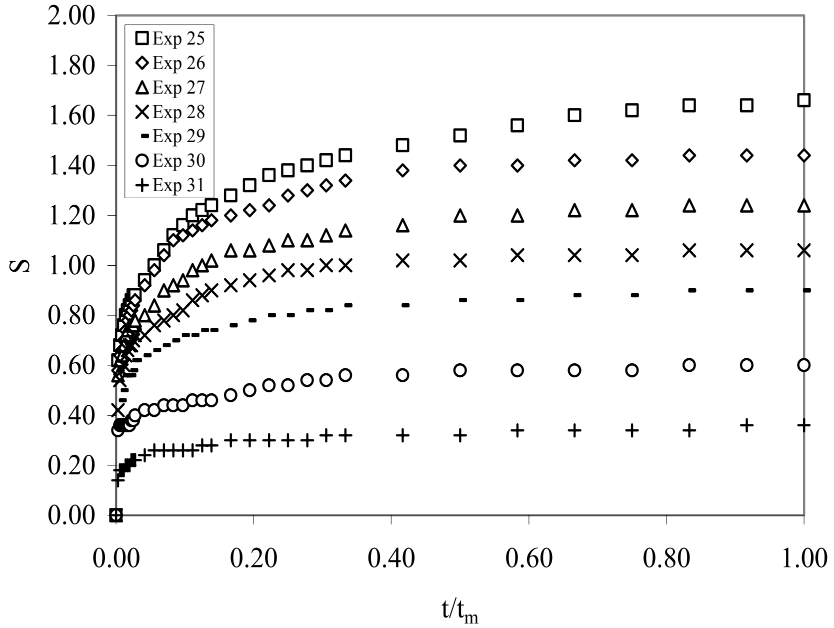

Figure 3.9. Temporal variation of scour depths for Experiments 25-31

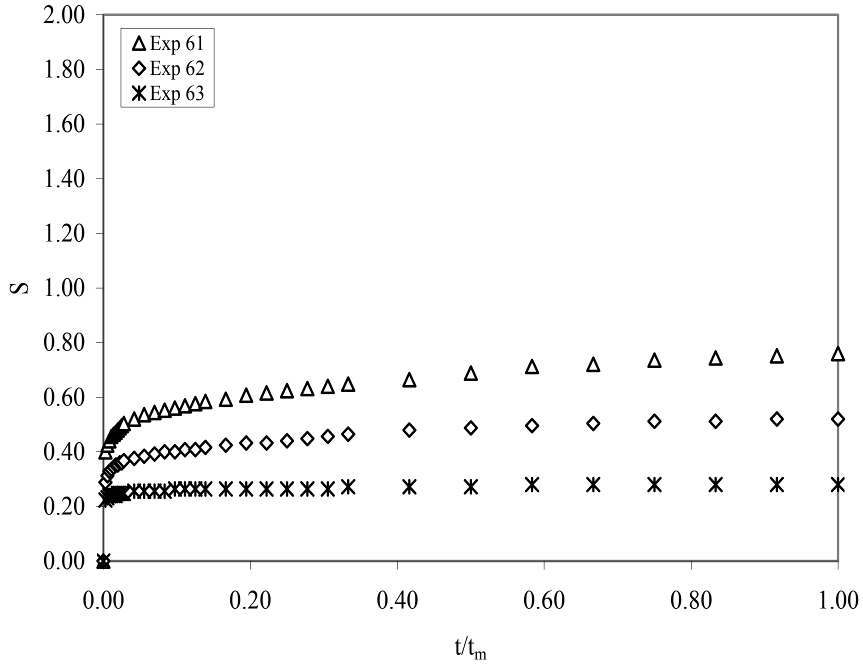

Figure 3.10. Temporal variation of scour depths for Experiments 61-63

.

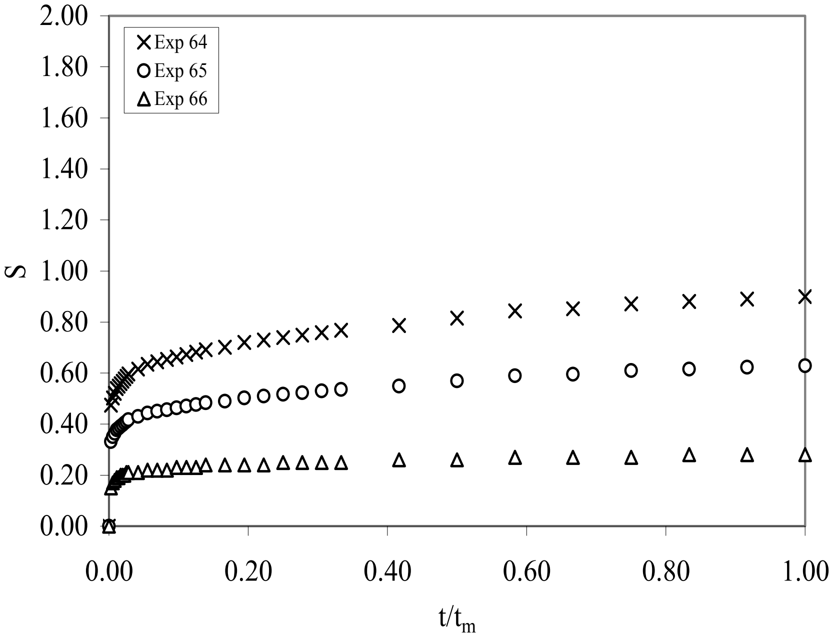

Figure 3.11. Temporal variation of scour depths for Experiments 64-66

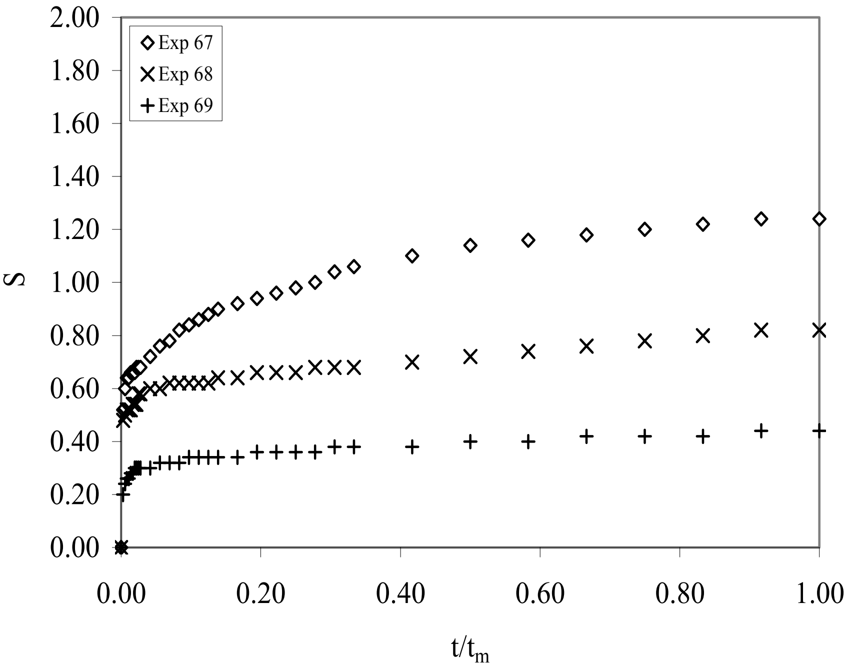

Figure 3.12. Temporal variation of scour depths for Experiments 67-69

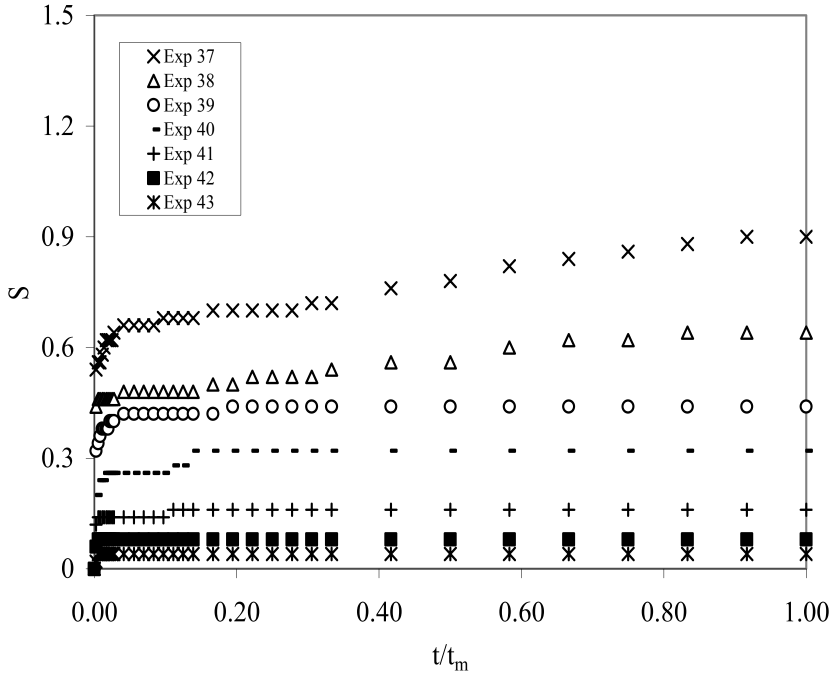

Figure 3.13. Temporal variation of scour depths for Experiments 37-43

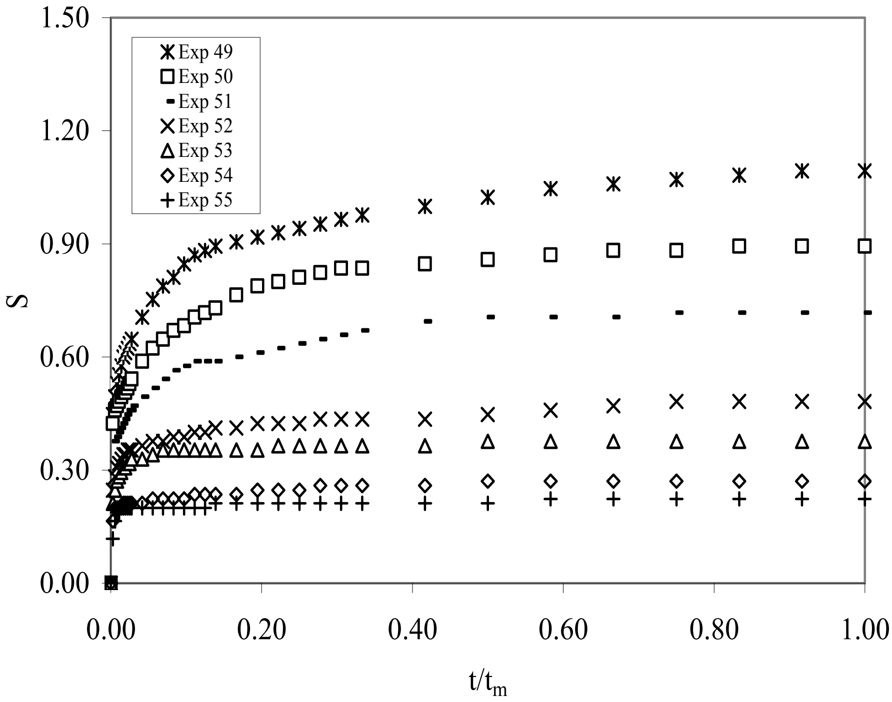

Figure 3.14. Temporal variation of scour depths for Experiments 49-55

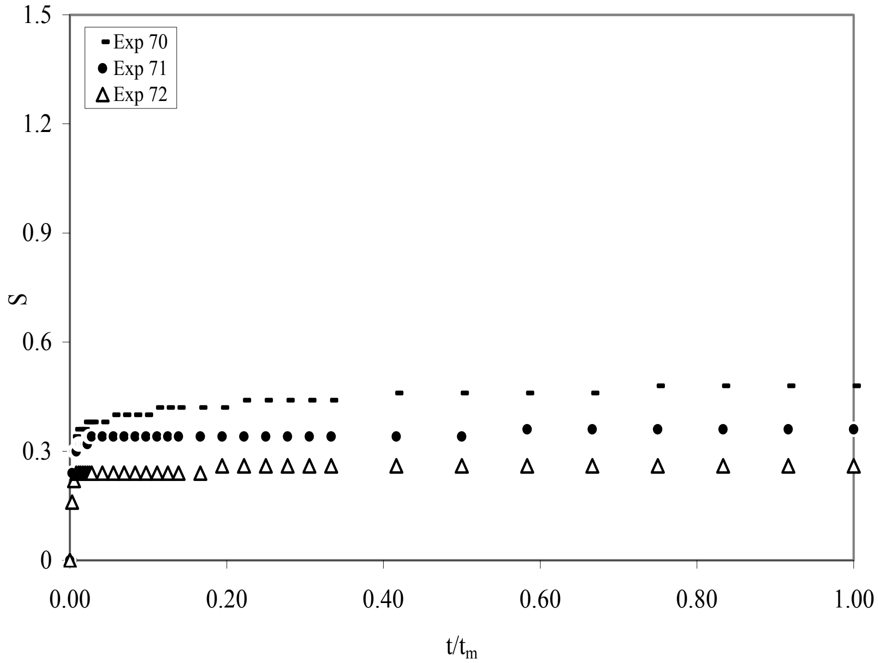

Figure 3.15. Temporal variation of scour depths for Experiments 70-72

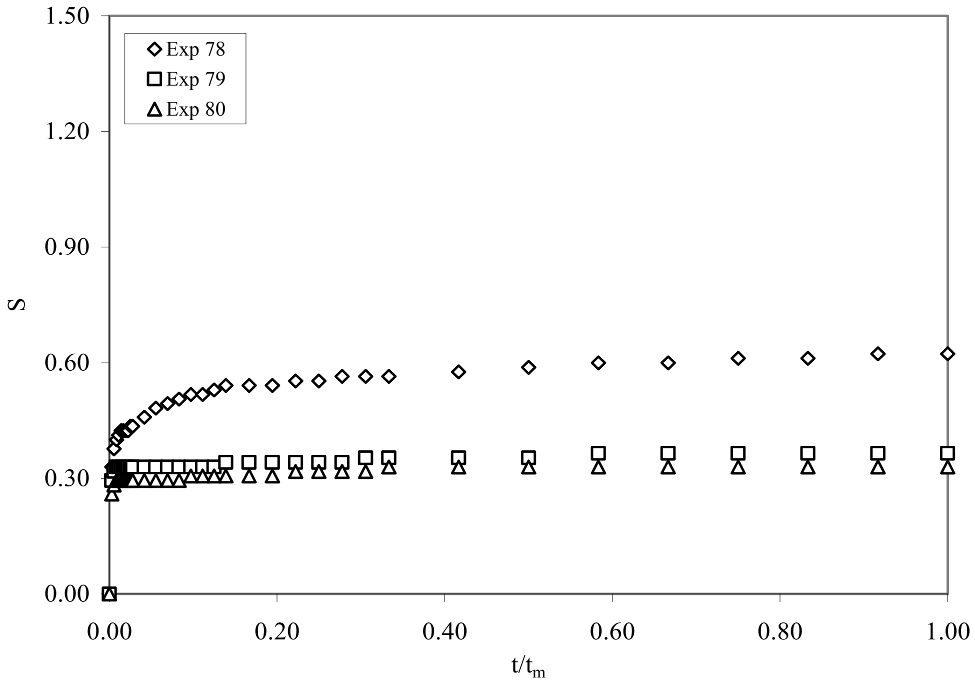

Figure 3.16. Temporal variation of scour depths for Experiments 78-80

The principal observations during the course of the experiments are summarized below. Detailed discussion will be presented in Chapter 4 which gives further analysis of the experimental results.

a) The depths of scour around vertical-wall abutments are found to be greater than those of wing-wall abutments. This is mainly due to stronger separation of flow at the upstream corner of the vertical-wall abutment, which lead to greater zone for the development of primary vortices. Once eroded particles are carried by the flow in the downstream direction, they are deposited in the dead zone behind the abutment where the velocities are very small.

b) In wing-wall abutments, the depth of scour increases when the acute angle, which is the angle between side inclination of the abutment and the horizontal, increases since small acute angles exhibit less disturbance to the flow in close vicinity to the upstream corner of the abutment.

c) All scour hole contour plots demonstrate that the scour hole is geometrically similar under steady flow conditions. Also scour hole preserves its geometric shape throughout its development.

d) The slope of the scour hole in the upstream direction is steeper than the slope in the downstream direction. The value of the slope angle in the upstream direction is very close to natural angle of repose of the sediment. The distance between the scour hole depth and top of the accumulated sand bar decreases as the abutment length decreases.

In the development of the semi-empirical model for temporal variation of scour around vertical-wall abutments, which will be presented in Chapter 5, an expression giving the volume of scour hole around the abutment model is needed. To this end, sequential experiments were performed under a densimetric particle Froude number (based on shear velocity of approach flow) of $N=u_*/(\Delta g D_{50})^{0.5}=0.164$ using

D_{50}=1.8 mm to determine time-dependent volume expression of scour holes around the vertical-wall abutments. These experiments were performed using both abutment sizes, i.e. L=12.5 cm (Experiments 8 through 12) and L=10 cm (Experiments 20 through 24). Experiments were stopped at the end of different test durations; namely 5, 20, 60, 100, and 150 min to determine the contours of the scour hole around abutment models using point gages. A coordinate system was placed at the mid-width of the abutment at the original bed level (See Figure 3.17). The coordinate-x' is along the flow direction, whereas the coordinate-y' is across the flume. The z'-coordinate is in the downward direction.

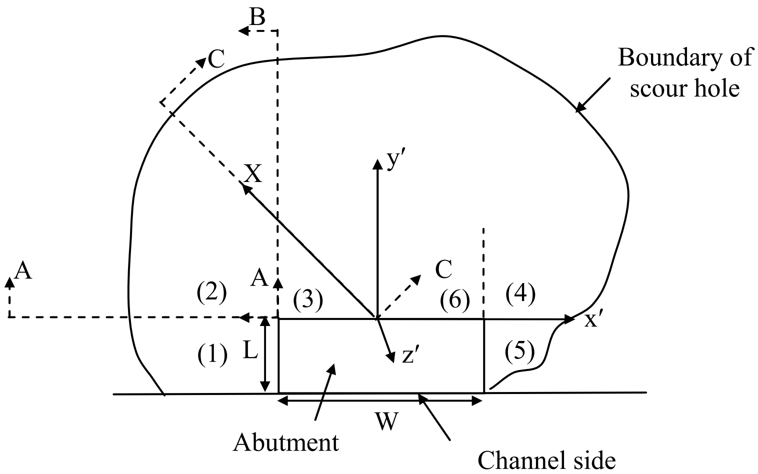

Figure 3.17. Coordinate system of scour hole

At the end of an experiment, water was removed gently from the channel not to disturb the bed topography and measurements were carried out in a grid system around the abutment composed of joints separated by 2 cm intervals along and across the channel according to the aforementioned coordinate system. However, abrupt local changes in bed topography were also measured by taking the data in smaller meshes. After each run, the bed was flattened to run the experiment with the next duration. Scour contours measured at the end of the specified test durations are presented in Figures 3.18 through 3.52.

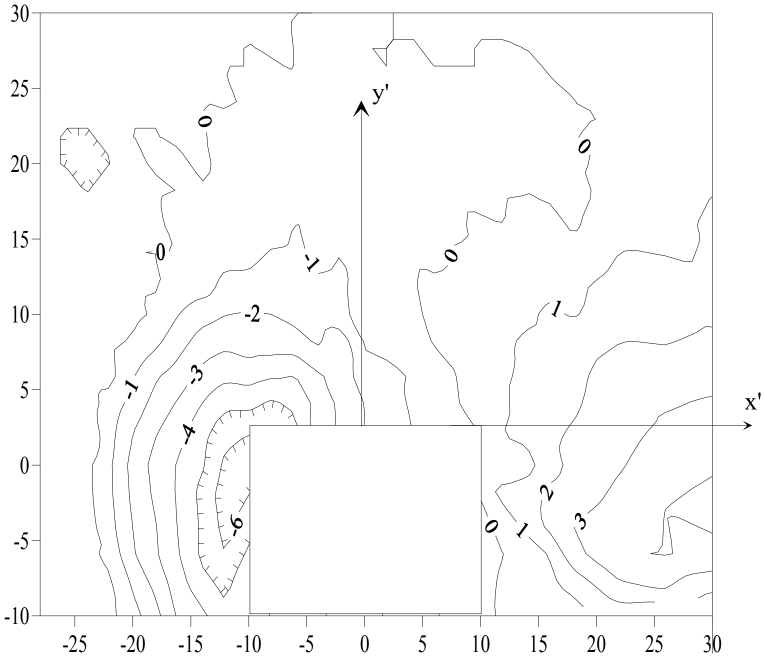

Figure 3.18. Scour hole contours in cm (Experiment No: 8, t = 5 min)

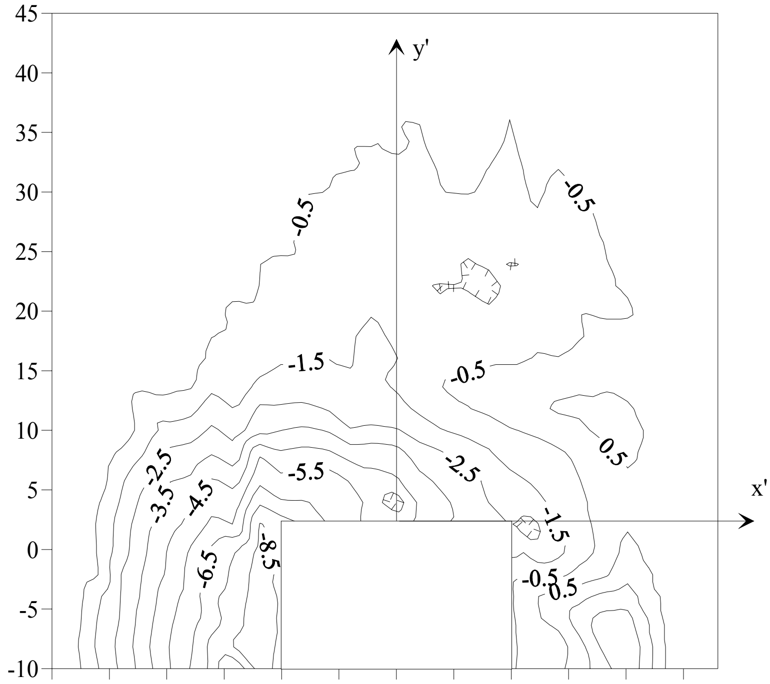

Figure 3.19. Scour hole contours in cm (Experiment No: 9, t = 20 min)

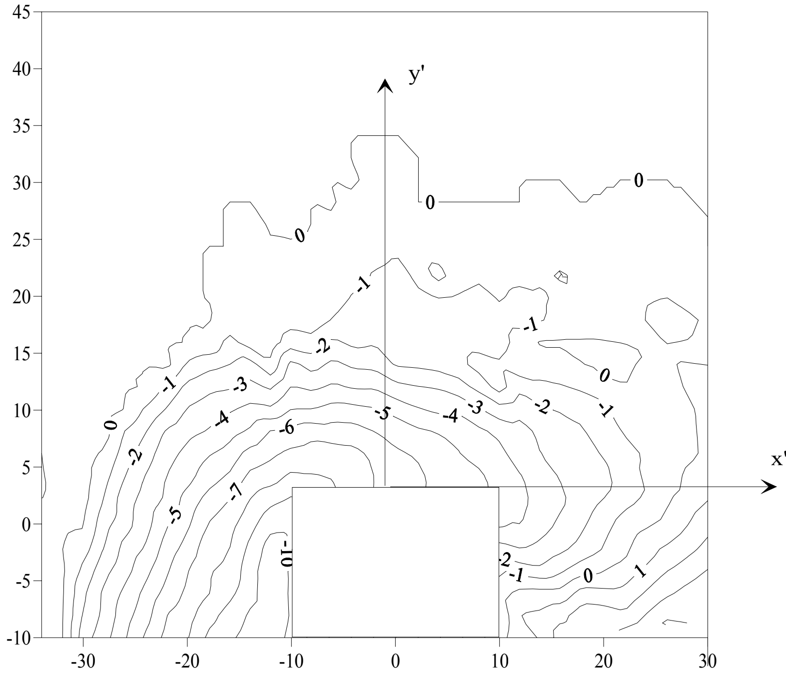

Figure 3.20. Scour hole contours in cm (Experiment No: 10, t = 60 min)

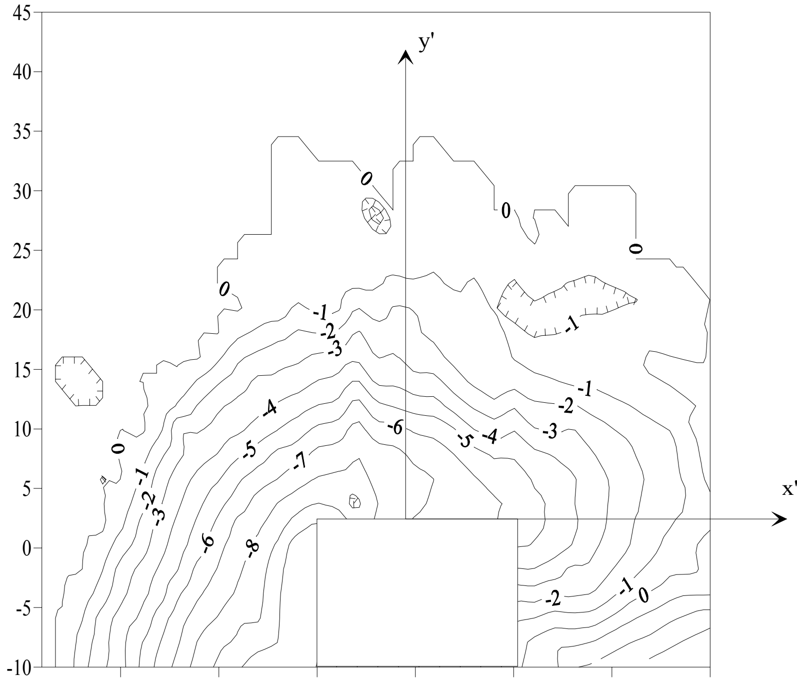

Figure 3.21. Scour hole contours in cm (Experiment No: 11, t = 100 min)

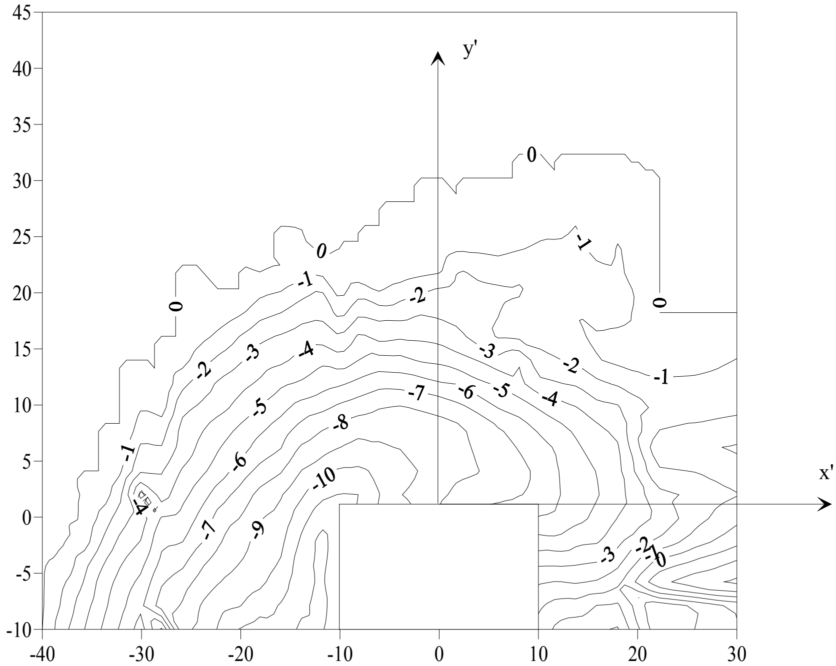

Figure 3.22. Scour hole contours in cm (Experiment. No: 12, t = 150 min)

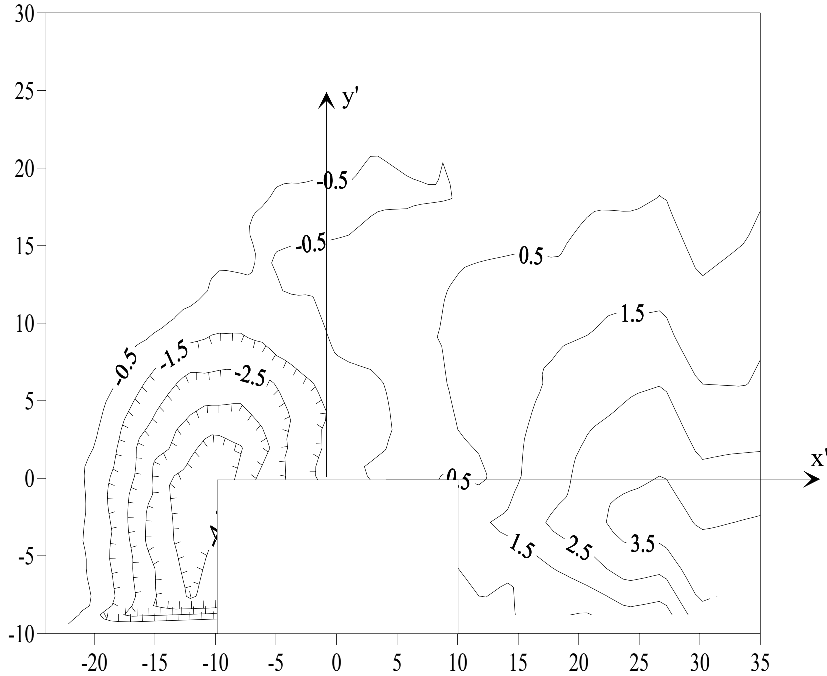

Figure 3.23. Scour hole contours in cm (Experiment No: 20, t = 5 min)

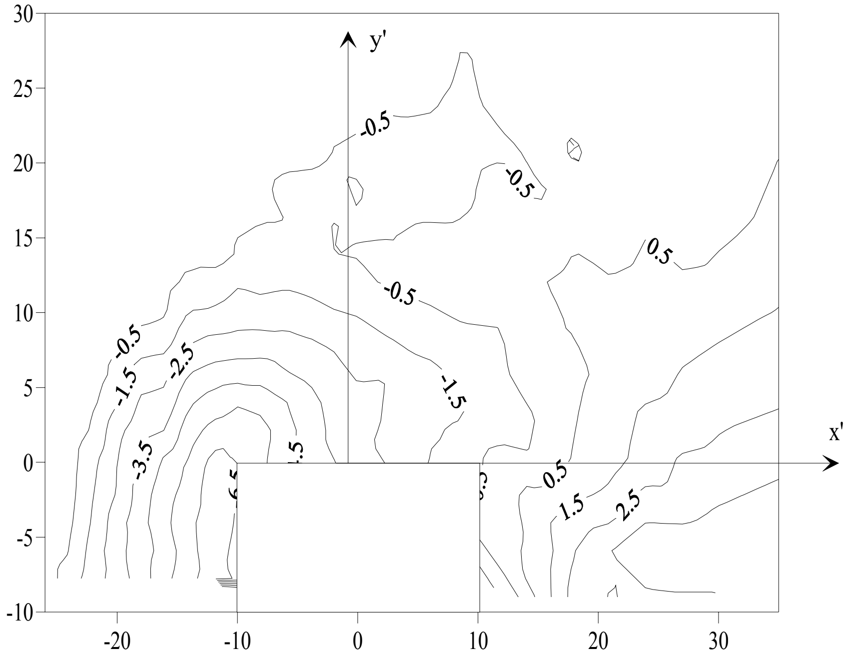

Figure 3.24. Scour hole contours in cm (Experiment No: 21, t = 20 min)

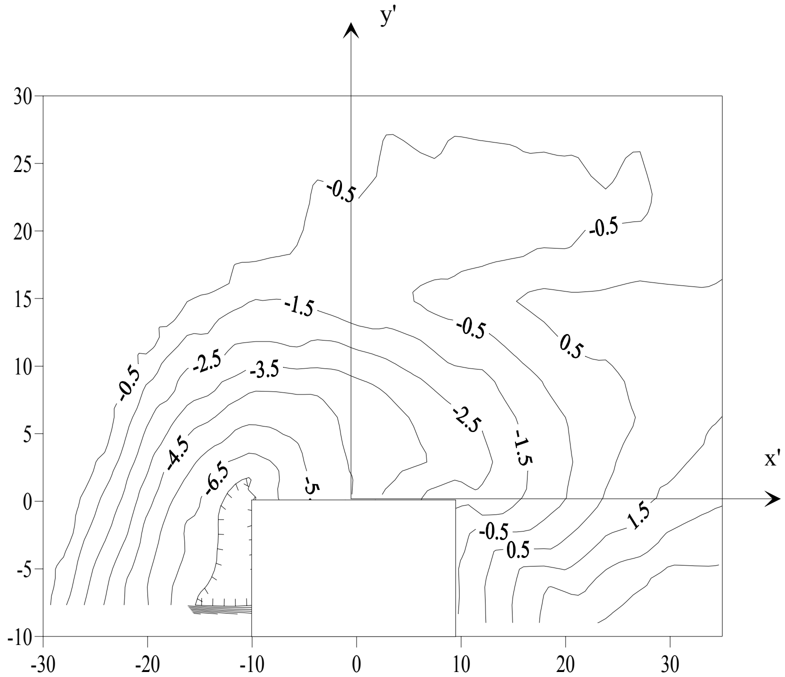

Figure 3.25. Scour Hole contours in cm (Experiment No: 22, t = 60 min)

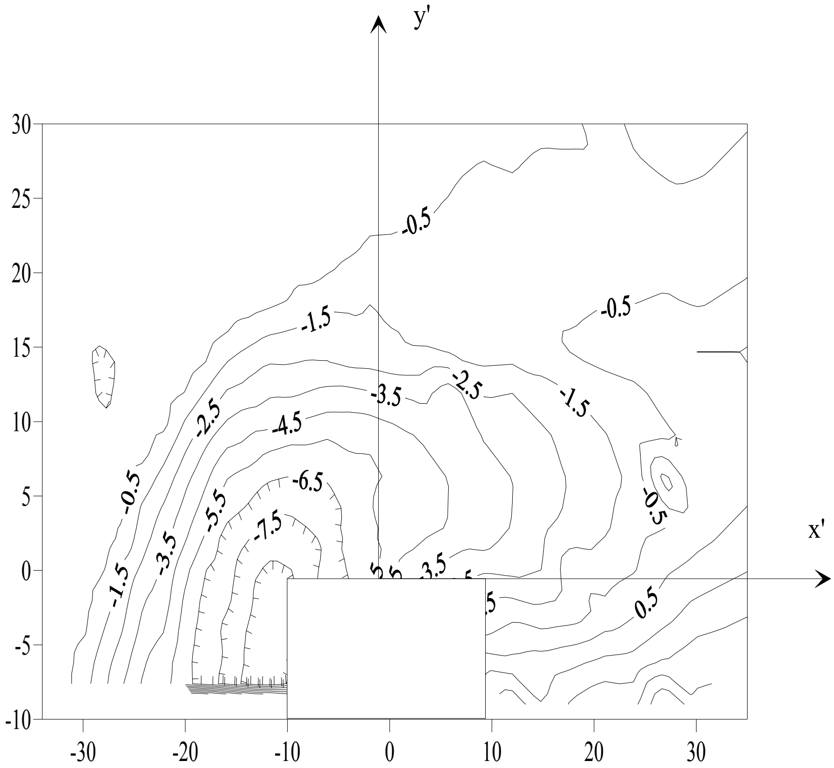

Figure 3.26. Scour hole contours in cm (Experiment No: 23, t = 100 min)

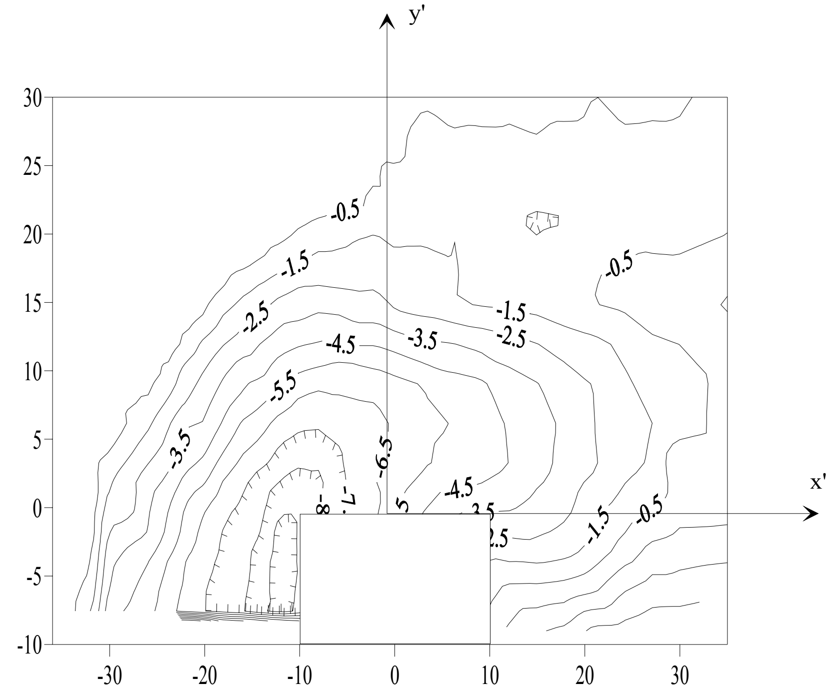

Figure 3.27. Scour hole contours in cm (Experiment No: 24, t = 150 min)

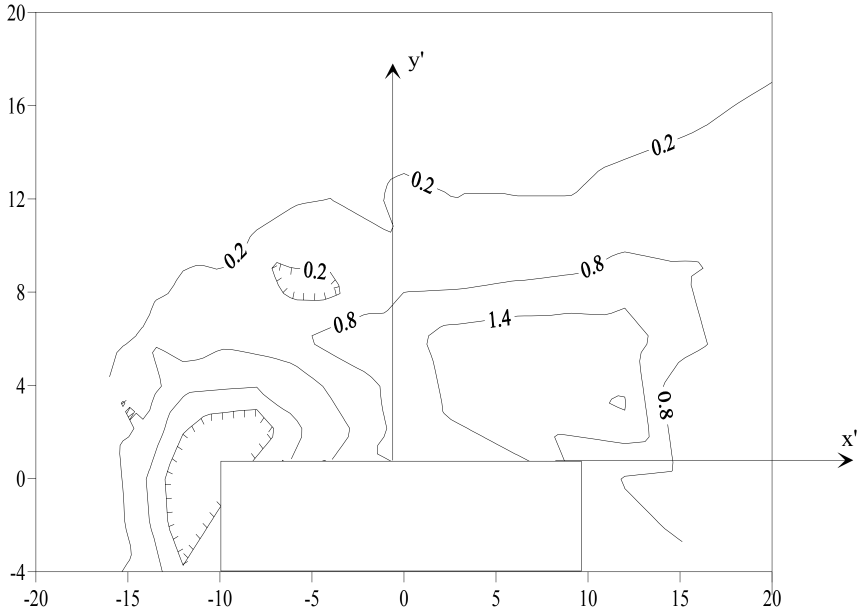

Figure 3.28. Scour hole contours in cm (Experiment No: 32, t = 5 min)

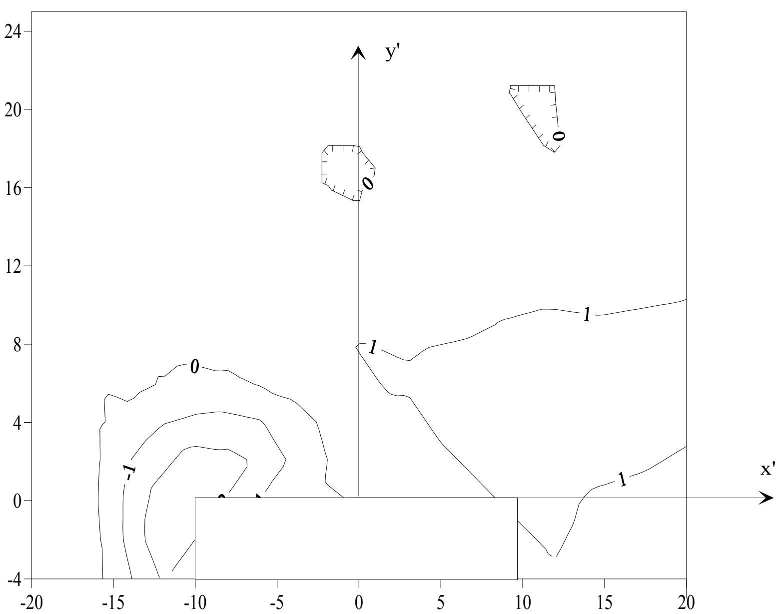

Figure 3.29. Scour hole contours in cm (Experiment No: 33, t = 20 min)

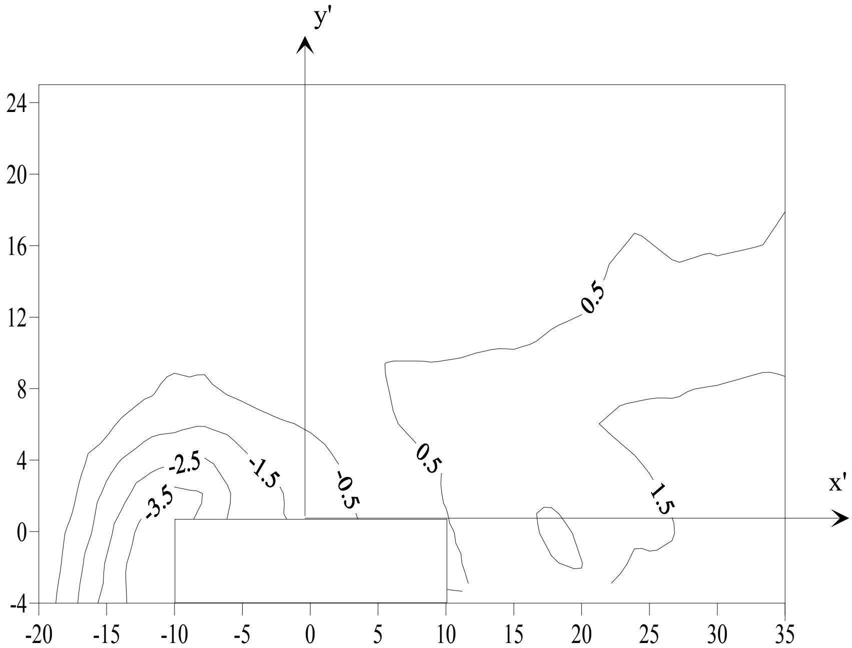

Figure 3.30. Scour hole contours in cm (Experiment No: 34, t = 60 min)

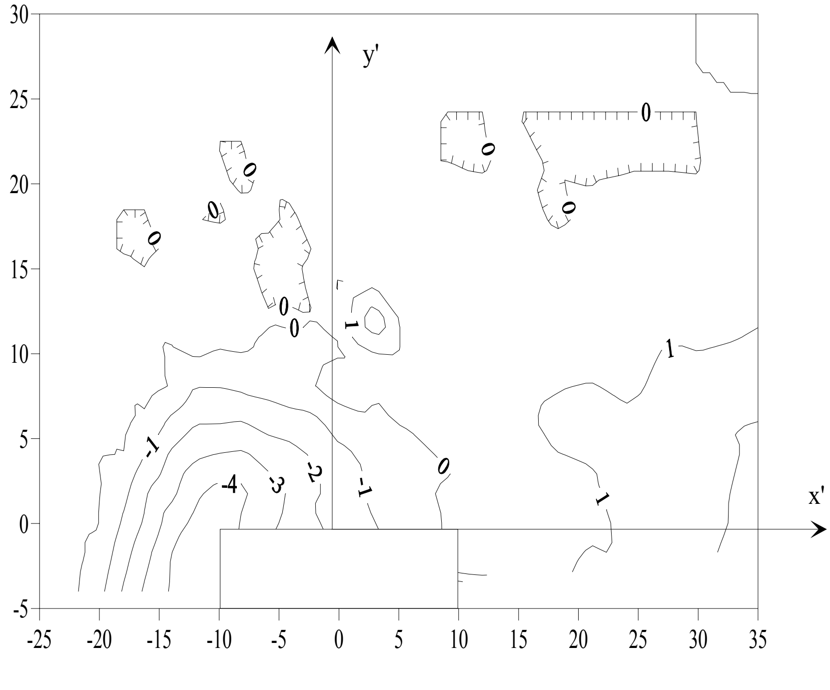

Figure 3.31. Scour hole contours in cm (Experiment No: 35, t = 100 min)

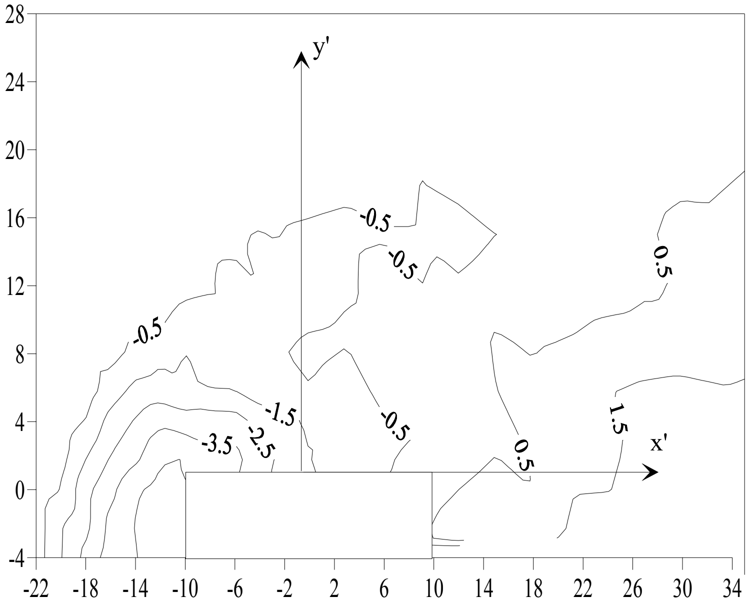

Figure 3.32. Scour hole contours in cm (Experiment No: 36, t = 150 min)

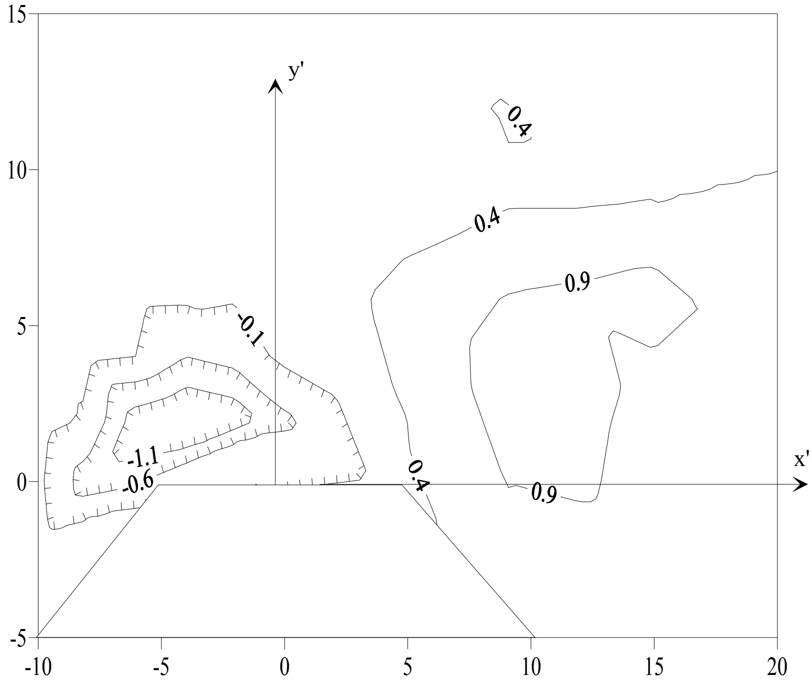

Figure 3.33. Scour hole contours in cm (Experiment No: 44, t = 5 min)

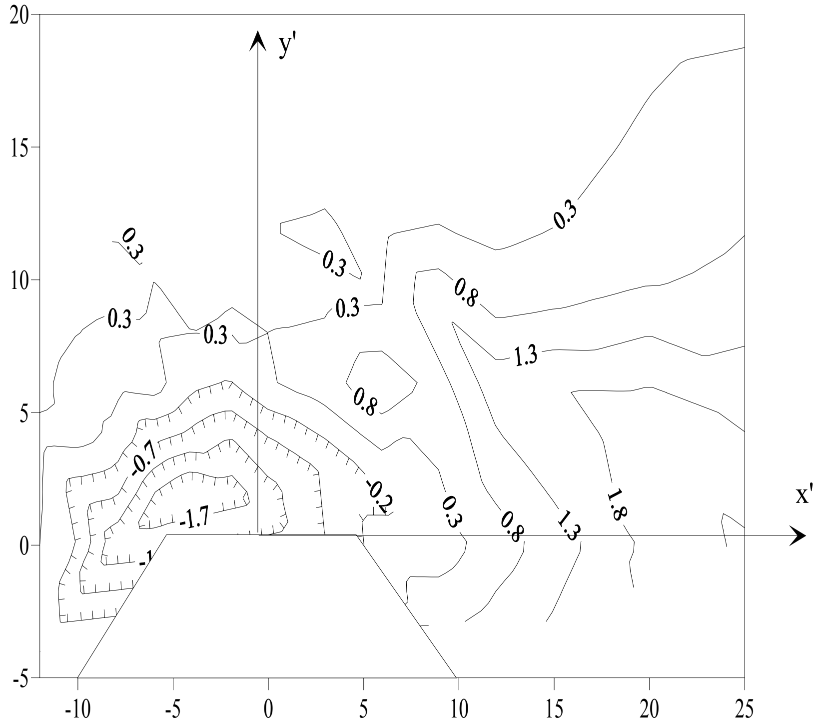

Figure 3.34. Scour hole contours in cm (Experiment No: 45, t = 20 min)

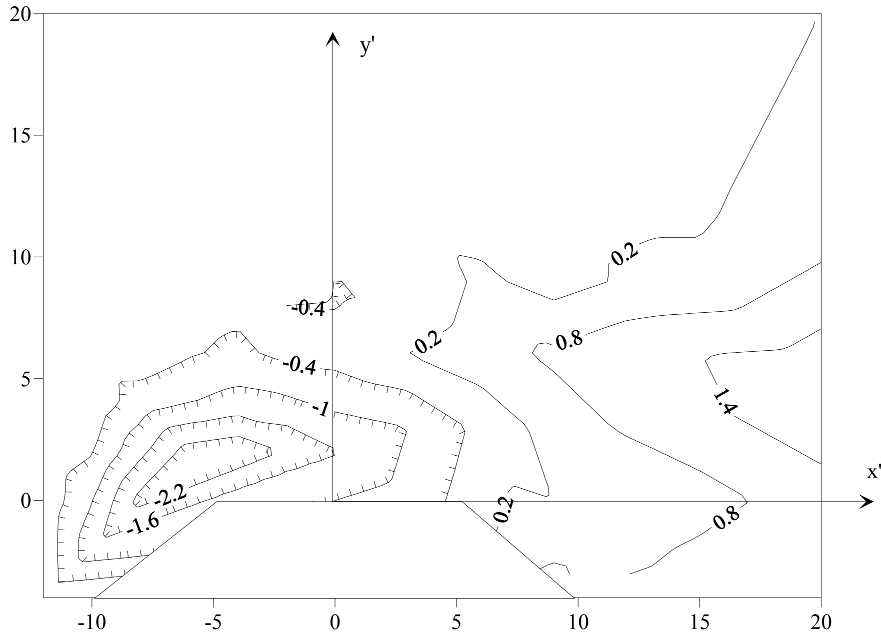

Figure 3.35. Scour hole contours in cm (Experiment No: 46, t = 60 min)

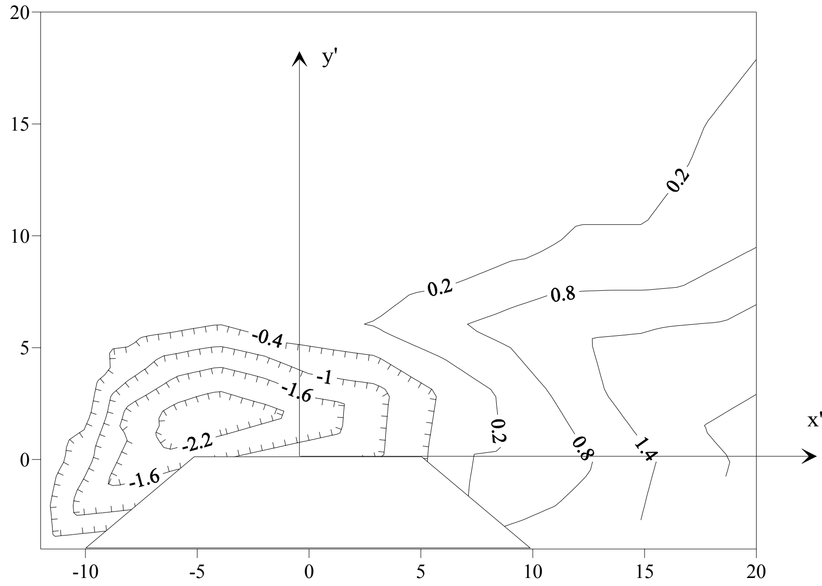

Figure 3.36. Scour hole contours in cm (Experiment No: 47, t = 100 min)

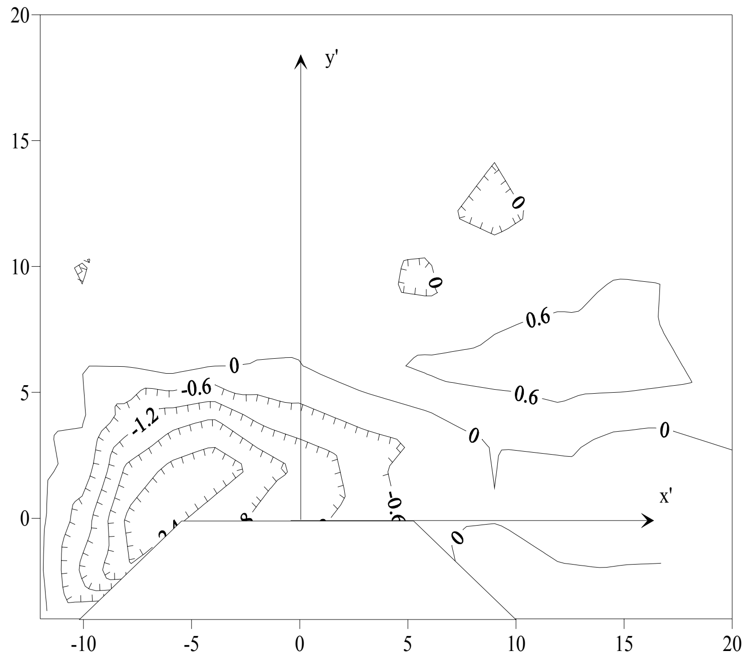

Figure 3.37. Scour hole contours in cm (Experiment No: 48, t = 150 min)

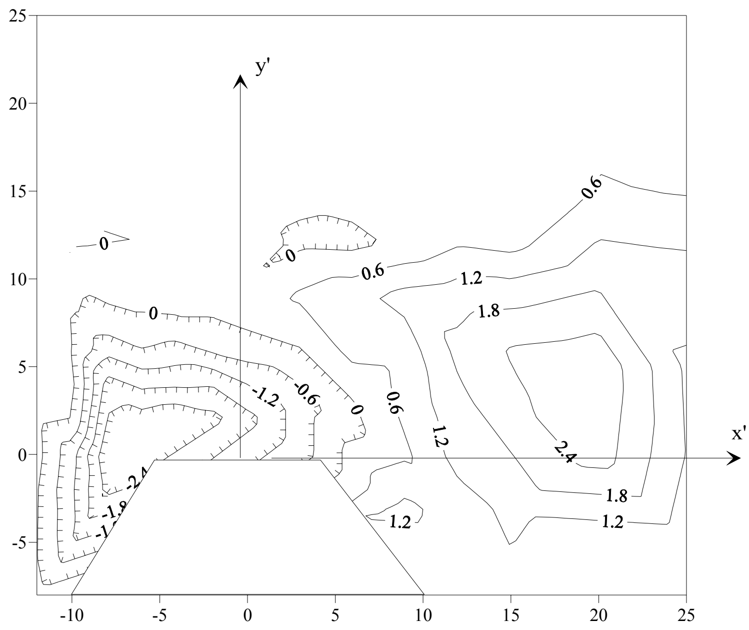

Figure 3.38. Scour hole contours in cm (Experiment No: 56, t = 5 min)

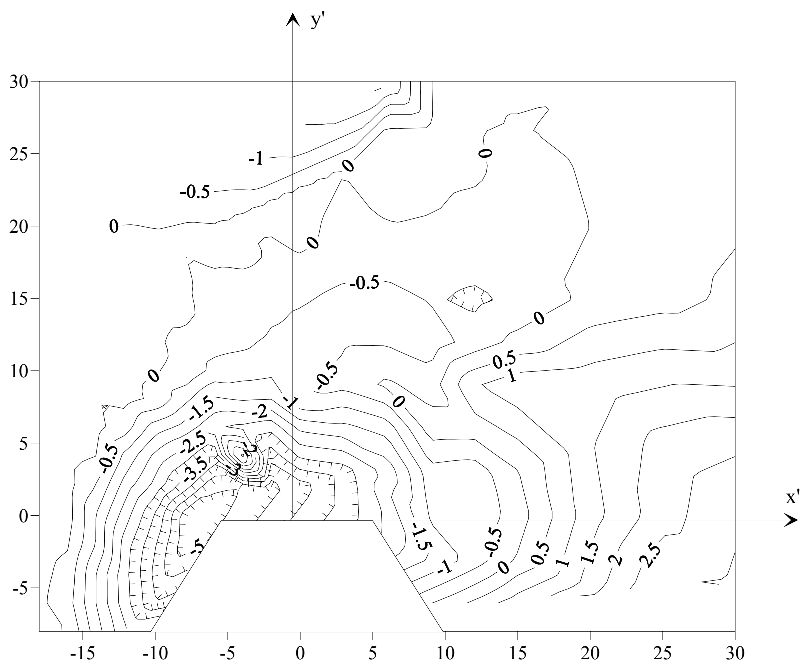

Figure 3.39. Scour hole contours in cm (Experiment No: 57, t = 20 min)

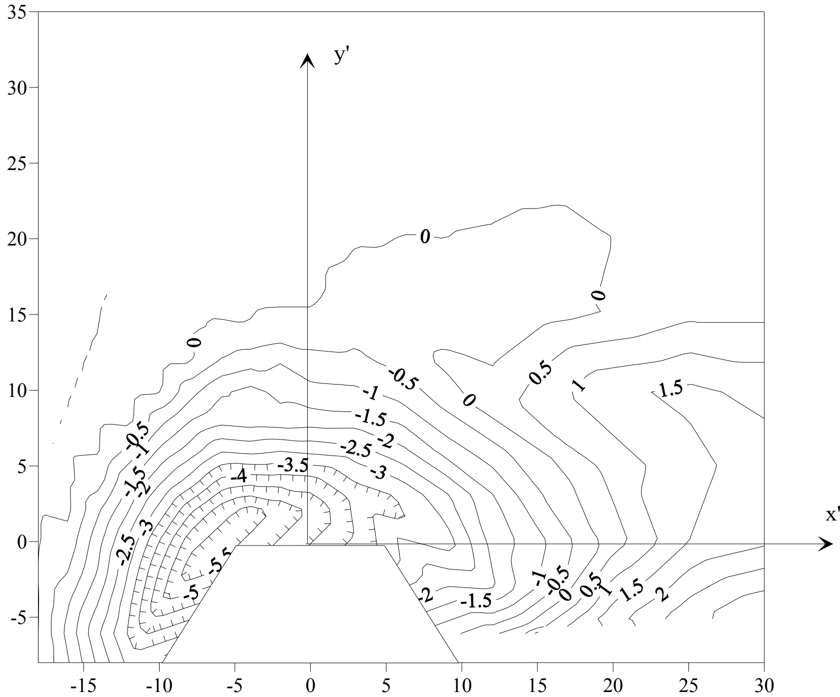

Figure 3.40. Scour hole contours in cm (Experiment No: 58, t = 60 min)

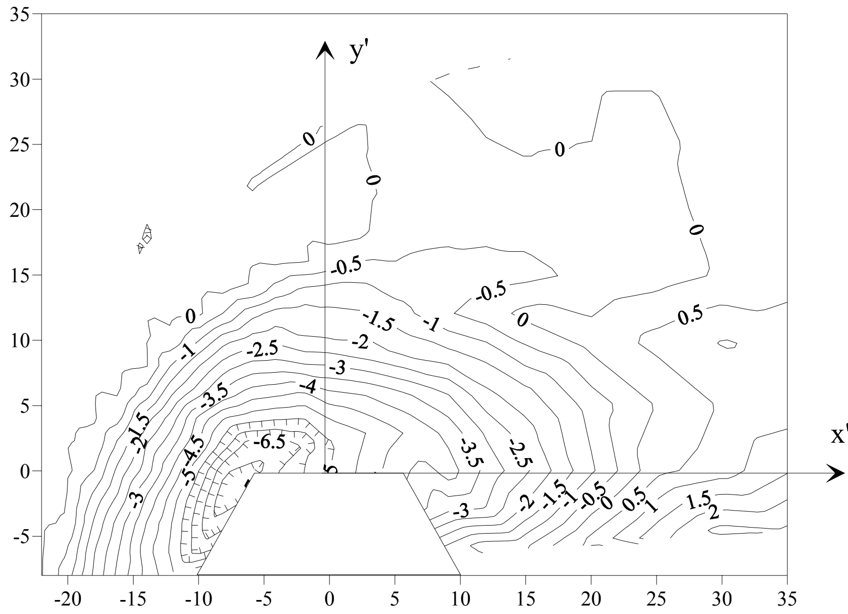

Figure 3.41. Scour hole contours in cm (Experiment No: 59, t = 100 min)

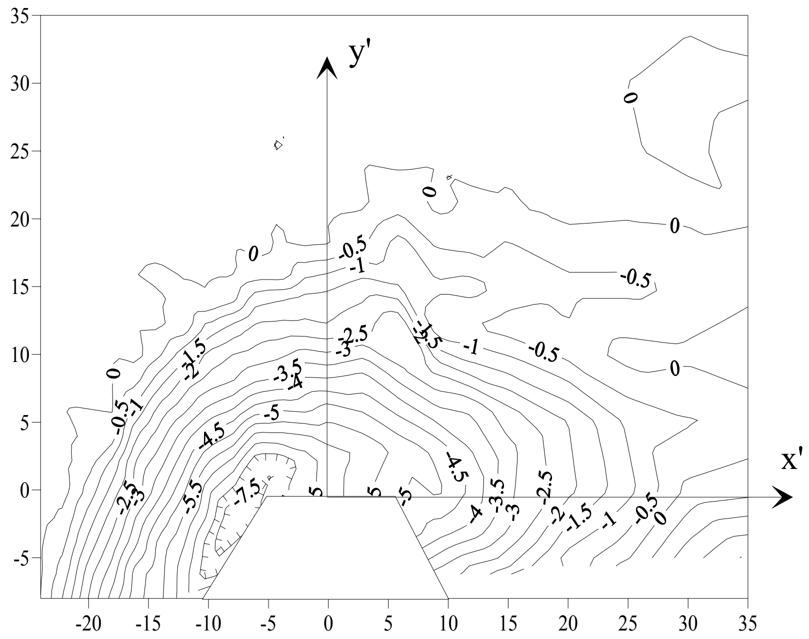

Figure 3.42. Scour hole contours in cm (Experiment No: 60, t = 150 min)

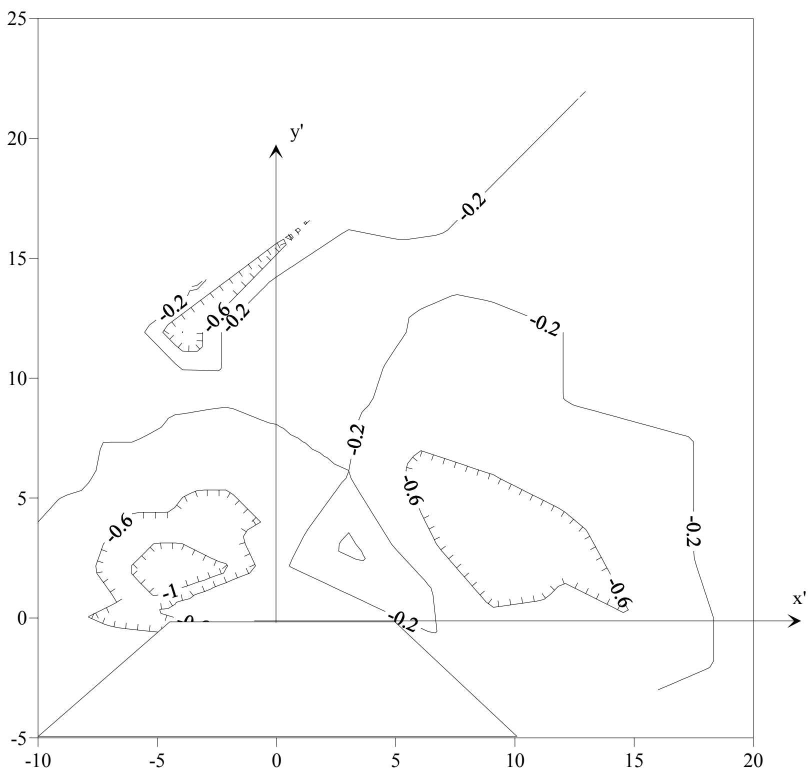

Figure 3.43. Scour hole contours in cm (Experiment No: 73, t = 5 min)

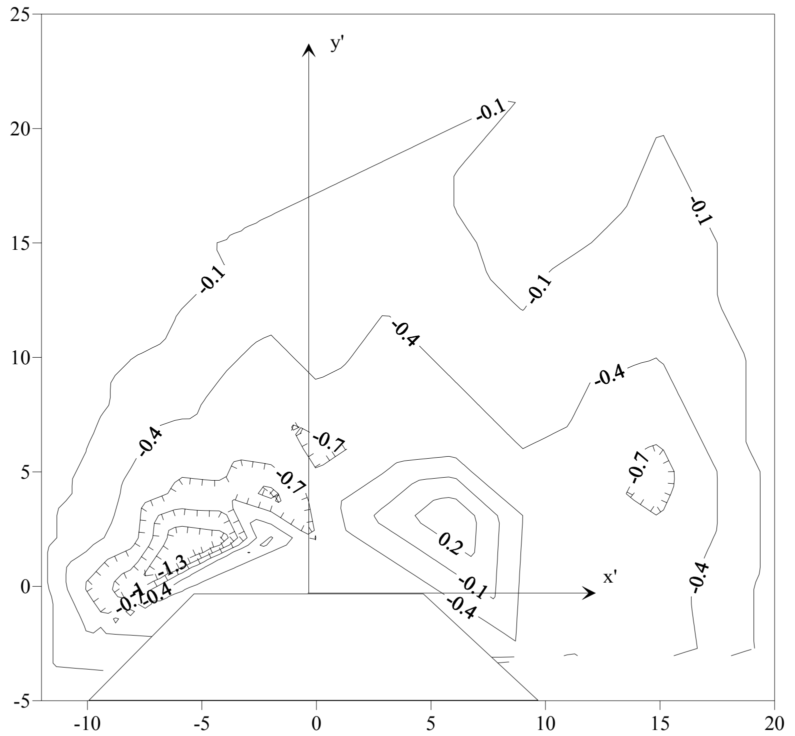

Figure 3.44. Scour hole contours in cm (Experiment No: 74, t = 20 min)

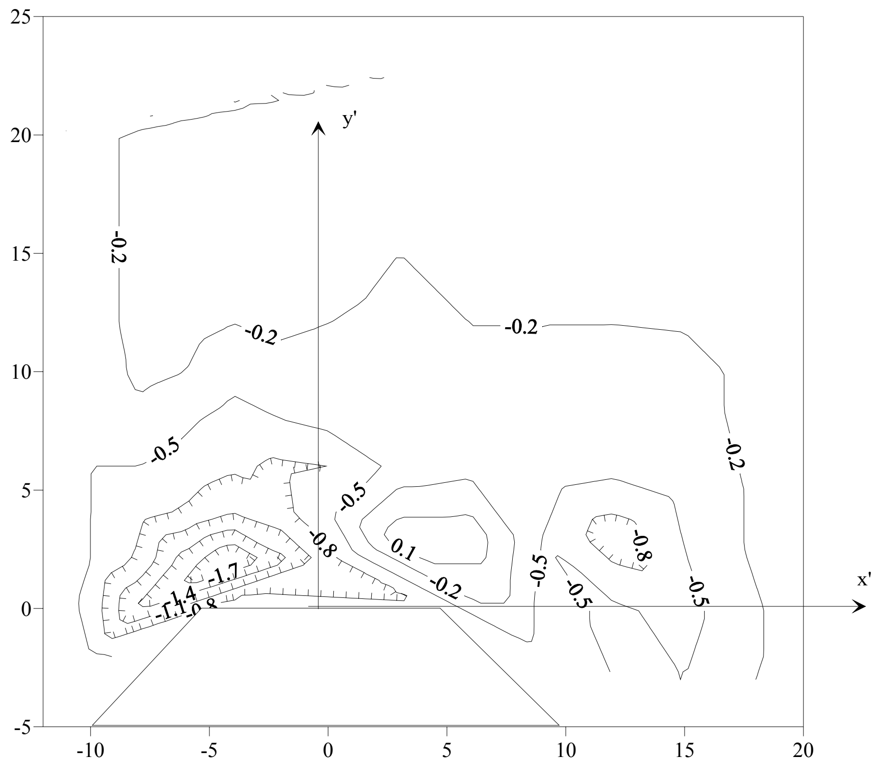

Figure 3.45. Scour hole contours in cm (Experiment No: 75, t = 60 min)

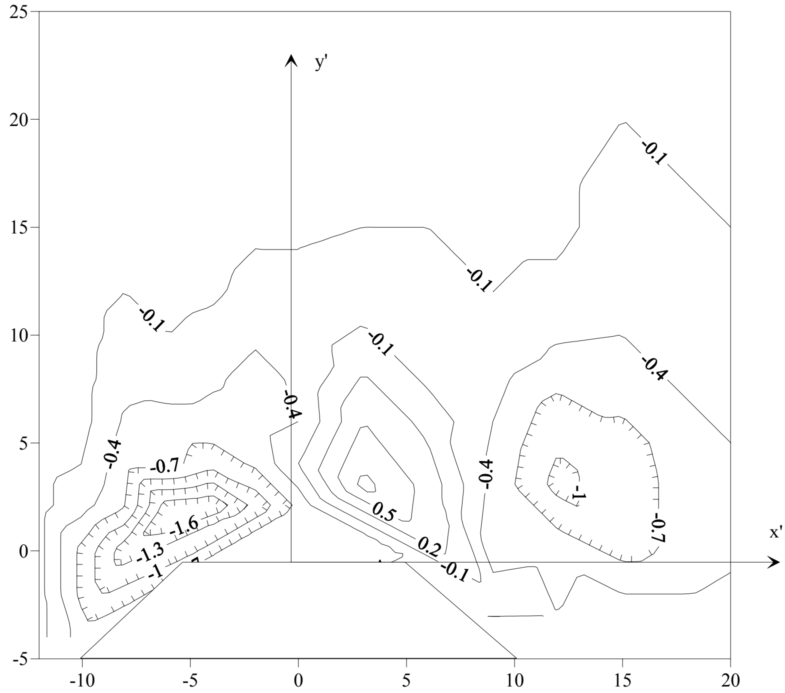

Figure 3.46. Scour hole contours in cm (Experiment No: 76, t = 100 min)

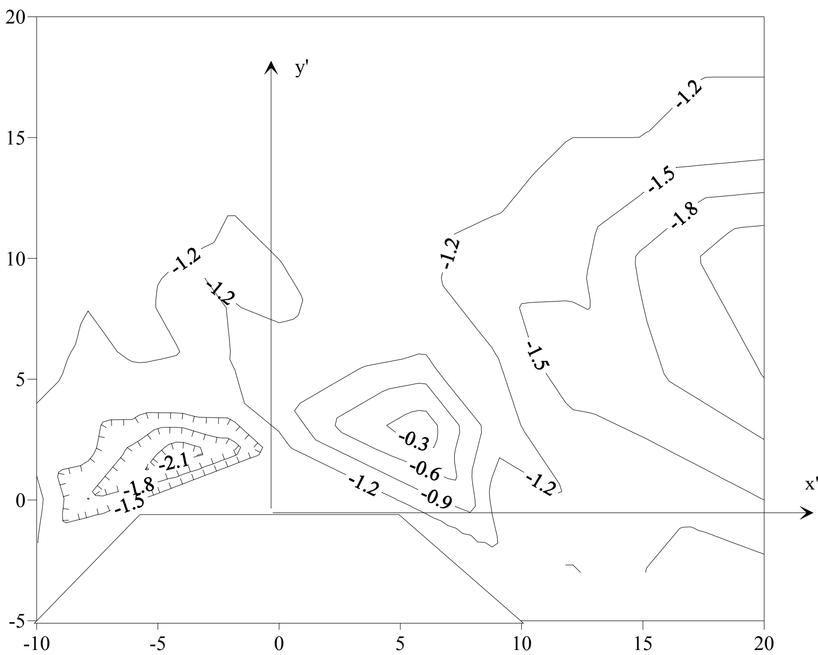

Figure 3.47. Scour hole contours in cm (Experiment No: 77, t = 150 min)

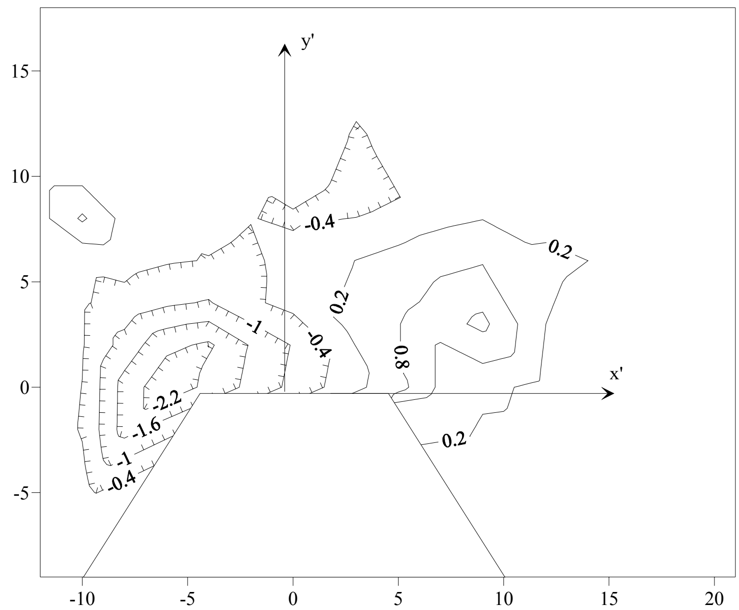

Figure 3.48. Scour hole contours in cm (Experiment No: 81, t = 5 min)

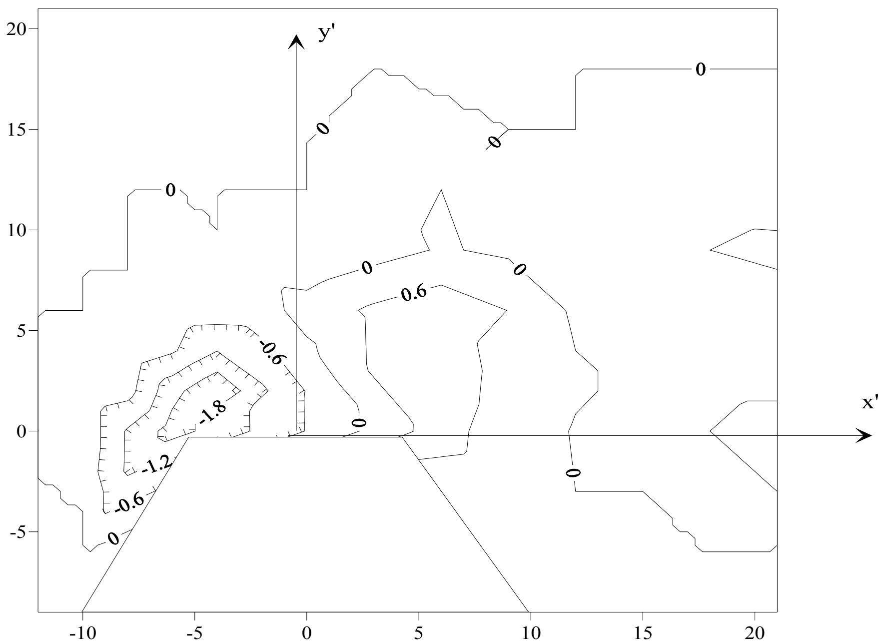

Figure 3.49. Scour hole contours in cm (Experiment No: 82, t = 20 min)

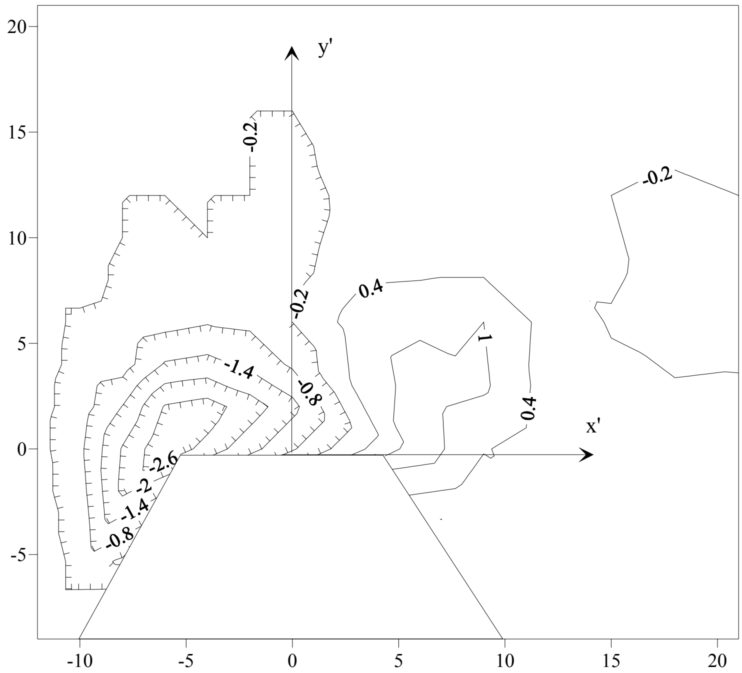

Figure 3.50. Scour hole contours in cm (Experiment No: 83, t = 60 min)

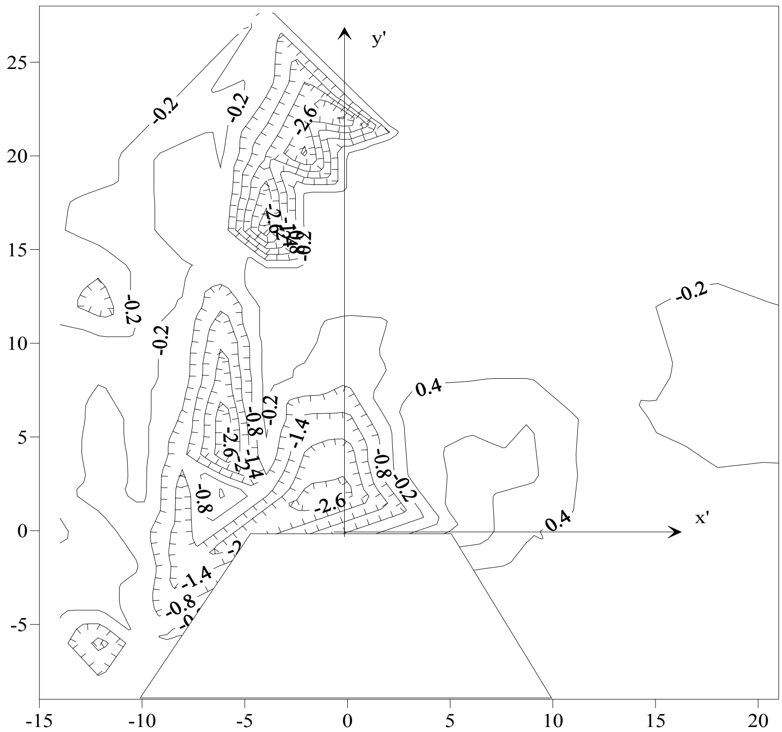

Figure 3.51. Scour hole contours in cm (Experiment No: 84, t = 100 min)

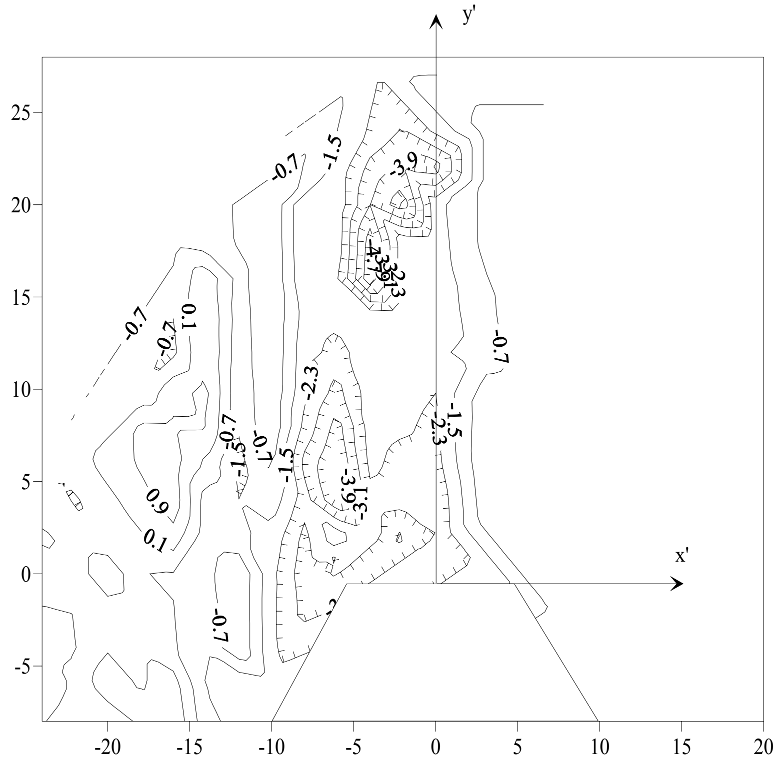

Figure 3.52. Scour hole contours in cm (Experiment No: 85, t = 150 min)

Further information on the findings of the scour measurements and their interpretations will be provided in Chapter 4.

CHAPTER 4

ANALYSIS OF EXPERIMENTAL RESULTS

4.1. Introductory Remarks

This chapter deals with the analysis and interpretation of the experimental results. The order of magnitudes of scour depths measured around vertical-wall and wing-wall abutments as well as the rate of scour evolution will be discussed. The findings of this chapter will form the basis for the semi-empirical model, which will be introduced in Chapter 5.

4.2. Interpretation of the Results Obtained from Vertical-wall Abutments

Wide ranges of experiments have been carried out for the observation of temporal variation of scour depths at vertical-wall abutments. As stated before, the range of flow rates was decided such that clear water conditions prevailed on the flume bed for the bed materials tested. This study is intended to develop a methodology for semi-empirical analysis of temporal variation in clear water scouring at vertical-wall abutments. The author conducted extensive laboratory measurements on abutment scouring. However, for some of the experiments, almost equilibrium conditions were achieved shortly under small densimetric Froude numbers with small abutment lengths. Therefore, it is assumed that a subset of the experimental data having similar scour evolution tendency as the previously reported popular empirical models, e.g. Coleman et al. (2003) and Oliveto and Hager (2002) will be used in the calibration data. To this end, a new data set is organized and recalled as the calibration data set (Table 4.1) for the vertical-wall abutments. The equations for equilibrium scour depth were applied to the experimental sets for the vertical-wall abutments as shown in Table 4.1 in which columns 5 and 6 present equilibrium parameters of Melville and Coleman (2000) and Coleman et al. (2003) using Equations (2.7) and (2.8 or 2.9), whereas column 7 gives the equilibrium scour depths computed from Dey and Barbhuiya equation, i.e. Equation (2.22).

Table 4.1. Calibration data for vertical-wall abutments

Experiment No (1)	Experiment No in calibration set (2)	L (cm) (3)	d_s (m) (4)	d_{se} (m) (5)	t_e (hr) (6)	d_{se} (m) (7)	t_m (min) (8)
1	1	12.5	0.126	0.164	61.52	0.209	360
2	2	12.5	0.123	0.153	55.81	0.200	360
3	3	12.5	0.121	0.143	51.77	0.194	360
4	4	12.5	0.116	0.131	45.53	0.185	360
5	5	12.5	0.105	0.119	39.58	0.170	360
6	6	12.5	0.074	0.107	34.14	0.154	360
8	C1	12.5	0.066	0.164	61.52	0.209	5
9	C2	12.5	0.092	0.164	61.52	0.209	20
10	C3	12.5	0.107	0.164	61.52	0.209	60
11	C4	12.5	0.11	0.164	61.52	0.209	100
12	C5	12.5	0.123	0.164	61.52	0.209	150
13	7	10.0	0.121	0.147	55.39	0.185	360
14	8	10.0	0.115	0.137	50.76	0.177	360
15	9	10.0	0.109	0.128	47.68	0.172	360
16	10	10.0	0.097	0.118	42.37	0.163	360
17	11	10.0	0.077	0.107	37.18	0.151	360
18	12	10.0	0.05	0.095	32.40	0.136	360
20	C6	10.0	0.055	0.147	55.39	0.185	5
21	C7	10.0	0.0715	0.147	55.39	0.185	20
22	C8	10.0	0.084	0.147	55.39	0.185	60
23	C9	10.0	0.096	0.147	55.39	0.185	100
24	C10	10.0	0.102	0.147	55.39	0.185	150
25	13	5.0	0.083	0.078	72.48	0.127	360
26	14	5.0	0.072	0.075	68.66	0.121	360
27	15	5.0	0.062	0.074	68.11	0.117	360
28	16	5.0	0.054	0.071	64.19	0.112	360
61	17	12.5	0.095	0.159	112.19	0.175	360
62	18	12.5	0.065	0.133	83.93	0.162	360
64	19	10.0	0.09	0.142	106.60	0.155	360
65	20	10.0	0.063	0.119	80.49	0.143	360
67	21	5.0	0.062	0.099	175.21	0.106	360

As can also be seen from Table 4.1, the test durations range between 3.5 to 38% of the equilibrium test durations according to the Coleman et al. (2003) method using Equations (2.8) and (2.9). That is why the scour depths obtained at the end of 6 hours test durations are relatively smaller than those of the equilibrium scour depths computed from Coleman et al. (2003) and Dey and Barbhuiya (2005) approaches. Moreover, equilibrium scour depth equation of Dey and Barbhuiya (2005), i.e. Equation (2.22), resulted in greater values than the findings of Coleman et al. (2003) method. Based on these observations it can be stated that derivation of empirical equations based on the final scour depths obtained at the end of six hours of test duration would not be realistic. On the contrary, analysis of time-dependent patterns of scour depths and contours would provide relevant information for flows having durations within physical limits of practical interest.

The results of this study will be compared with the results of previous studies dealing with temporal variation of scour depth, which exhibit similar scour evolution tendencies as those of the present study. The results of Cardoso and Bettess (1999) cannot be used in the comparison since their study was conducted in a two-stage channel reflecting different flow conditions, i.e. long abutments, floodplain effects, etc., compared to the present experimental studies. Ballio and Orsi (2000) did not provide explicit relations for the equilibrium scour depth, which was required in Equation (2.19) for computing temporal variation of the scour depth at vertical-wall abutments. Hence, their method will not be considered in the validation stage. Therefore, the results of this study will be compared with the findings of a semi-empirical model developed by Dey and Barbhuiya (2005) and two empirical models, which were proposed by Coleman et al. (2003) and Oliveto and Hager (2002).

Suitability of Dey and Barbhuiya (2005) method for the verification purpose can be checked using the results of the experimental study. To this end dimensionless scour depth measurements were compared with the solution of Dey and Barbhuiya (2005) method using Equation (2.21) for all data sets. For the sake of brevity, only the results of two experiments, i.e. Experiments 1 and 13 were given. As can be seen from Figures 4.1 and 4.2, Dey and Barbhuiya (2005) model relatively overpredict the dimensionless scour depths for T_s>50. Therefore, this method will also be disregarded in the comparative analysis of the results.

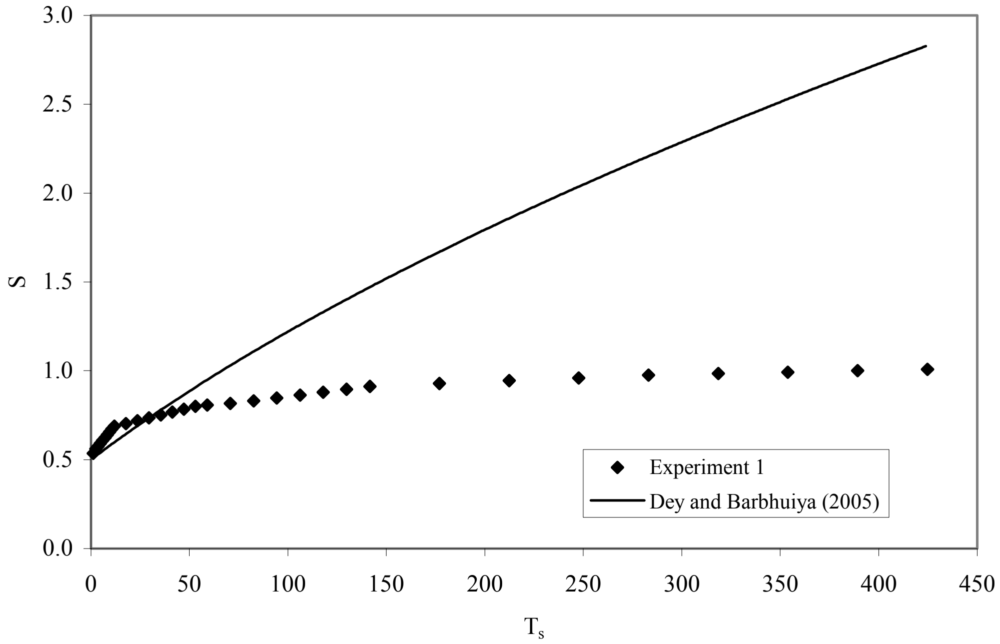

Figure 4.1. Comparison of Dey and Barbhuiya (2005) model with Experiment 1

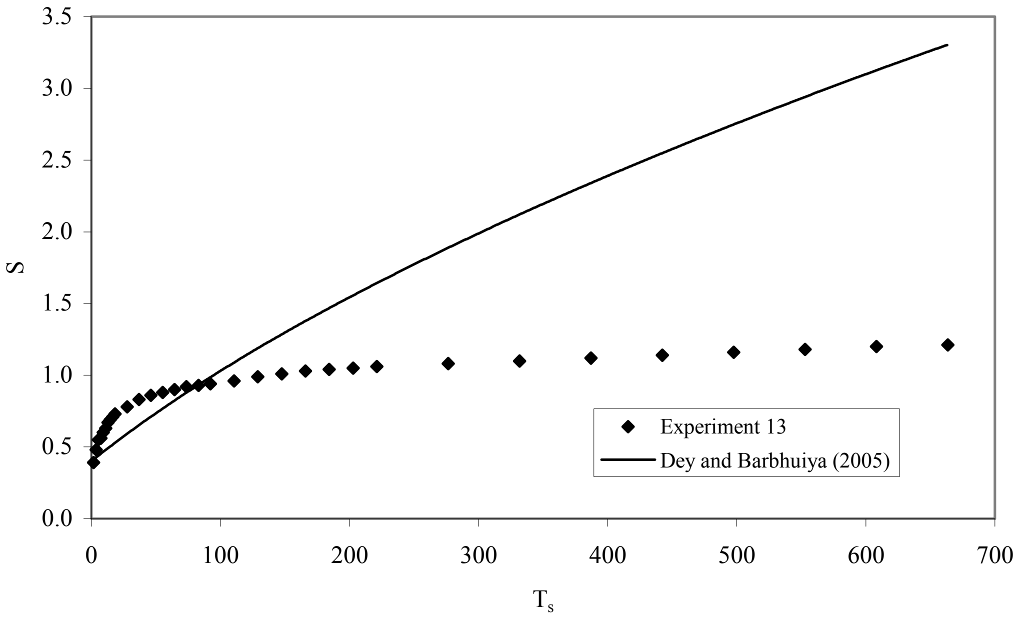

Figure 4.2. Comparison of Dey and Barbhuiya (2005) model with Experiment 13

In the second phase of the analysis, the geometric characteristics of the scour holes around the abutment are investigated. In order to observe the locations of the maximum depths of scour and accretion around abutment models, the coordinate system shown in Figure 3.17 is used. For the purpose of comparison, the surrounding of the abutment models is divided into 6 zones. The observations made on the locations of the maximum scour and accretion zones were stated in Table 4.2.

Table 4.2. Description of maximum scour and accretion zones

Experiment No (1)	L (cm) (2)	t_m (min) (3)	d_s (m) (4)	Maximum Scour zone (5)	Maximum Accreation zone (6)
8	12.5	5	0.066	1	5
9	12.5	20	0.092	1	5
10	12.5	60	0.107	1	5
11	12.5	100	0.110	1	5
12	12.5	150	0.123	1	5
20	10	5	0.055	1	5
21	10	20	0.072	1	5
22	10	60	0.084	1	5
23	10	100	0.096	1	5
24	10	150	0.102	1	5
32	5	5	0.016	1	4
33	5	20	0.028	1	4
34	5	60	0.043	1	4
35	5	100	0.049	1	6
36	5	150	0.054	1	5
44	Wing-wall, 45^o	5	0.016	3	4
45	Wing-wall, 45^o	20	0.022	3	4
46	Wing-wall, 45^o	60	0.026	3	4
47	Wing-wall, 45^o	100	0.027	3	4
48	Wing-wall, 45^o	150	0.028	3	4
56	Wing-wall, 60^o	5	0.029	3	4
57	Wing-wall, 60^o	20	0.053	1	5
58	Wing-wall, 60^o	60	0.058	1	5
59	Wing-wall, 60^o	100	0.074	3	5
60	Wing-wall, 60^o	150	0.080	1	5
73	Wing-wall, 45^o	5	0.014	3	6
74	Wing-wall, 45^o	20	0.015	3	6
75	Wing-wall, 45^o	60	0.020	3	6
76	Wing-wall, 45^o	100	0.021	3	6
77	Wing-wall, 45^o	150	0.024	3	6
81	Wing-wall, 60^o	5	0.026	1	6
82	Wing-wall, 60^o	20	0.028	3	5
83	Wing-wall, 60^o	60	0.030	3	5
84	Wing-wall, 60^o	100	0.037	3	5
85	Wing-wall, 60^o	150	0.053	3	4

During the course of the experiments, it was observed that the maximum scour depths occurred in region 1 close to the upstream corner for all vertical-wall abutments, whereas the maximum accretions were observed in the wake zone, i.e. zone 5 for L=12.5 and 10 cm case, whereas the maximum accretions were observed in zones 4, 5 and 6 for L=5 cm. Since the stream power in the bridge constriction is small for L=5 cm compared to the thicker abutments with L=12.5 and 10 cm, the eroded sediments could not be carried until the wake region and may partially accumulate in zones 6 and 4. It was also observed that the horizontal distance between the locations of maximum depths of scour and accretion decreased with decreasing length of vertical wall abutment. At the early stages, the maximum scours observed in zone 1 close to the upstream corner of the abutment. As time elapsed, the surface area of the scour hole enlarged with almost uniformly spaced contours towards the downstream corner. Scour contours surrounded the downstream corner for increasing time.

4.3. Interpretation of the Results Obtained from Wing-wall Abutments

Similar zones as in the case of vertical-wall abutments can also be defined for wing-wall abutments. Observations on the locations of maximum scour and accretion zones for the wing-wall abutments are also outlined in Table 4.2. Because of inclination of the upstream face of the wing-wall abutment towards the centerline of the bridge opening, the dominancy of the downflow is shifted with the flow action such that the maximum scour depths were mainly observed in zone 3. The maximum accretion zones for most cases were observed in zones 4 and 6. Scour contours were evolved in zone 2 and propagated towards the downstream with respect to time. However, even under the maximum test duration for contour measurements the scour contours could not reach the wake region of the abutment having 60° of acute angle. In case 45° acute angle, however, the scour contours evolved in zone 2 and exceeded the downstream corner towards the wake region with respect to time. Another by-product of the analysis is that the shapes of scour contours around wing-wall abutments are more rounded compared to the case of vertical-wall abutments. This may be due to stronger separation around the upstream corner of the vertical-wall abutment in which greater area is under the effect of rotational flow.

4.4. Use of Scour Contours for Practical Applications

The volume and surface area of the scour hole around the abutments were computed at the aforementioned test durations using a software based on triangularization technique. This program is capable of evaluating the area and volume elements bounded by irregular contours. For the sake of practical applications, dimensionless scour hole volume and surface area expressions are defined as $V^*=V/(d_sL^2)$ and $A^*=A/(WL)$, respectively, where V is the volume, A is the surface area of the scour hole around the abutment, and W is the width of the abutment parallel to the flow direction. Variations of dimensionless scour area and volume with respect to dimensionless time, T_s, are shown in Figures 4.3 and 4.4, respectively.

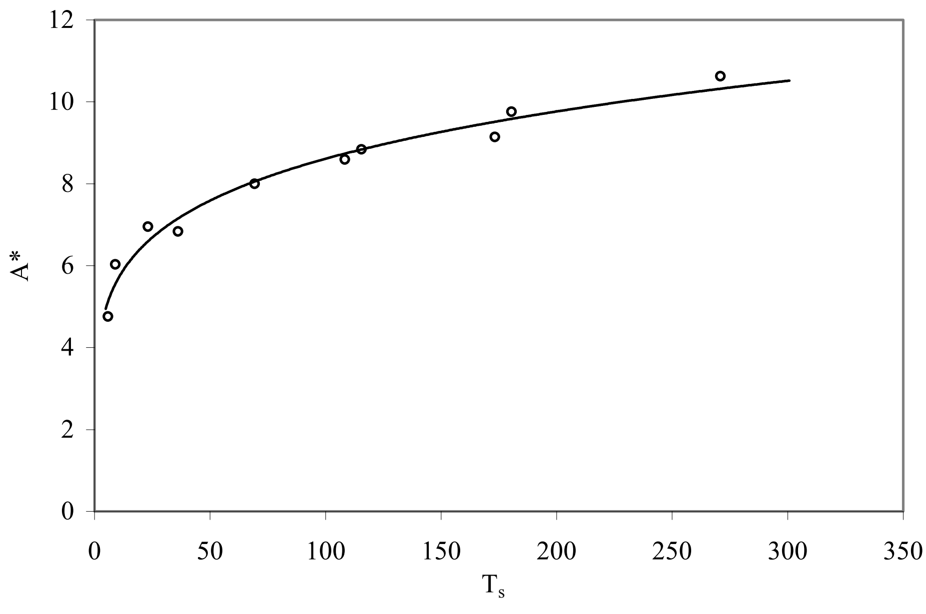

Figure 4.3. Variation of dimensionless scour area with dimensionless time

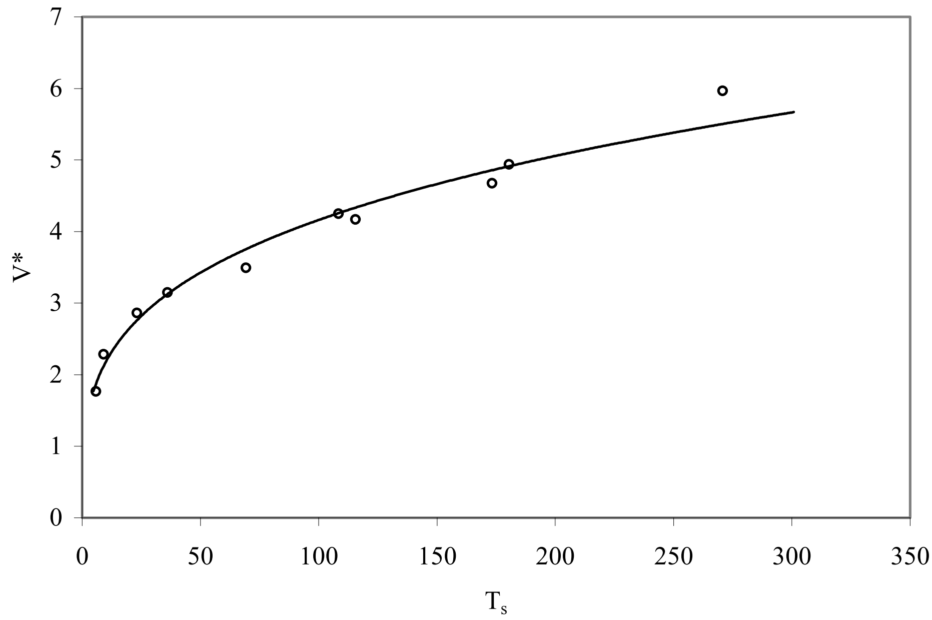

Figure 4.4. Variation of dimensionless scour volume with dimensionless time

The regression equations fitted to the data points in these figures with the corresponding coefficients of determination (R^2) are obtained as

$$A^* = 3.722T_s^{0.182} \qquad (R^2=0.962) \tag{4.1}$$

$$V^* = 1.142T_s^{0.281} \qquad (R^2=0.980) \tag{4.2}$$

As can be seen from Figures 4.3 and 4.4, the rates of change of A* and V* decrease with respect to T_s. The order of magnitude of the time required to reach the equilibrium conditions can be found in such a way that the corresponding rate of change of dimensionless volume is almost zero.

In order to have information for the equilibrium value of T_s under the experimental conditions, the method of Coleman et al. (2003) is applied to the data. As a result, a value of T_s=13048 is obtained, which gives an equilibrium test duration of 184 h. In actual prototype conditions, the corresponding flow duration would be extremely long for the practical ranges of design flow conditions. With the extrapolation of Equation (4.1), it can be observed that the rate of change of A* is negligibly small for T_s>4500. This limiting value gives approximately A*=17. In other words, the surface area of the scour hole is about A=17WL and its further development is negligibly small. This value can be used as an approximate area of coverage of the bed with an armoring countermeasure, e.g. riprap.

There exist some methods in the literature giving the appropriate riprap size to be placed around abutments, which are outlined by Melville and Coleman (2000). However, the studies dealing with the placement details of riprap around abutments are limited. Therefore, riprap coverage area of A=17WL may be used as a preliminary design value. A semi-circular area with the origin shown in Figure 4.5, which is expressed in Equation (4.3), may be adopted for the riprap coverage at the bed level around the abutment. The suggested placement area of riprap armoring is illustrated in Figure 4.5.

$$A = \frac{\pi}{2}\left(3.5L + \frac{W}{2}\right)^2 - WL \qquad (4.3)$$

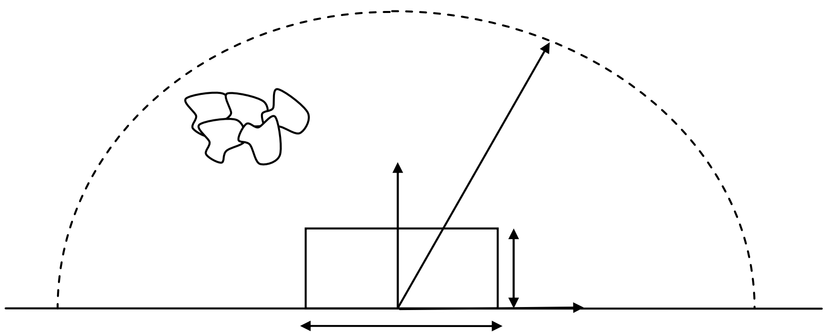

Figure 4.5. Placement of riprap around abutment as scour countermeasure

The surface elevation of riprap layer can be placed at the mean bed level or at a lower elevation not to create extra turbulence at the bed. It should be emphasized, however, that additional experiments need to be conducted to generalize the design details of this armoring countermeasure, i.e. the extension of the area of protection as well as the size, layer thickness, and surface elevation of the riprap.

CHAPTER 5

DEVELOPMENT OF SEMI-EMPIRICAL MODEL

This chapter presents the development of a semi-empirical model for determining clear water scour evolution at vertical-wall abutments. A similar study can also be carried out for wing-wall abutments for a potential future research. The model is based on the application of the sediment continuity equation to the scour hole around the abutment. The volume of the scour hole around the vertical-wall abutment is determined using an analytical approach and an empirical approach, which will be designated as the Approach 1 and Approach 2.

5. 1. Framework for Model Development-Approach 1

A new semi-empirical model will be developed for determining temporal variation of clear water scour depth around vertical-wall abutments. Sediment continuity equation for the scour hole around an abutment is

$$\frac{dV}{dt} = Q_{so} - Q_{si} \tag{5.1}$$

where V=scour hole volume around the abutment, Q_{so}=volumetric rate of sediment being carried out from the scour hole, and Q_{si}=volumetric rate of sediment being carried into the scour hole. For clear water conditions, Q_{si}=0. The volumetric rate of sediment out of the scour hole can be determined using a sediment pickup function as follows

$$Q_{so} = f\,\frac{EA_p}{\Delta\rho_s} \tag{5.2}$$

where f=coefficient of proportionality to account for the geometric features of the scour hole around the abutment as well as flow and sediment properties, E=sediment pickup rate in mass per unit time and area, and A_p=unit area from which sediment is picked up. Several sediment pickup functions have been reported in the literature for flat beds composed of uniform materials, e.g. equations proposed by LeFeuvre and Altınbilek (1970), Fernandez Luque (1974), Nagakawa and Tsujimoto (1980), and Van Rijn (1984). A recent sediment pickup function valid for sloping beds with uniform and non-uniform materials was proposed by Dey and Debnath (2001). This equation giving the pickup rate in kg/m^2/s is

$$E = 0.0006 T D_*^{0.24} \sigma^{1.9} \rho_s \sqrt{\Delta g D_{50}} \tag{5.3}$$

where T=transport-stage parameter due to scouring, which is defined by $(\tau_b-\tau_{bc})/\tau_{bc}$, τ_b=bed shear stress on flat bed, $\tau_{bc}=\psi\tau_{cr}$=critical bed shear stress on sloping bed, τ_{cr}=critical bed shear stress on flat bed, ψ=a factor depending on turbulent fluctuations and oscillations of primary vortex, $D_*=D_{50}(\Delta g/\upsilon^2)^{1/3}$, and υ=kinematic viscosity of water. The value of ψ is normally less than 1.0 for the downward slope at the upstream side of the scour hole, whereas it may be greater than 1.0 for the rear side of the abutment. However, since it is very difficult to model the exact distribution of the critical bed shear stress along irregular contours within the scour hole, an average value may be taken for ψ. Considering the fundamental similarity of all clear water scouring situations, an average value of ψ=0.5 was taken in this study with reference to the work of Dey and Barbhuiya (2005) who used this value in the analysis of time variation of scour depth at abutments of various shapes.

The coefficient of proportionality, f, will be determined using the experimental results of this study. The determination of time-dependent shapes of scour holes around bridge abutments is the first step in the analysis. For this purpose sequential experiments were performed with F_d=2.384 and D_{50}=1.8 mm (Experiments 8-12, 20-24, and 32-36). Experiments were stopped at the end of different test durations; namely 5, 20, 60, 100, and 150 min to determine the contours of the scour hole around abutment models using point gages. After each run, the bed was flattened to run the experiment with the next duration. The scour contours obtained in tests were shown and analyzed in Chapter 4. Since the depths of scour around the abutment having L=5 cm were relatively small and equilibrium conditions were achieved shortly for small flow intensities, the scour contours obtained for L=5 cm will not be used in the model derivation.

The rate of change of the scour hole volume will be investigated by considering some axes around the upstream corner of the abutment. To this end, the cross-sections A-A, B-B, and C-C were taken as shown in Figure 3.17. To determine the rate of change of side inclination of the scour hole, a three-dimensional coordinate system was placed at the initial bed level. The coordinates x' and y' are along the sections A-A and B-B, respectively, whereas the z'-coordinate is located along the face of the abutment in the downward direction. In the analysis, x_t', y_t', and z_t' are the time-dependent coordinates of the scour hole, whereas x'_{tmax}, y'_{tmax}, and z'_{tmax} are the maximum coordinates of the scour hole measured at the end of the tests. The correlations between x_t'/x'_{tmax} or y_t'/y'_{tmax} (or X_t/X_{tmax}) and $z_t'/z_t'_{max}$ were investigated to examine the rate of change of the side inclination of the scour hole at different axes. As observed in Figures 5.1 through 5.3, the discrepancy of the data points from the bisector line, representing the line of best agreement, was small. It can, therefore, be accepted that the shape of the scour hole remains almost unchanged with respect to time. However, the rate of change decelerated as time elapsed. Another by-product of this study was that the side angles of the scour hole, except the rear face of the abutment, was approximately equal to the angle of repose, θ, of the sediment. In this study, the values of angles of repose for the bed materials were taken as 31°and 30° for D_{50}=1.8 mm and 0.9 mm, respectively. Dey and Barbhuiya (2005) also observed that the upstream scour holes around abutment models of different shapes had a similarity at different times. They concluded that this implied a layer-by-layer scouring process until an equilibrium state was achieved. As a result, the volume of scour hole can be approximated by an inverted semi-cone having a rectangular base with dimensions W and L. This definition is also consistent with that used for cylindrical and square piers by Yanmaz (1989).

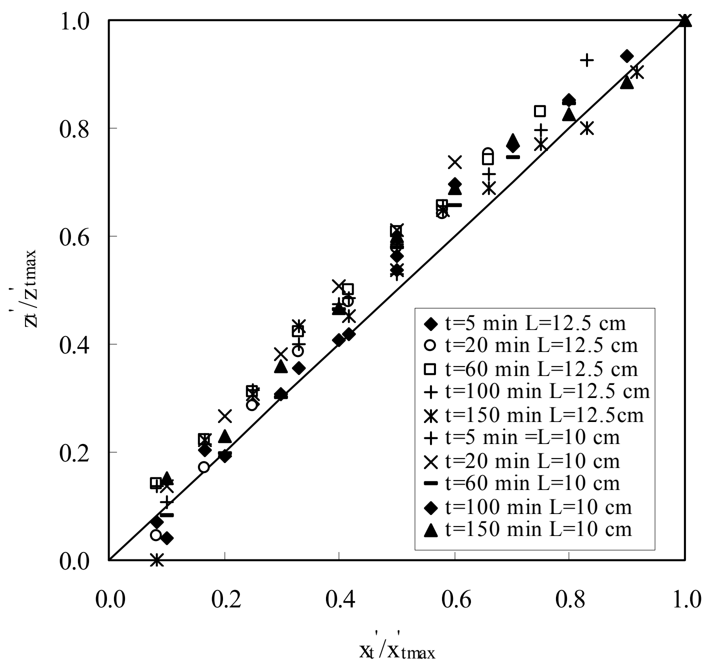

Figure 5.1. Correlation between x_t'/x'_{tmax} and z_t'/z'_{tmax} (Section A-A in Fig. 3.17)

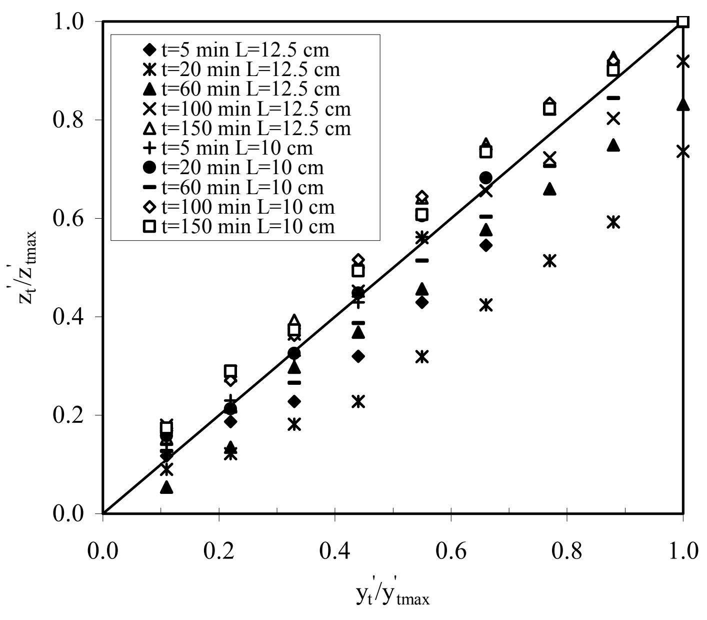

Figure 5.2. Correlation between y_t'/y'_{tmax} and z_t'/z'_{tmax} (Section B-B in Fig. 3.17)

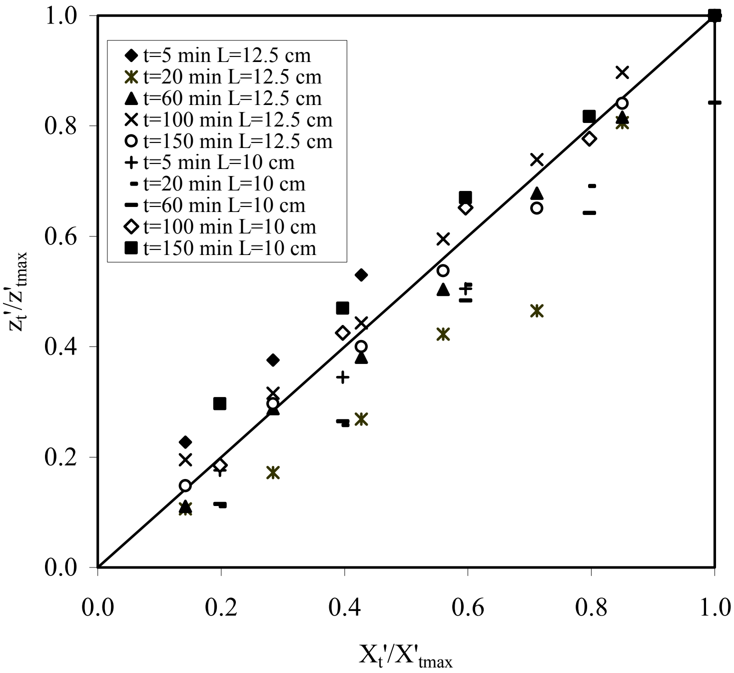

Figure 5.3. Correlation between x_t/x_{tmax} and z_t'/z'_{tmax} (Section C-C in Fig. 3.17)

5.1.1. Determination of Scour Hole Volume

Volume expression of the scour hole will be derived on the basis of the above approximation using Figure 5.4. To define the geometric characteristics of the scour hole, several points were considered on the volume element as shown in Figure 5.4. The coordinates of points P, Q, M, P′, Q′, and M′ in Figure 5.4 are

$P=(a, a\tan\phi, 0)$

$Q=(B'\cos\phi, B'\sin\phi, d_s)$

$M=((1-\eta)P+ \eta Q)$ where $0\leq \eta \leq 1.0$

$P'=(\xi a, \xi a\tan\phi, 0)$ where $0\leq\xi\leq 1.0$

$Q'=(\xi B'\cos\phi, \xi B'\sin\phi, d_s)$

$M'=((1- \eta)P'+ \eta Q')$

The parameters η and ξ are used to define the coordinates of the points. Substituting the values of P' and Q' into M' lead to

$x=(1-\eta)\xi a+\eta\xi B'\cos\phi=f_1(\eta, \xi, \phi)$

$y=(1-\eta)\xi a\tan\phi+\eta\xi B'\sin\phi=f_2(\eta, \xi, \phi)$

$z=\eta d_s=f_3(\eta)$

where $a=W/2$, $B'=(L+d_s/\tan\theta)$.

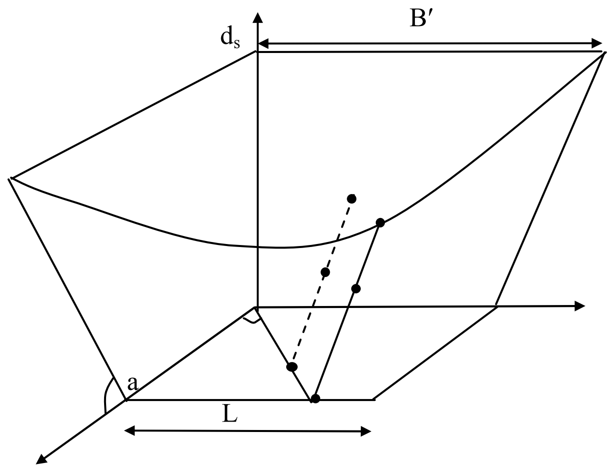

Figure 5.4. Geometric description of the scour hole model

The total volume of the scour hole around the abutment is $V=2(V_1+V_2)-LWd_s$, where V_1 and V_2 are the volume elements having triangular bases on x-y plane with $0\leq\phi\leq\arctan(2L/W)$ and $\arctan(2L/W)<\phi\leq\pi/2$, respectively. The volume element V_1 can be determined from

$$V_1 = \int_0^{\arctan\left(\frac{2L}{W}\right)} \left(\int_0^1 \left(\int_0^1 |J| d\eta \right) d\xi \right) d\phi \tag{5.4}$$

in which $|J|$=the determinant of the Jacobian of the transformation from the Cartesian coordinates to the coordinate system shown in Figure 5.4 and can be obtained as

$$J = \begin{vmatrix} \frac{\partial f_1}{\partial \eta} & \frac{\partial f_1}{\partial \xi} & \frac{\partial f_1}{\partial \phi} \\ \frac{\partial f_2}{\partial \eta} & \frac{\partial f_2}{\partial \xi} & \frac{\partial f_2}{\partial \phi} \\ \frac{\partial f_3}{\partial \eta} & \frac{\partial f_3}{\partial \xi} & \frac{\partial f_3}{\partial \phi} \end{vmatrix} \tag{5.5}$$

Taking the respective derivatives in this determinant,

$$\frac{\partial f_1}{\partial \eta} = -\xi a + \xi B' \cos \phi$$

$$\frac{\partial f_2}{\partial \eta} = -\xi a \tan \phi + \xi B' \sin \phi$$

$$\frac{\partial f_3}{\partial \eta} = d_s$$

$$\frac{\partial f_1}{\partial \xi} = (1-\eta)a + \eta B' \cos \phi$$

$$\frac{\partial f_2}{\partial \xi} = (1-\eta)a \tan \phi + \eta B' \sin \phi$$

$$\frac{\partial f_3}{\partial \xi} = 0$$

$$\frac{\partial f_1}{\partial \phi} = -\eta \xi B' \sin \phi$$

$$\frac{\partial f_2}{\partial \phi} = (1-\eta)\xi a \sec^2 \phi + \eta \xi B' \cos \phi$$

$$\frac{\partial f_3}{\partial \phi} = 0$$

Inserting these derivatives into Equation (5.5), the Jacobian determinant reduces to

$$J=\begin{vmatrix} -\xi a+\xi B'\cos\phi & (1-\eta)a+\lambda B'\cos\phi & -\eta\xi B'\sin\phi \\ -\xi a\tan\phi+\xi B'\sin\phi & (1-\eta)a\tan\phi+\lambda B'\sin\phi & (1-\eta)\xi a\sec^2\phi+\eta\xi B'\cos\phi \\ d_s & 0 & 0 \end{vmatrix}$$

which can be expanded as

$$J=(-\xi a+\xi B'\cos\phi)\begin{vmatrix} (1-\eta)a\tan\phi+\eta B'\sin\phi & (1-\eta)\xi a\sec^2\phi+\eta B'\xi\cos\phi \\ 0 & 0 \end{vmatrix}-$$

$$[(1-\eta)a+\eta B\cos\phi]\begin{vmatrix} -\xi a\tan\phi+\xi B'\sin\phi & (1-\eta)\xi a\sec^2\phi+\eta B'\xi\cos\phi \\ d_s & 0 \end{vmatrix}+$$

$$(-\eta\xi B'\sin\phi)\begin{vmatrix} -\xi a\tan\phi+\xi B'\sin\phi & (1-\eta)a\tan\phi+\eta B'\sin\phi \\ d_s & 0 \end{vmatrix}$$

Computing the above determinants and inserting the results into Equation (5.4), the volume element V_1 is obtained as

$$V_1=\frac{d_s WL}{12}+\left(\frac{d_s WL}{12}+\frac{W{d_s}^2}{12\tan\theta}\right)A+\left(\frac{d_s L^2}{6}+\frac{2L{d_s}^2}{6\tan\theta}+\frac{{d_s}^3}{6\tan^2\theta}\right)B \tag{5.6}$$

The volume element V_2 can also be determined in a similar manner as

$$V_2=\frac{Ld_s}{6}\left(L+\frac{d_s}{\tan\theta}\right)C+\frac{1}{6}\left(L+\frac{d_s}{\tan\theta}\right)^2 d_s D+\frac{d_s L^2}{6}\left(\frac{W}{2L}\right) \tag{5.7}$$

where

$A=\ln\left|\sec(\arctan(2L/W))+2L/W\right|$
$B=\arctan(2L/W)$
$C=\ln\left|\sec(\arctan(W/(2L)))+W/(2L)\right|$
$D=\arctan(W/(2L))$.

Since the total volume of the scour hole is $V=2(V_1+V_2)-LWd_s$, one can obtain

$$V = \left[\begin{array}{l} \dfrac{d_s WL}{3} + \left(\dfrac{d_s WL}{6} + \dfrac{W d_s^{\ 2}}{6 \tan\theta} \right) A + \left(\dfrac{d_s L^2}{3} + \dfrac{2 L d_s^{\ 2}}{3 \tan\theta} + \dfrac{d_s^{\ 3}}{3 \tan^2\theta} \right) B + \\ \dfrac{C}{3} \left(L^2 d_s + \dfrac{L d_s^{\ 2}}{\tan\theta} \right) + \dfrac{D}{3} \left(d_s L^2 + \dfrac{2 L d_s^{\ 2}}{\tan\theta} + \dfrac{d_s^{\ 3}}{\tan^2\theta} \right) \end{array} \right] - WLd_s \qquad (5.8)$$

The predictive ability of Equation (5.8) needs to be checked by the application of a software, which is capable of evaluating the area and volume elements bounded by irregular contours using the triangularization technique. The volumes computed from the program, V_p, are compared with the volumes obtained from Equation (5.8), V_m, for different test durations used in tests 8 through 12 and 20 through 24 (See Figure 5.6). At the early stages, the model predicts the scour hole volumes relatively well. As time elapses, i.e. at t=100 min and 150 min, the model slightly underestimates the scour hole volumes than the findings of the program, but the average percent difference between two approaches is about 13%, which can be accepted reasonable. Therefore, Equation (5.8) is accepted to represent the scour hole volume expression around vertical-wall abutments.

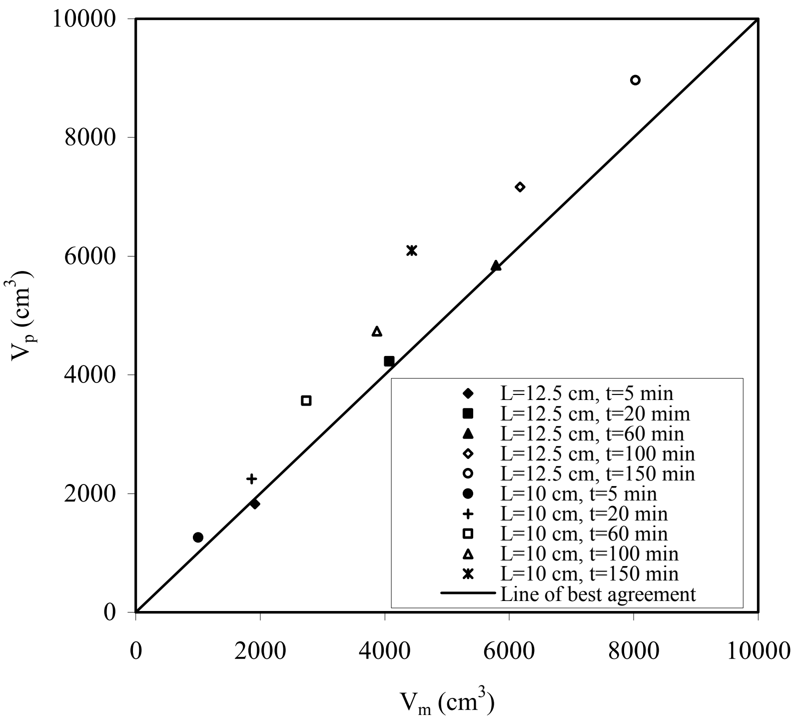

Figure 5.5. Comparison of the computed and measured scour hole volumes

To determine the temporal variation of the scour depth, Equation (5.1) is to be solved taking Q_{si}=0 and using the expressions given in Equations (5.2) and (5.8). Time derivative of Equation (5.8) is

$$\frac{dV}{dt}=\frac{d(d_s)}{dt}\left[\begin{array}{l}\frac{-2WL}{3}+\left(\frac{WL}{6}+\frac{Wd_s}{3\tan\theta}\right)A+\left(\frac{L^2}{3}+\frac{4Ld_s}{3\tan\theta}+\frac{{d_s}^2}{\tan^2\theta}\right)B+\\ \frac{C}{3}\left(L^2+\frac{2Ld_s}{\tan\theta}\right)+\frac{D}{3}\left(L^2+\frac{4Ld_s}{\tan\theta}+\frac{3{d_s}^2}{\tan^2\theta}\right)\end{array}\right] \tag{5.9}$$

The coefficient of proportionality, f, can then be determined from

$$f=\frac{\Delta\rho_s}{EA_p}\frac{dV}{dt} \tag{5.10}$$

Since sediment pickup rate is defined as the mass per unit area and time, a representative unit area needs to be defined. The upstream side of the scour hole is under the influence of primary vortices, where maximum scouring occurs. The part of the scour hole at the rear side of the abutment is subject to accretion. The side of the abutment parallel to the flow direction is under the effect of accelerated flow due to bridge constriction, which retards the sediment pickup from the side of the scour hole. Therefore, the whole perimeter of the scour hole cannot contribute to the sediment pickup. As a result, the upstream side of the scour hole can be considered for the definition of the unit area for sediment pickup. To this end, the unit area, A_p, from which sediment is picked up can be approximately taken as the projected width of the scour hole perpendicular to flow direction times the particle size, i.e. $((d_s\cot\theta+L)D_{50})$, where the term $d_s\cot\theta$ gives approximately the surface width of the scour hole measured from its edge to the face of the abutment (See Figure 5.6). This definition was first applied by Yanmaz and Altınbilek (1991) and was reused by Yanmaz (2006) for bridge piers. Since the sediment pickup rate is coupled with a unit area, the term EA_p accounts for the time-dependent changes of the sediment transport rate out of the scour hole.

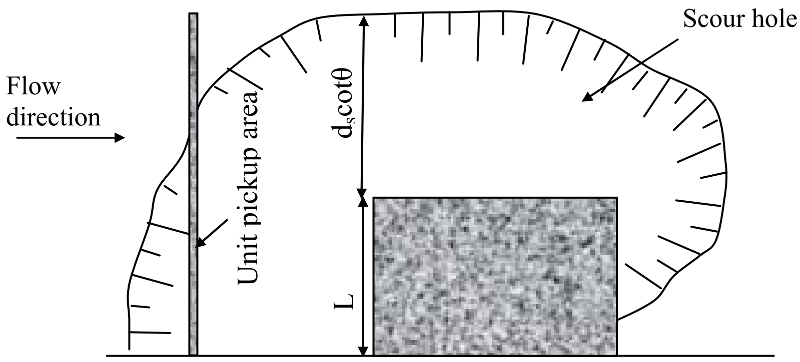

Figure 5.6. Definition sketch for unit sediment pickup area

Using the sediment pickup function proposed by Dey and Debnath (2001) and by inserting the relevant parameters into Equation (5.10), one obtains

$$f = \frac{\int_{ds1}^{ds2} \Delta\rho_s G d(d_s)}{\int_{t1}^{t2} 0.0006\rho_s \sqrt{\Delta g D_{50}}\, T D_*^{0.24} \sigma^{1.9} \left(\frac{d_s}{\tan\theta} + L \right) D_{50} dt} \tag{5.11}$$

where

$$G = \left[\frac{-2WL}{3} + \left(\frac{WL}{6} + \frac{Wd_s}{3\tan\theta} \right) A + \left(\frac{L^2}{3} + \frac{4Ld_s}{3\tan\theta} + \frac{d_s^{\,2}}{\tan^2\theta} \right) B + \frac{C}{3}\left(L^2 + \frac{2Ld_s}{\tan\theta} \right) + \frac{D}{3}\left(L^2 + \frac{4Ld_s}{\tan\theta} + \frac{3d_s^{\,2}}{\tan^2\theta} \right) \right]$$

Successive values of f can be computed from Equation (5.11) using the experimental values of d_s versus t in the calibration data outlined in Chapter 4, for the limits of the integration. An inspection of the computed f values indicates that the rate of sediment transport is inversely proportional to the instantaneous scour depth. At the early stages of each experiment, the net rate of sediment transport out of the scour hole is very high leading to large values of f. As the depth of scour increases, the net rate of sediment transport out of the scour hole decreases. This observation was also supported by Dargahi (1990) who investigated the temporal variation of Q_{so}.

Since f reflects the geometric characteristics of the scour hole as well as flow and sediment properties, it needs to be expressed explicitly by a suitable dimensionless form accounting for these effects. Successive trials have been carried out to establish a functional relationship for the coefficient of proportionality, f. To this end, various combinations of dimensionless parameters reflecting these aspects, i.e. shear velocity of the approach flow (u_*), time (t), median sediment size (D_{50}), angle of repose of the sediment (θ), flow intensity (u/u_c), and abutment length are formed and tested to achieve a form having the highest coefficient of correlation. A list of combinations of such dimensionless parameters is shown below:

$$f = h\left(\frac{u_* t D_{50}}{L^2}, \frac{u_* t}{L,}, \frac{d_s \cot\theta}{L}, \frac{u}{u_c}\right) \tag{5.12}$$

where h is a function. In this study, the following functional forms are considered for f:

$$f_1 = c_0 \left(\frac{u_* t}{L}\right)^{c_1} \left(\frac{d_s \cot\theta}{L}\right)^{c_2} \tag{5.13}$$

$$f_2 = c_0 \left(\frac{u_* t D_{50}}{L^2}\right)^{c_1} \left(\frac{d_s \cot\theta}{L}\right)^{c_2} \tag{5.14}$$

$$f_3 = c_0 \left(\frac{u_* t}{L}\right)^{c_1} \left(\frac{d_s \cot\theta}{L}\right)^{c_2} \left(\frac{u}{u_c}\right)^{c_2} \tag{5.15}$$

in which c_0 is a coefficient, and c_1, c_2, and c_3 are the powers of the expressions given in Equations (5.13) through (5.15) which attain different values for each functional form of f. The coefficient and powers of these expressions can be obtained from multiple regression analysis. The results of these manipulations are presented in Table 2. Equation (5.13) was accepted to represent the form of f since it resulted in the maximum coefficient of correlation. The correlation between the computed (f_c) and predicted (f_p) values is shown in Figure 5.7.

Table 5.1. Selection criterion for f values

Function	c_0	c_1	c_2	c_3	R^2
f_1	1205	-0.90	0.016	-	0.80
f_2	32	-1.06	1.47	-	0.76
f_3	560	-0.85	-0.37	-2.09	0.77

Equations (5.9), (5.10), and (5.13) are then combined and solved for $d(d_s)/dt$ to obtain

$$\frac{d(d_s)}{dt} = \frac{0.438\left(\dfrac{d_s}{L\tan\theta}\right)^{-0.90}\left(\dfrac{u_* t}{L}\right)^{0.016} T D_*^{0.24}\sigma^{1.9}\sqrt{\Delta g D_{50}}\left(\dfrac{d_s}{\tan\theta}+L\right)D_{50}}{G} \tag{5.16}$$

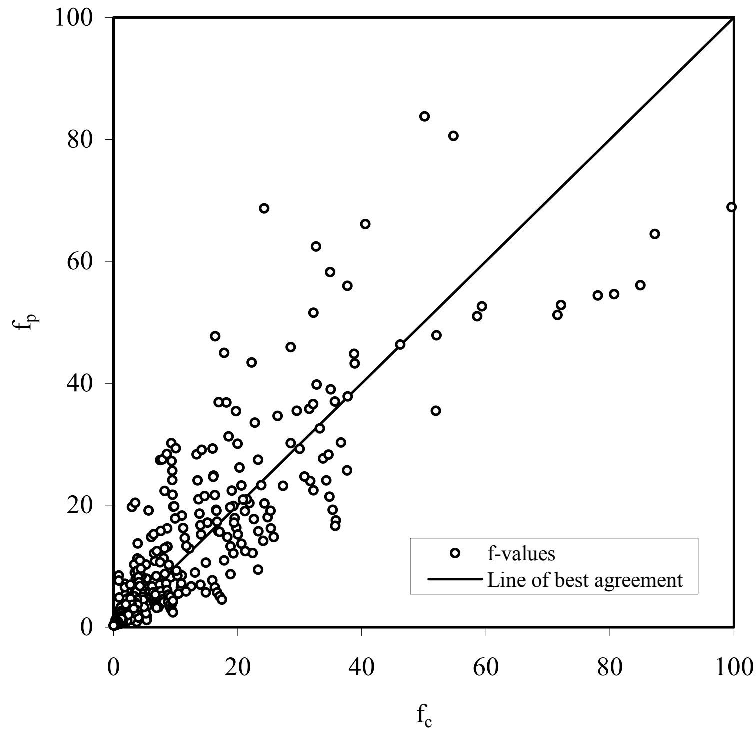

Figure 5.7. Correlation between predicted and computed f-values

Solution of Equation (5.16) is presented in Figures 5.8 through 5.28 for the experimental sets of the calibration data. In the solution, the value of the relative density was selected as Δ=1.65 for quartz sand.

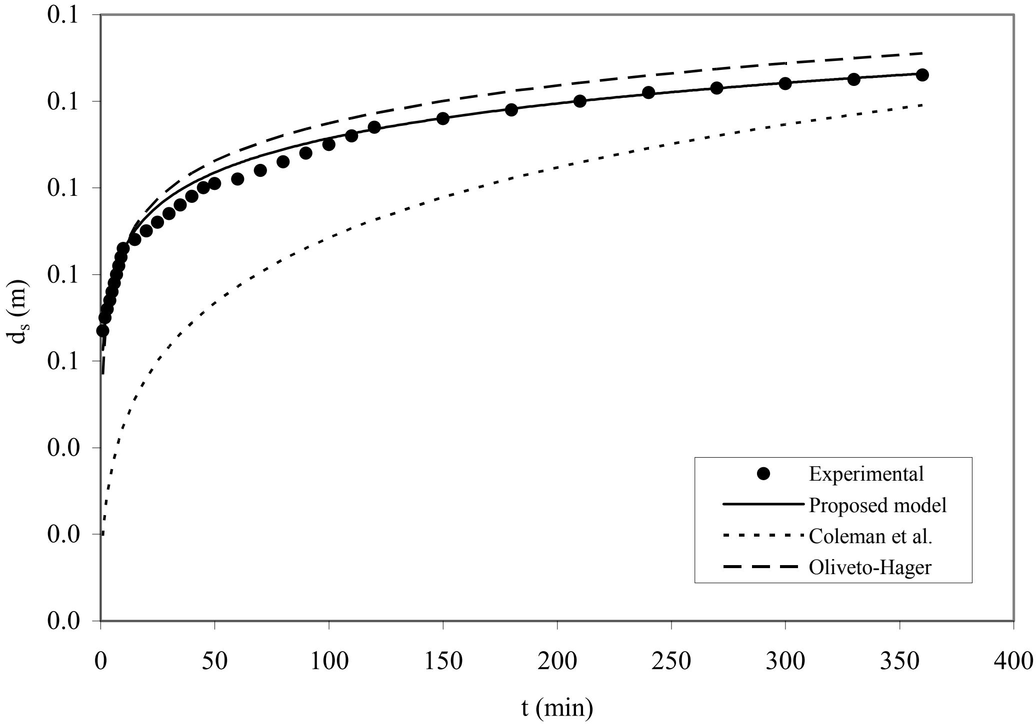

Figure 5.8. Computed versus experimental scour depths for Experiment 1

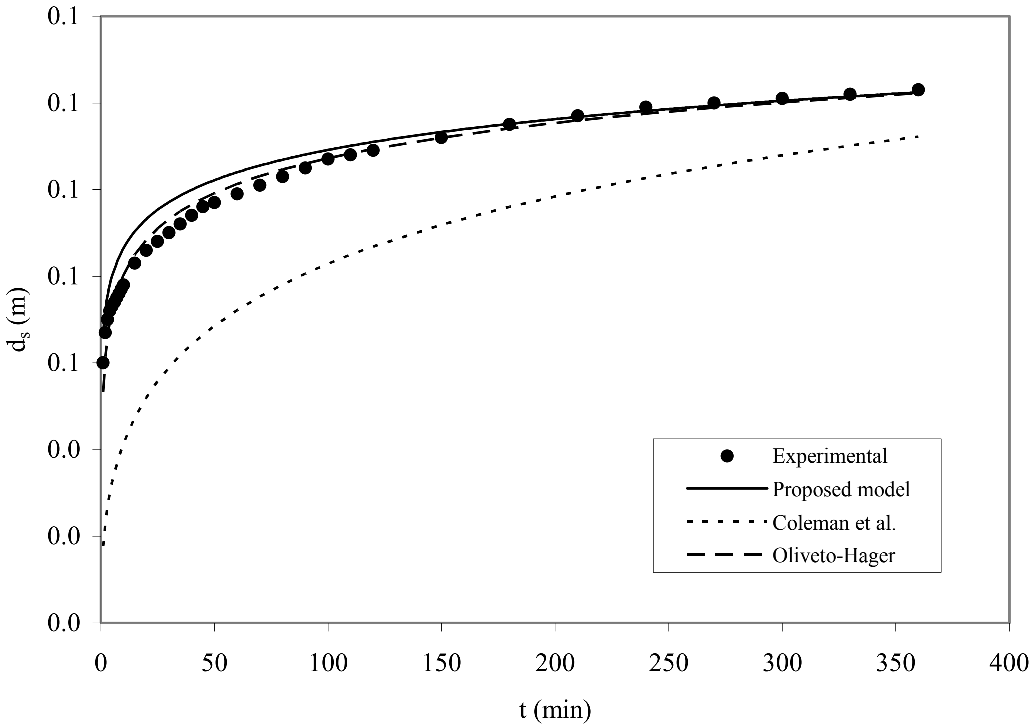

Figure 5.9. Computed versus experimental scour depths for Experiment 2

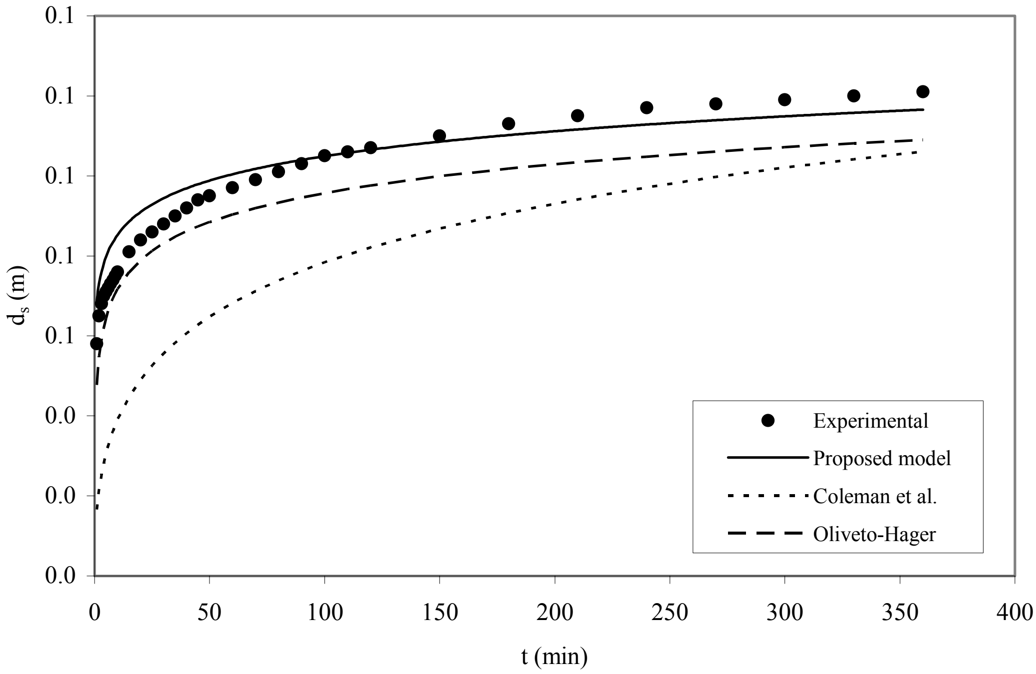

Figure 5.10. Computed versus experimental scour depths for Experiment 3

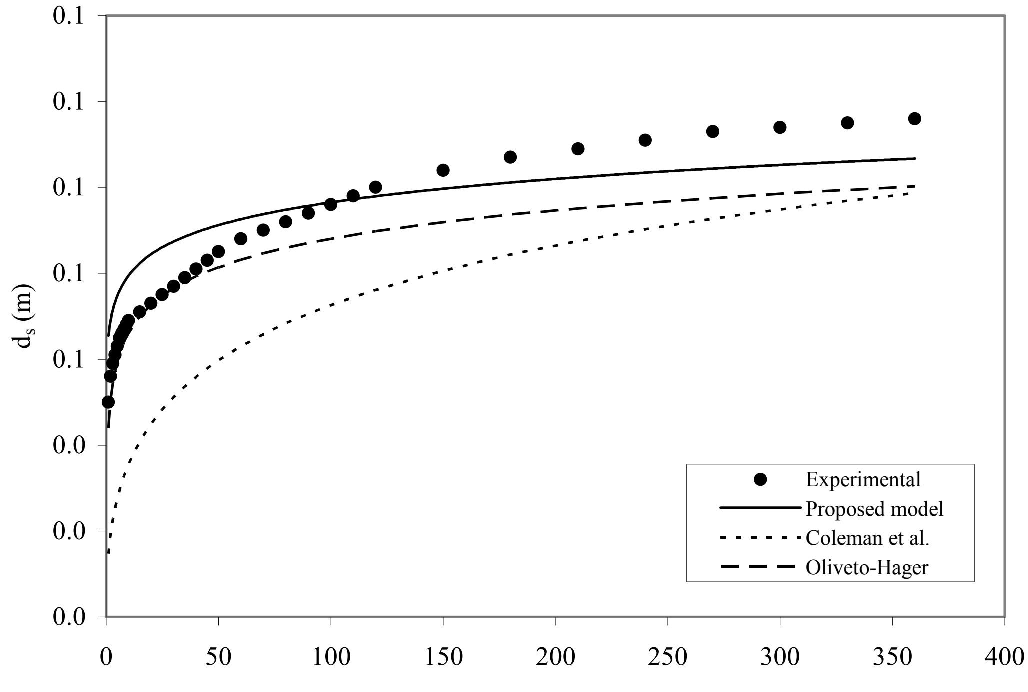

Figure 5.11. Computed versus experimental scour depths for Experiment 4

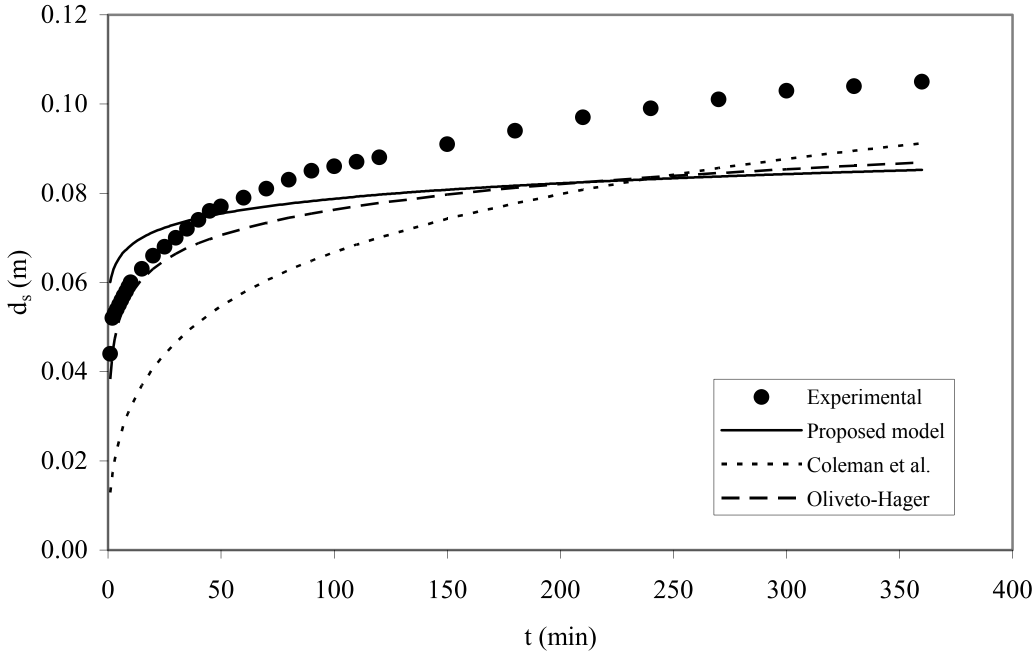

Figure 5.12. Computed versus experimental scour depths for Experiment 5

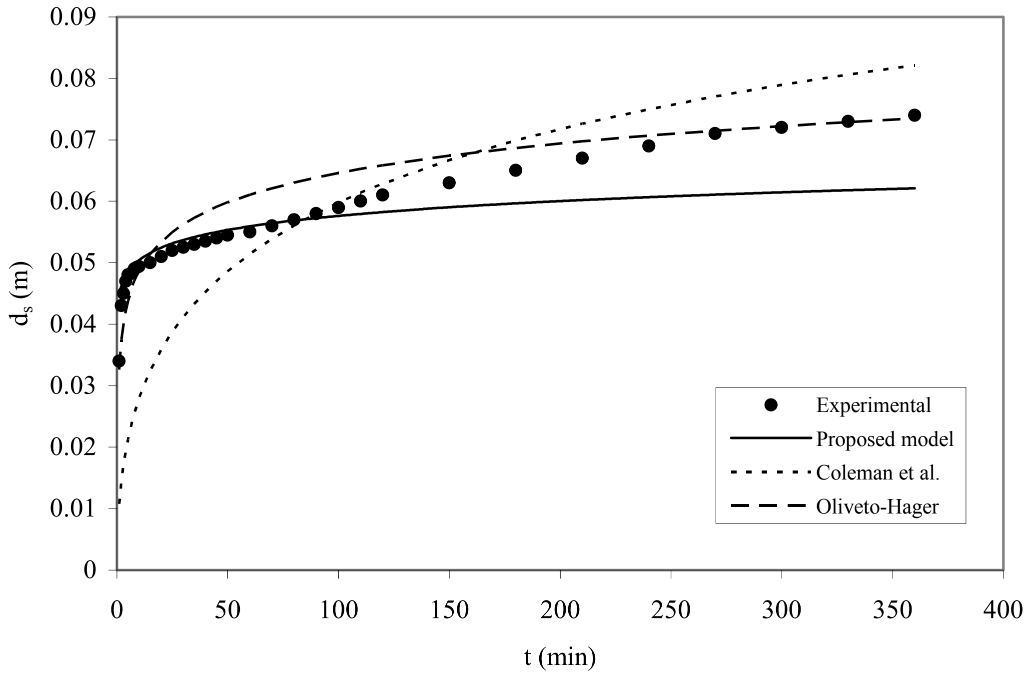

Figure 5.13. Computed versus experimental scour depths for Experiment 6

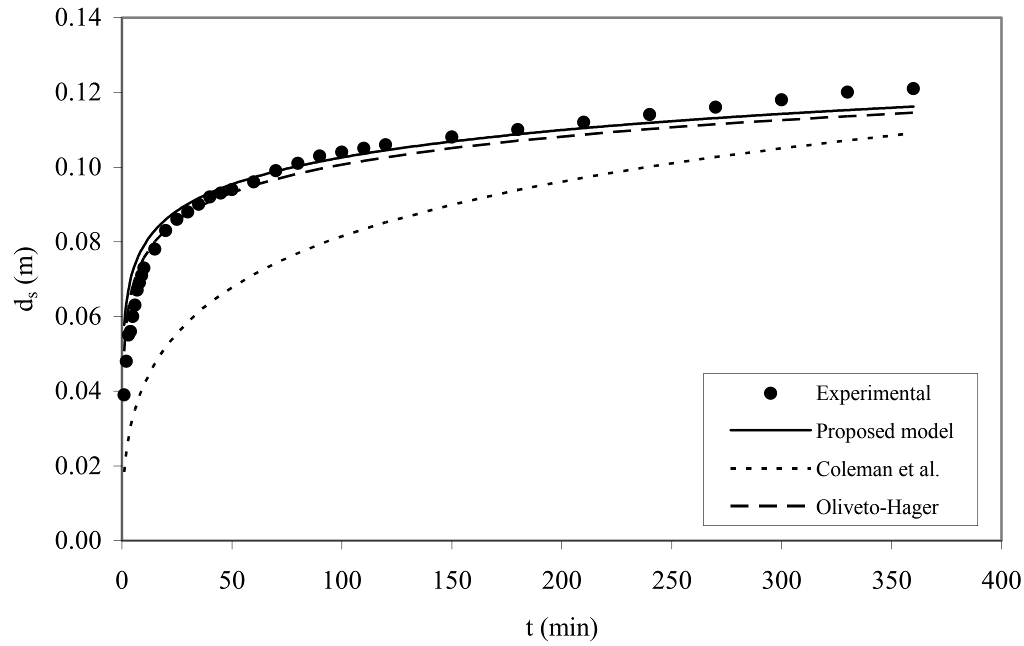

Figure 5.14. Computed versus experimental scour depths for Experiment 13

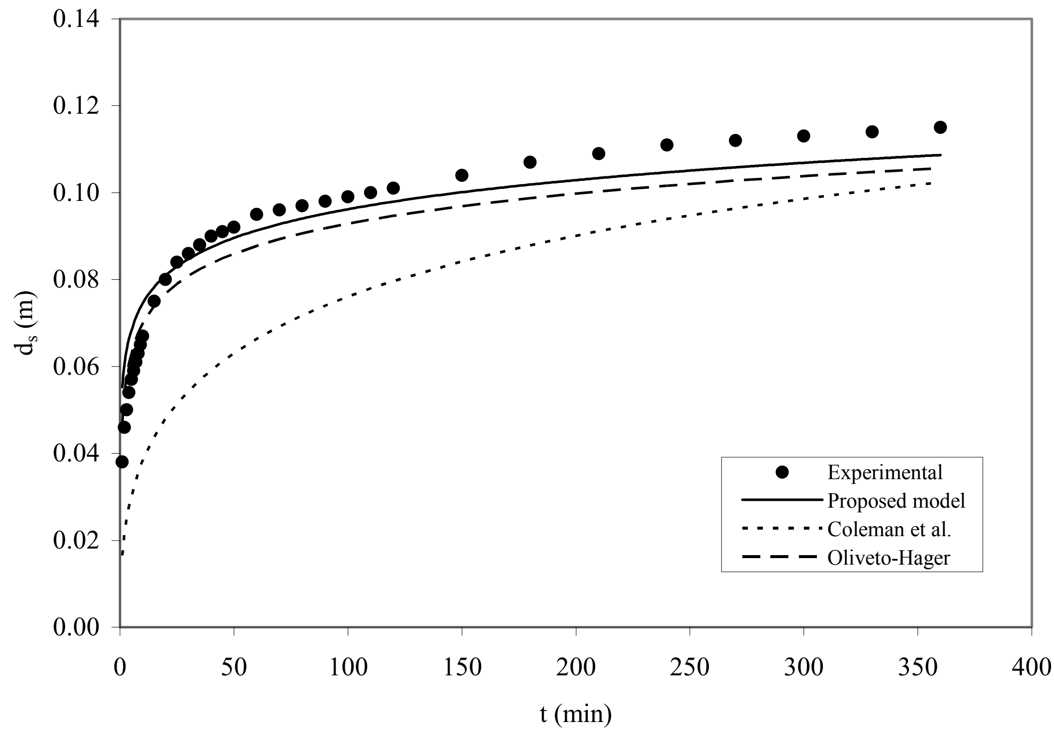

Figure 5.15. Computed versus experimental scour depths for Experiment 14

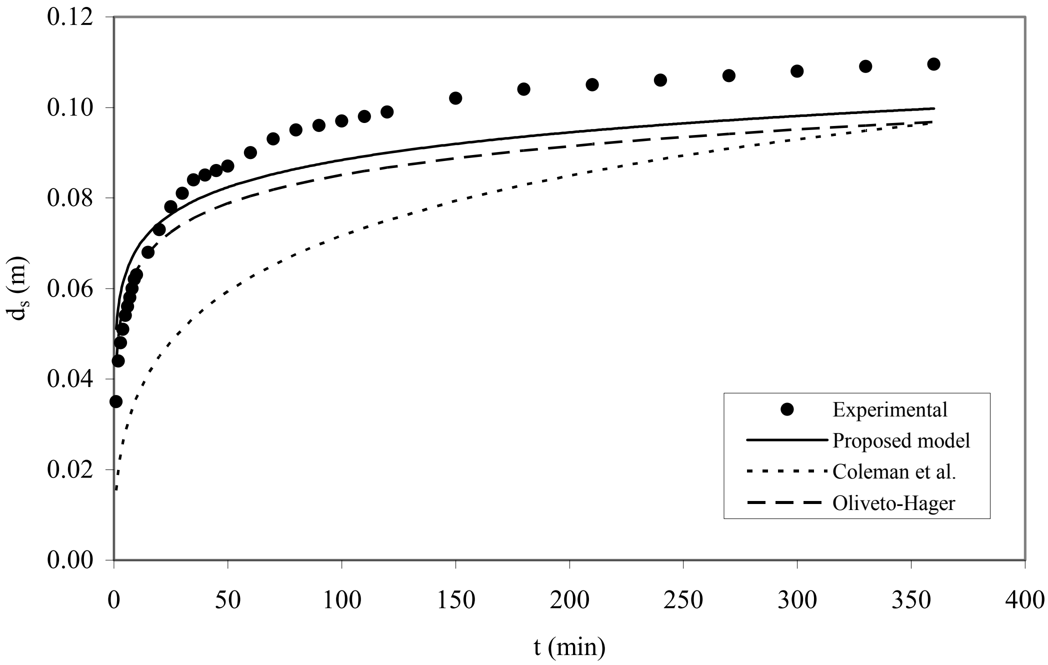

Figure 5.16. Computed versus experimental scour depths for Experiment 15

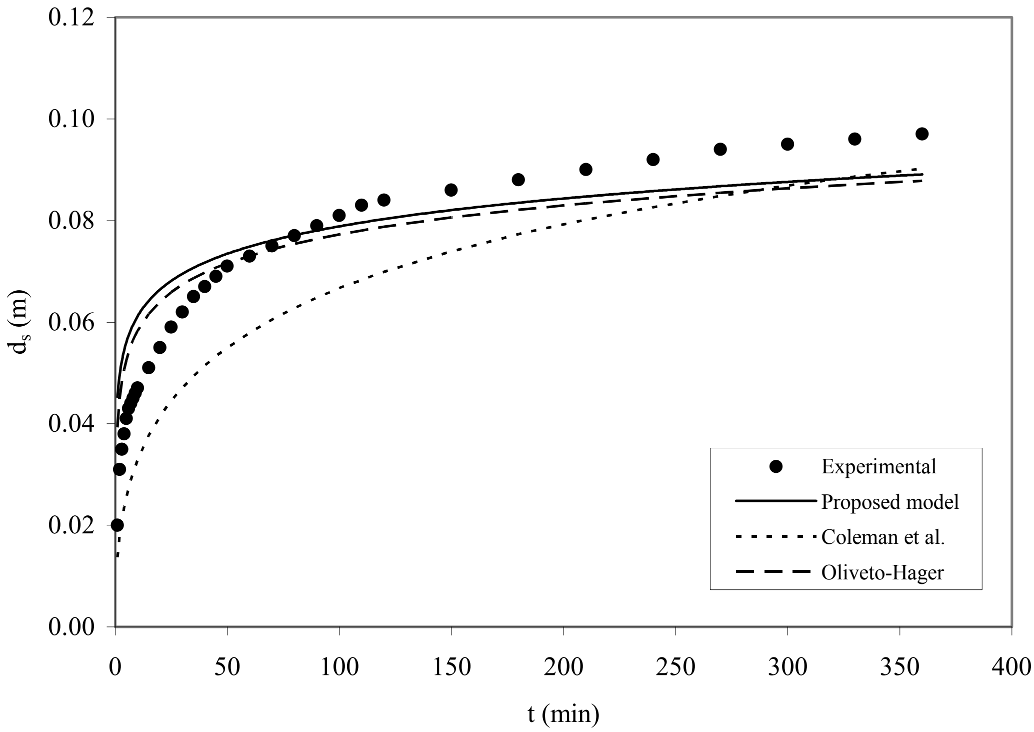

Figure 5.17. Computed versus experimental scour depths for Experiment 16

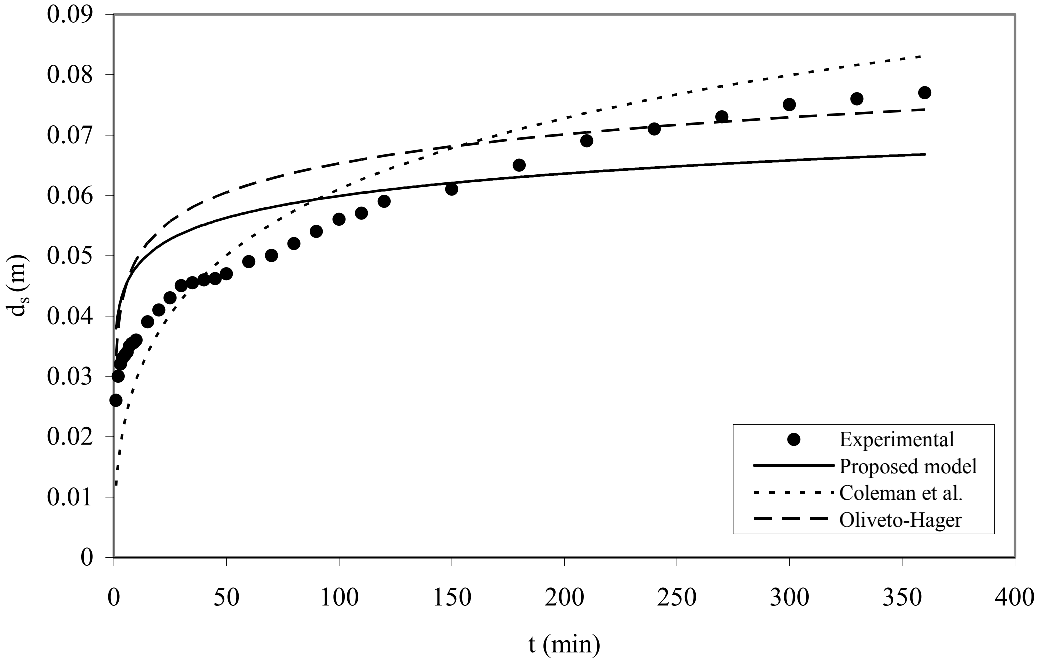

Figure 5.18. Computed versus experimental scour depths for Experiment 17

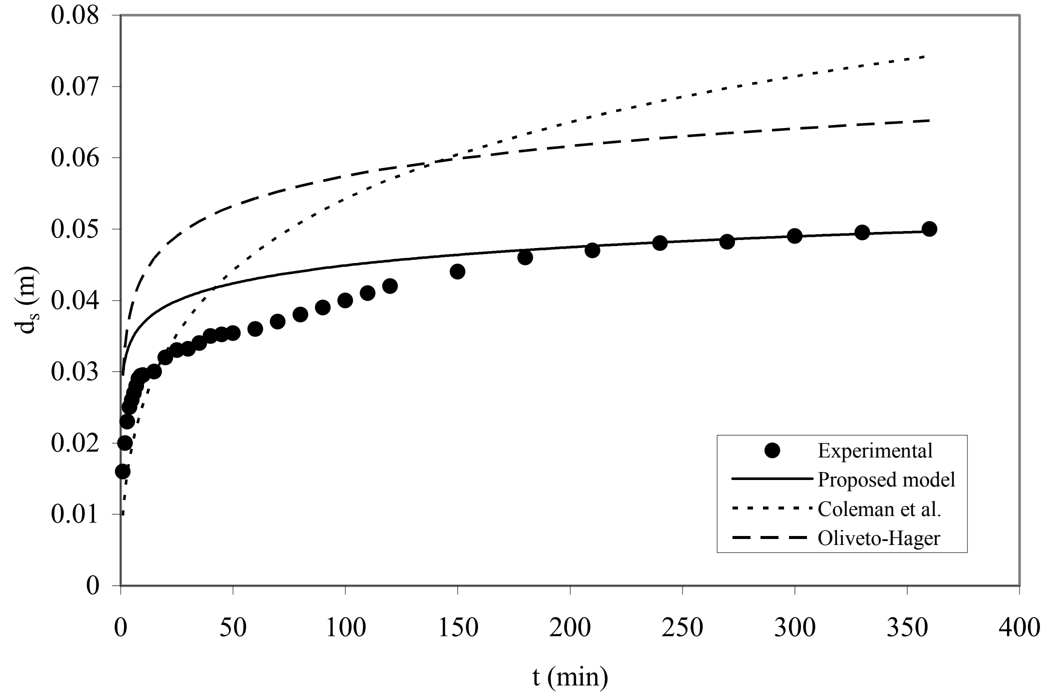

Figure 5.19. Computed versus experimental scour depths for Experiment 18

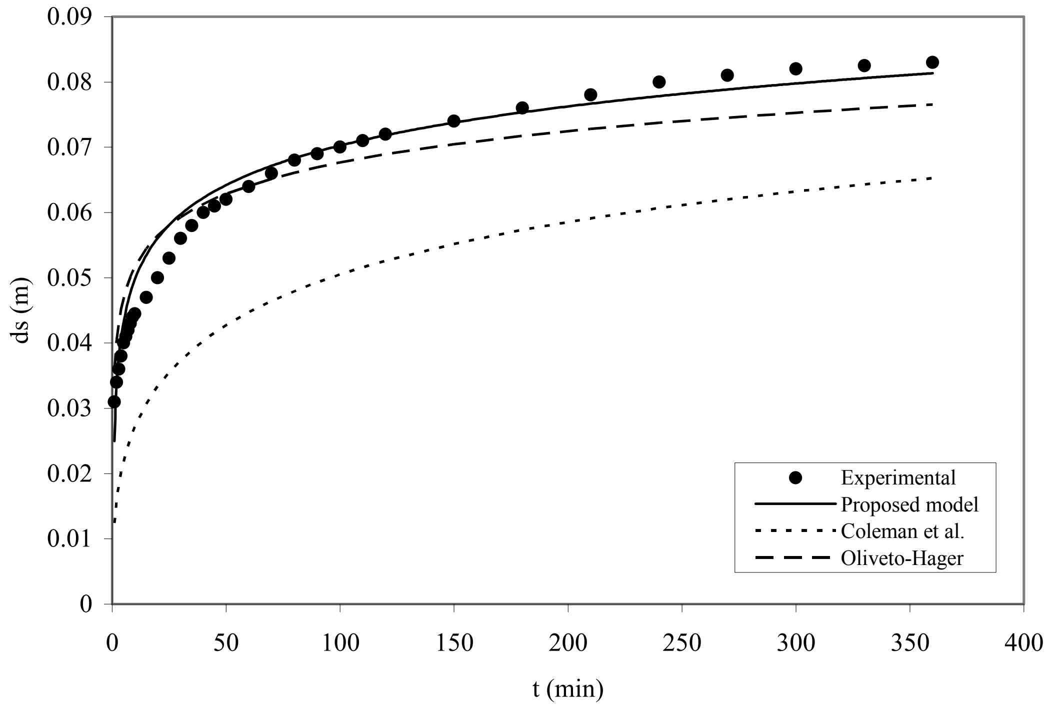

Figure 5.20. Computed versus experimental scour depths for Experiment 25

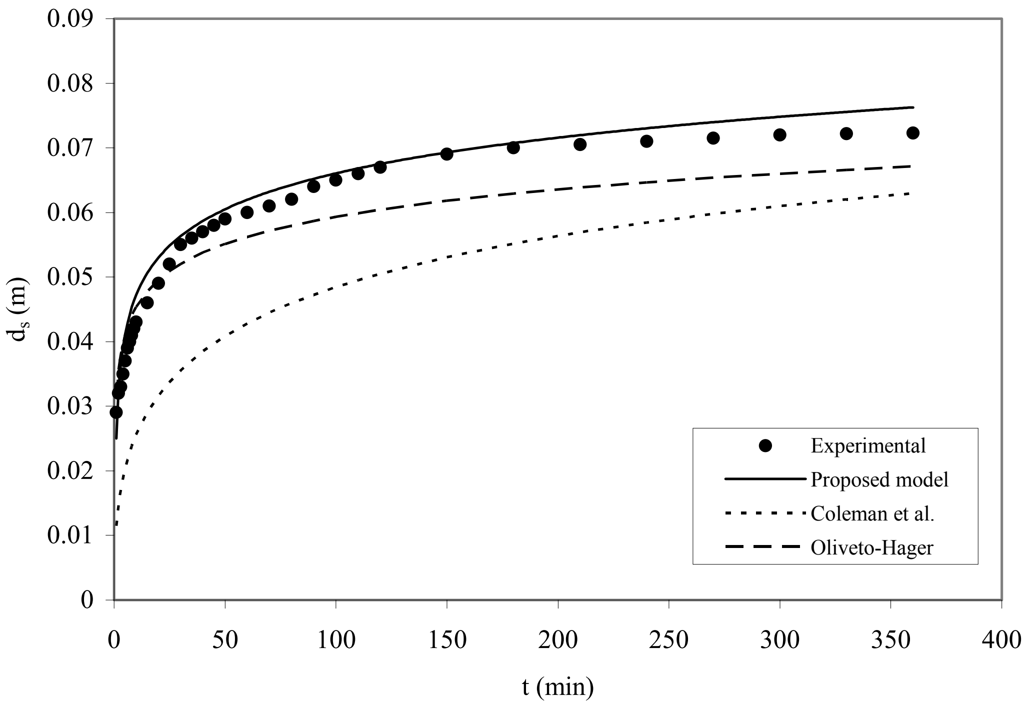

Figure 5.21. Computed versus experimental scour depths for Experiment 26

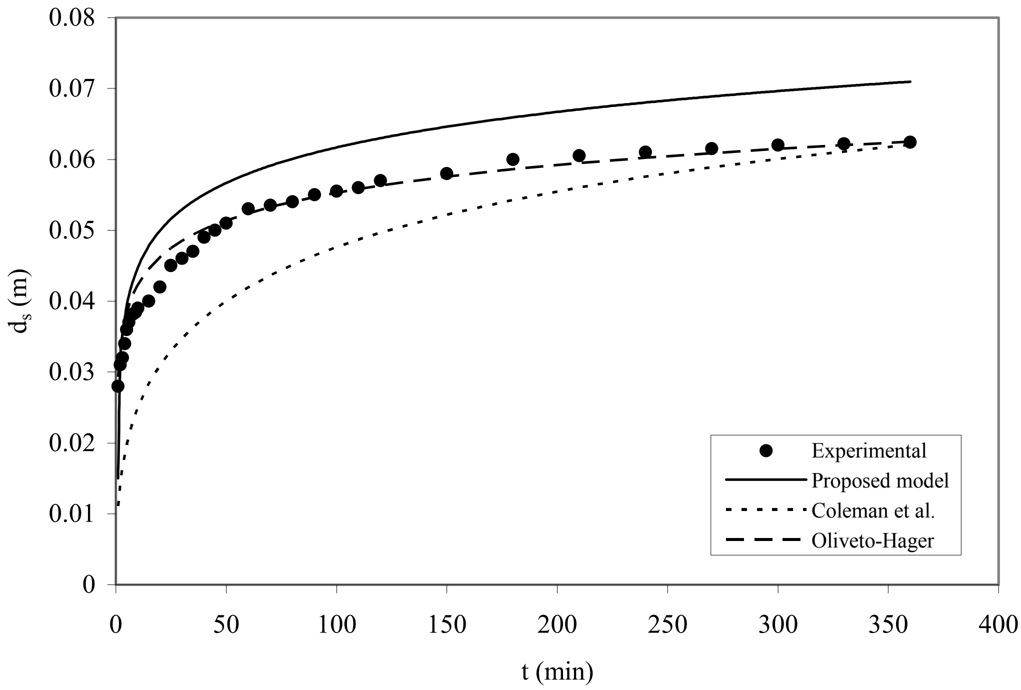

Figure 5.22. Computed versus experimental scour depths for Experiment 27

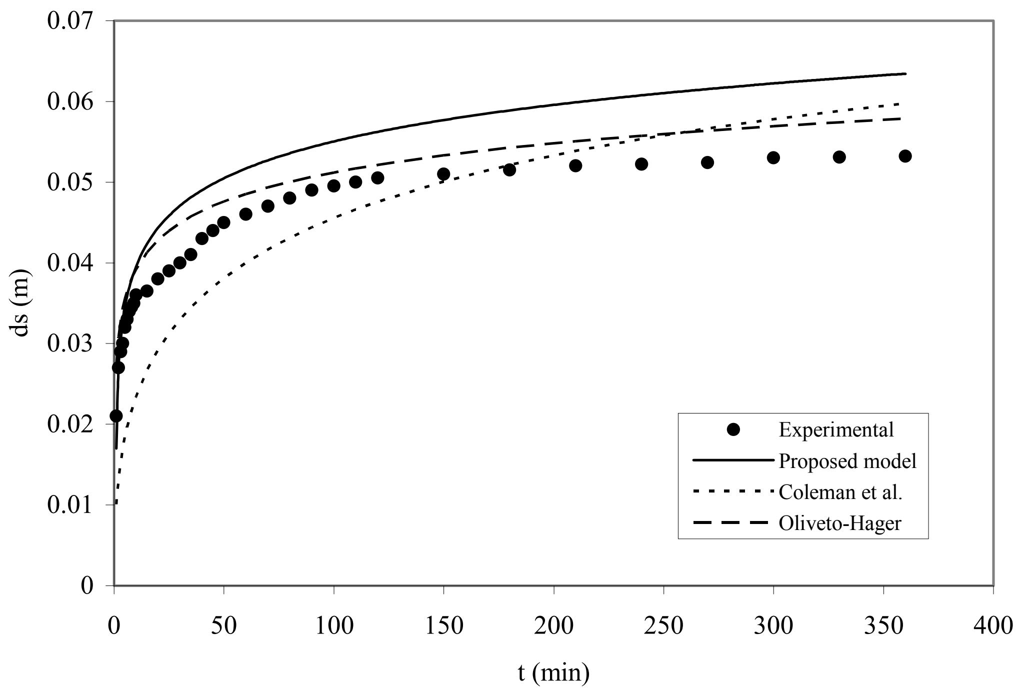

Figure 5.23. Computed versus experimental scour depths for Experiment 28

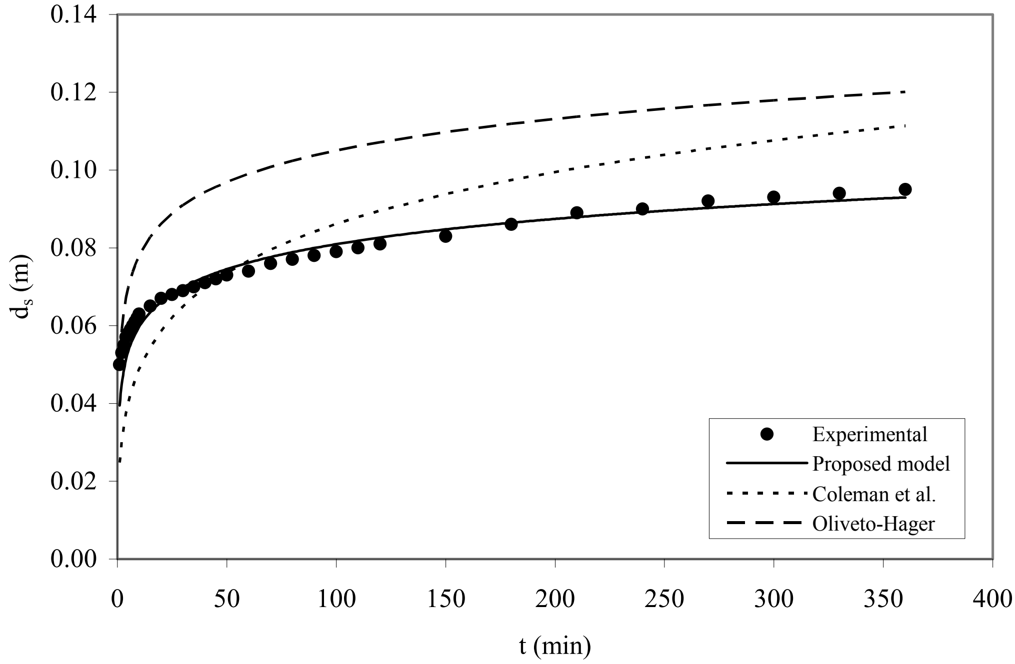

Figure 5.24. Computed versus experimental scour depths for Experiment 61

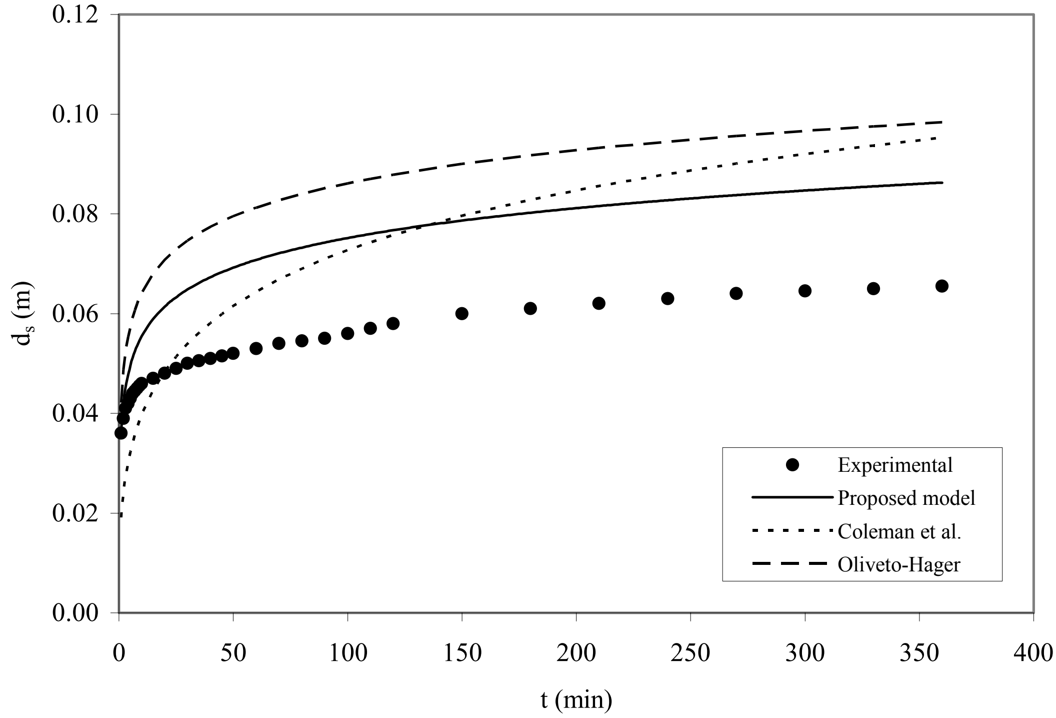

Figure 5.25. Computed versus experimental scour depths for Experiment 62

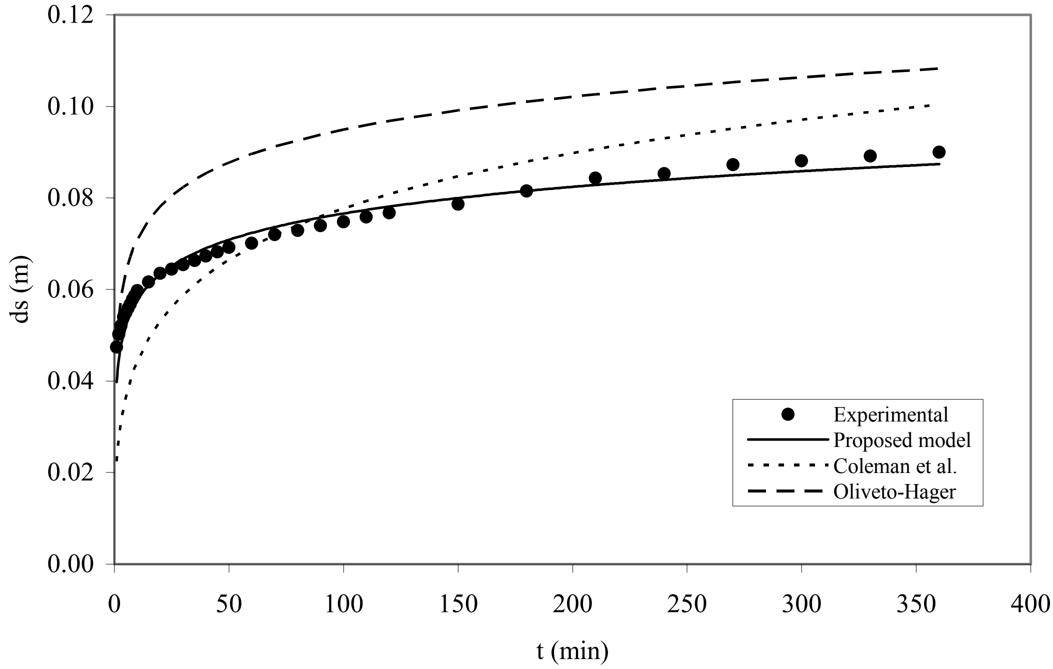

Figure 5.26. Computed versus experimental scour depths for Experiment 64

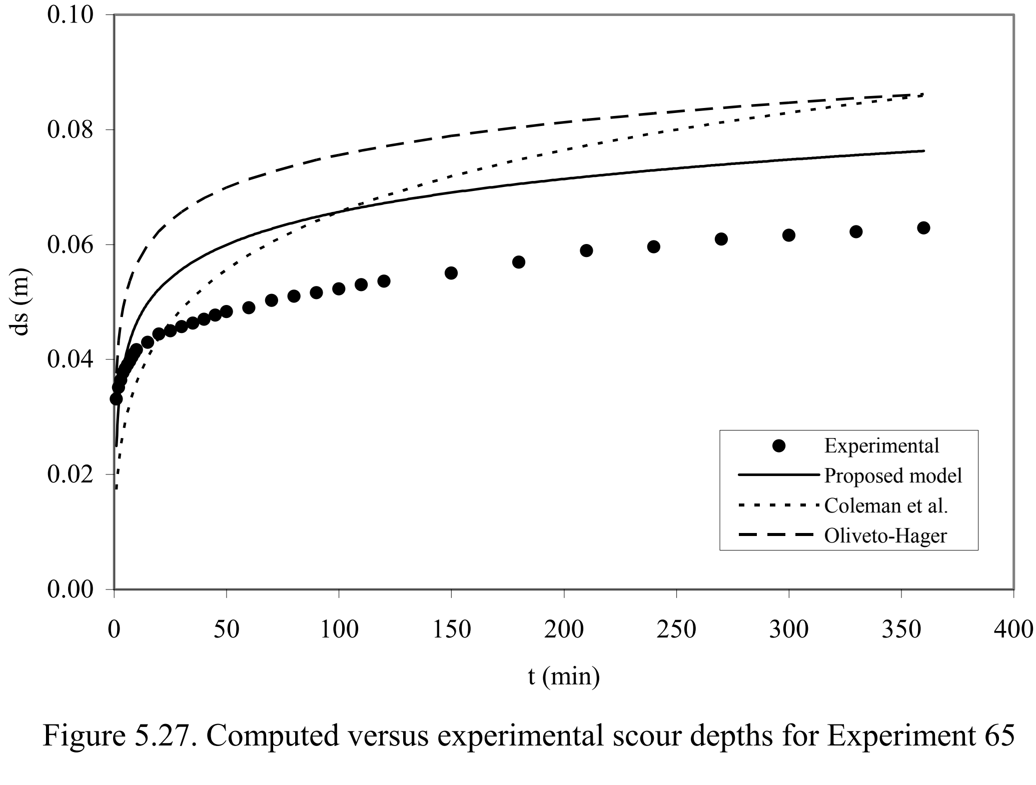

Figure 5.27. Computed versus experimental scour depths for Experiment 65

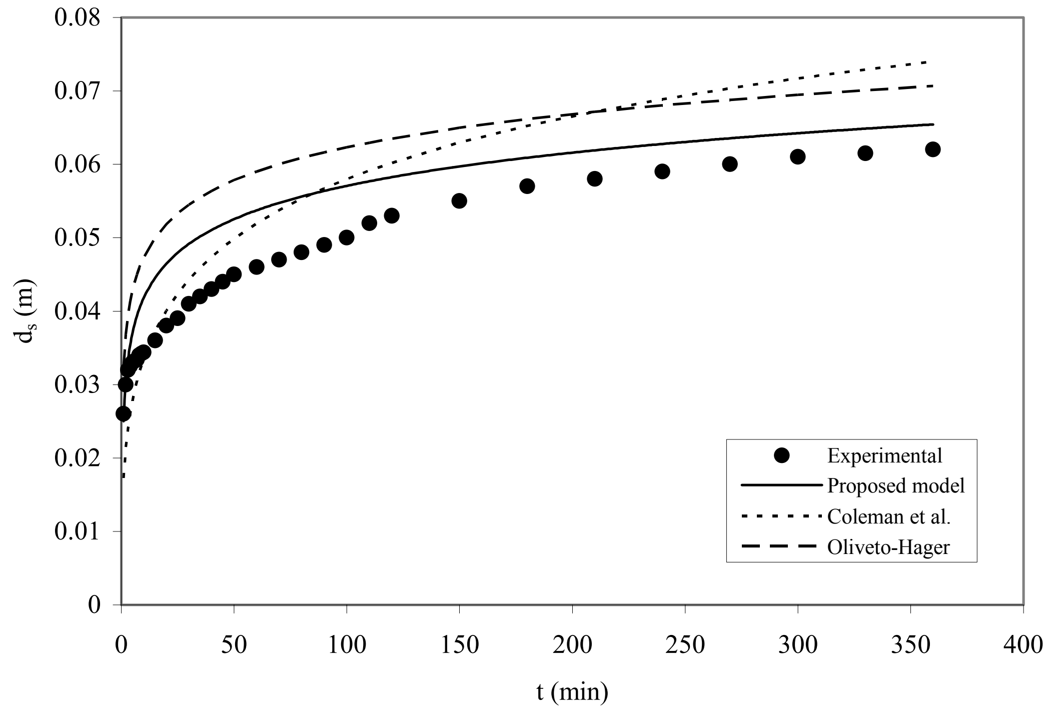

Figure 5.28. Computed versus experimental scour depths for Experiment 67

As can be seen from Figures 5.8 through 5.28, the results of the computed scour depths obtained from Equation (5.16) are in relatively good agreement with the experimental values. The agreement of the new model proposed herein with the methods proposed by Coleman et al. (2003) and Oliveto and Hager (2002) will be observed using the experimental data. Based on the discussion given in Chapter 4, other scour-prediction equations were not used in the comparison of the results of the proposed model.

To take into account the temporal discrepancy of the computed scour depths, the total time span was divided into sub-intervals, i.e. Δt_1 ($0<t\leq 20$ min), Δt_2 (20 min$<t\leq 45$ min), Δt_3 (45 min$<t\leq 100$ min), and Δt_4 (100 min$<t\leq 360$ min). A prediction factor, R, is defined as the ratio of the instantaneous values of the computed scour depth to the experimentally determined scour depth in these time intervals. Since the perfect agreement corresponds to R=1.0, then the standard error of estimate, S_e, of the prediction factors were computed in these time intervals. Mean prediction factor,

R_m, is used to assess the prediction level in a particular time interval. The results of this analysis are shown in Figures 5.29 through 5.33. These figures imply that the average predictive ability of the present model is higher than the aforementioned two methods. Moreover, the proposed model gives better prediction, i.e. R_m and S_e values decrease, with respect to time. Similar tendencies are also observed for the Oliveto-Hager (2002) and Coleman et al. (2003) approaches. In all the intervals tested, the Coleman et al. (2003) approach yielded smaller scour depths, whereas the Oliveto-Hager (2002) method predicted slightly greater scour depths than the experimental values.

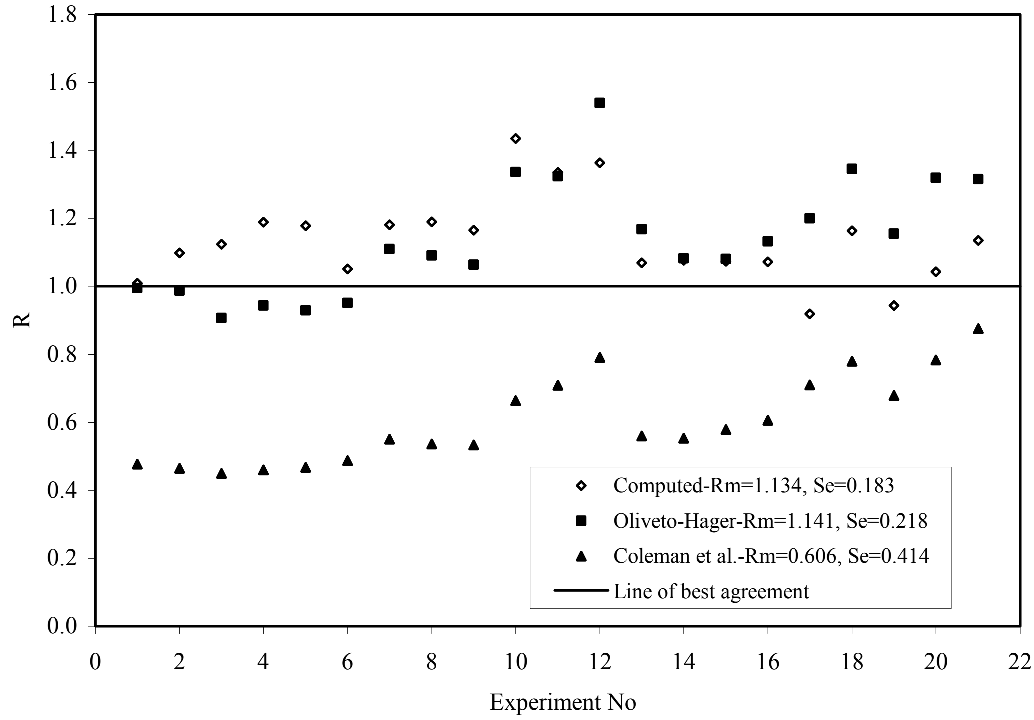

Figure 5.29. Scour prediction factors in time interval, Δt_1

Since the proposed model predicts the scour depths satisfactorily, presentation of Equation (5.16) in dimensionless form would be of practical interest. To this end, Equation (5.16) is transformed to dimensionless form. For dimensionless scour depth, $S=d_s/L$ term was used. For dimensionless time, $T_s=tD_{50}(\Delta g D_{50})^{0.5}/L^2$ was defined as it was also used previously by Yanmaz and Altinbilek (1991) for bridge piers and Dey And Barbhuiya (2005) for abutments. Use of T_s is assumed to be reasonable since it reflects the combined effects of time, sediment, and abutment length and it is independent of equilibrium scouring parameters.

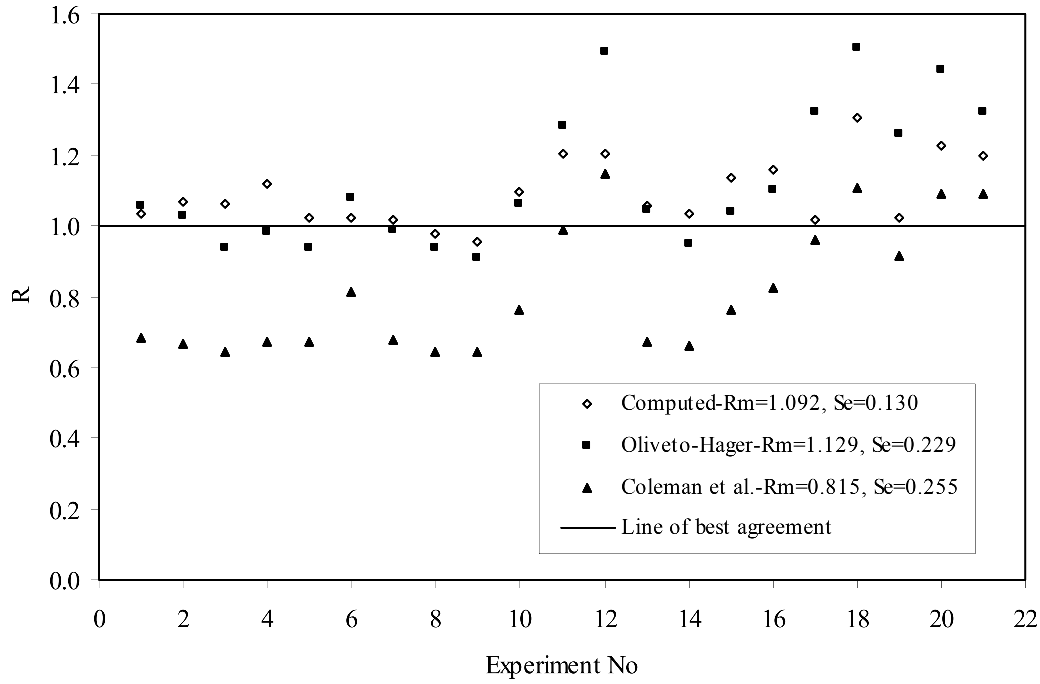

Figure 5.30. Scour prediction factors in time interval, Δt_2

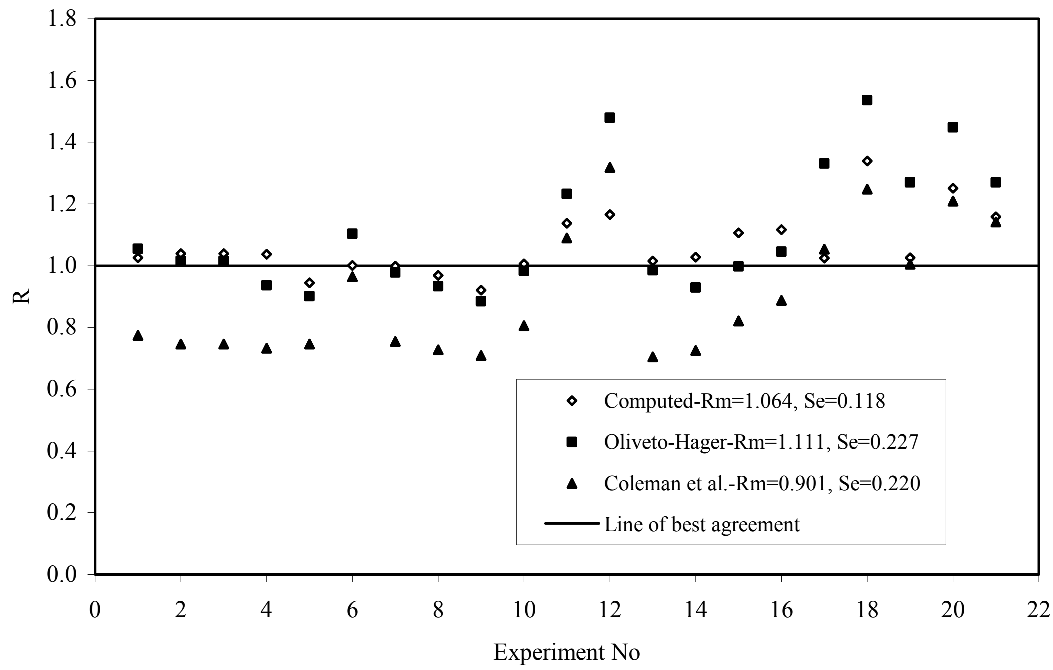

Figure 5.31. Scour prediction factors in time interval, Δt_3

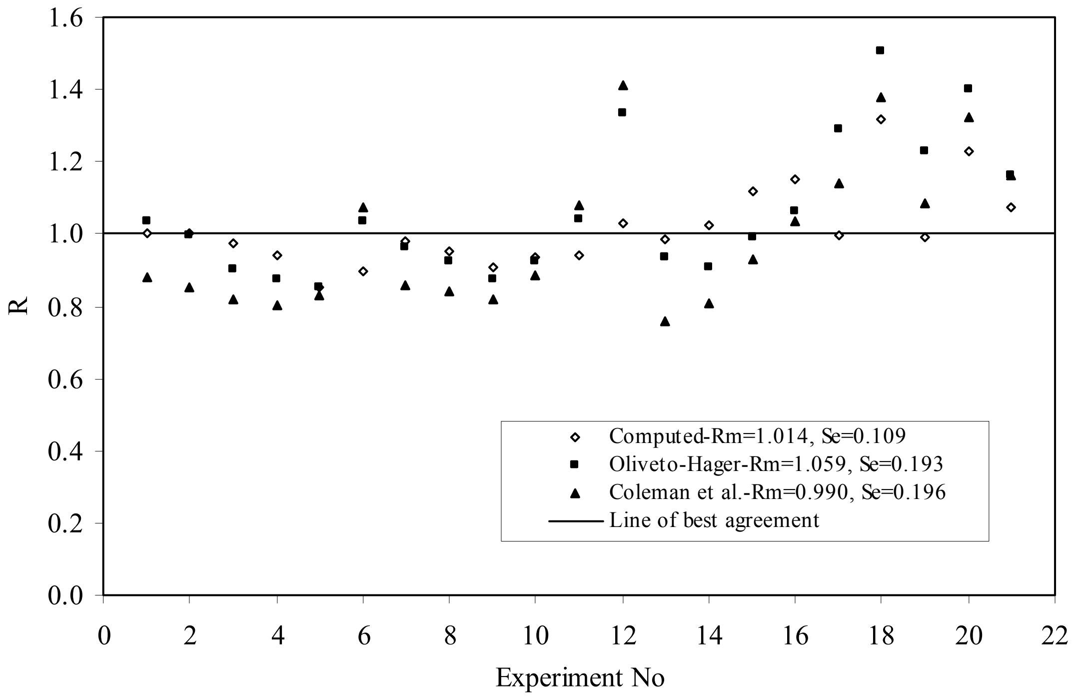

Figure 5.32. Scour prediction factors in time interval, Δt_4

By substituting S and T_s terms into Equation (5.16) the following dimensionless equation is obtained.

$$\frac{dS}{dT_s} = \frac{m(S\cot\theta)^{-0.90} T_s^{0.016}(S\cot\theta + 1)}{H} \tag{5.17}$$

$$H = \left[\begin{array}{l} \dfrac{-2\alpha}{3} + \left(\dfrac{\alpha}{6} + \dfrac{\alpha S}{3\tan\theta}\right)A + \left(\dfrac{1}{3} + \dfrac{4S}{3\tan\theta} + \dfrac{S^2}{\tan^2\theta}\right)B + \\ \dfrac{C}{3}\left(1 + \dfrac{2S}{\tan\theta}\right) + \dfrac{D}{3}\left(1 + \dfrac{4S}{\tan\theta} + \dfrac{3S^2}{\tan^2\theta}\right) \end{array}\right]$$

where α=W/L and m is as in the following:

$$m = 0.438\left(N\frac{L}{D_{50}}\right)^{0.016} TD_*^{0.24}\sigma^{1.9} \tag{5.18}$$

in which N is the densimetric particle Froude number based on the shear velocity of approach flow, $(u_*(\Delta g D_{50})^{0.5})$. For a particular combination of flow and sediment properties and a given value of abutment length, the value of m is computed. Therefore, the variation of dimensionless scour depth with respect to dimensionless time is obtained by the numerical solution of Equation (5.17), which is a first-order nonlinear differential equation. Graphical representation of this solution would greatly reduce the computational efforts. Figure 5.33 shows one of the charts with α=2.0 for a set of m values used in the calibration data. Similar graphs can also be obtained for different combinations of m and α values. Use of the chart in Figure 5.33 requires the computation of m using the input variables, i.e. the length of a vertical-wall abutment, design flow data, and sediment properties.

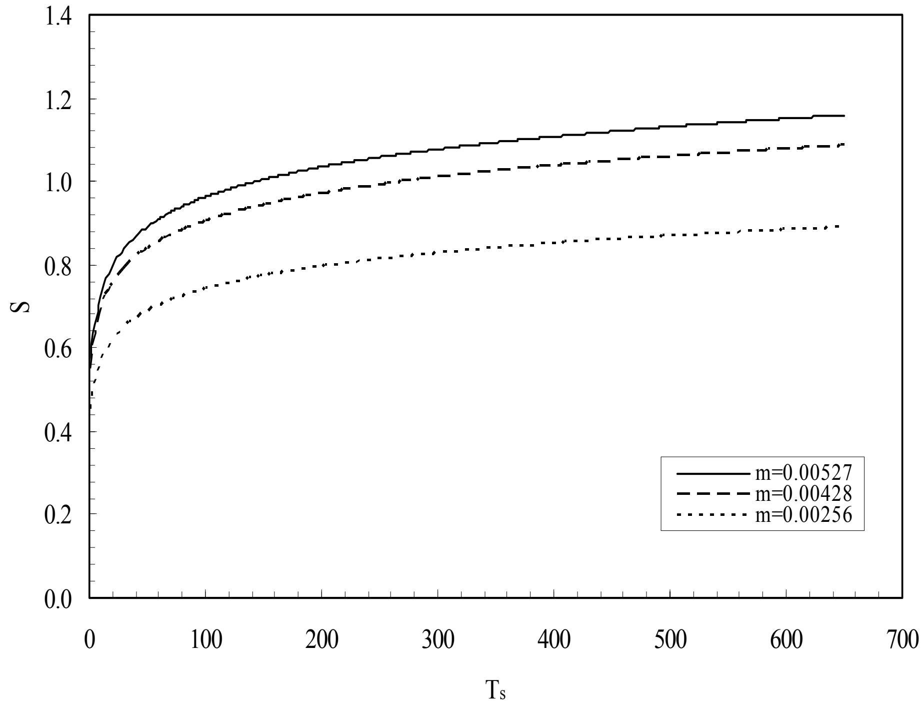

Figure 5.33. Dimensionless variation of scour depth for $\alpha = 2$

With the time to peak value of the design flood, the dimensionless time T_s is computed and the corresponding scour depth is determined from Figure 5.33 using the respective curve for m.

5.2. Model Development-Approach 2

This section presents development of another semi-empirical model, which uses an empirical relation, i.e. Equation (4.2) for the scour hole around a vertical-wall abutment. As stated before Equation (4.2) is based on using one type of sediment with two different abutment lengths. Although similar scouring characteristics are expected under different F_d values because of fundamental similarity of all types of clear water scouring conditions, potential effects of varying sediment sizes and abutment lengths on this expression may also be tested. Inspection of the time-dependent scour contours indicates that the rate of change of scour hole volume decreases with respect to time. This tendency can also be observed from Figure 4.4.

In the second approach, the same definition will also be used for the pickup area as was considered in the first approach. The coefficient of proportionality, f, will be determined using the experimental values in the calibration data. To determine the temporal variation of the scour depth, Equation (5.1) is to be solved with $Q_{si}=0$ using the expressions given in Equations (5.2), and (5.3). Inserting the values of V* and T_s into Equation (4.2), time derivative of the volume of the scour hole around the vertical-wall abutment is obtained as

$$\frac{dV}{dt} = ct^{0.281}\frac{dd_s}{dt} + \frac{0.281cd_s}{t^{0.719}} \tag{5.19}$$

where $c = 1.142L^{1.438}D_{50}^{0.281}(\Delta gD_{50})^{0.1405}$. Using the sediment pickup function given in Equation (5.3) and by inserting the relevant parameters into Equation (5.2), one obtains

$$f = \frac{\int_{ds1}^{ds2} m_c ct^{0.281} dd_s + \int_{t_1}^{t_2} 0.281mcd_s t^{-0.719} dt}{\int_{t_1}^{t_2} (d_s \cot\theta + L)dt} \tag{5.20}$$

where $m_c=\Delta\rho_s/(ED_{50})$. Successive values of f can be computed from Equation (5.20) using the d_s versus t values of the experiments in the calibration data for the limits of the integration. With reference to the similar discussion made for the form of f, the following equation has been obtained through a multiple linear regression analysis

$$f_1 = 143\left(\frac{u_* t}{L}\right)^{-0.31}\left(\frac{d_s \cot\theta}{L}\right)^{-2.95} \tag{5.21}$$

Equations (5.2), (5.19), and (5.21) combined to obtain

$$\frac{dd_s}{dt} = f\,\frac{(d_s \cot\theta + L)}{m_c c t^{0.281}} - \frac{0.281 d_s}{t} \tag{5.22}$$

Equation (5.22) was solved numerically using Euler's technique to compare its findings with the corresponding solutions obtained from the first approach. The results of this analysis are presented in Appendix 1. The non-dimensional form of Equation (5.22) can be obtained in a similar manner as performed in the first approach to obtain

$$\frac{dS}{dT_s} = \frac{125(S\cot\theta + 1)}{A_b (S\cot\theta)^{2.95} T_s^{0.591}} - \frac{0.281 S}{T_s} \tag{5.23}$$

where $A_b=m_c a^{0.31} D_{50}(\Delta g D_{50})^{0.5}$, is a parameter reflecting combined effects of flow, sediment, and abutment properties, which are normally the design inputs. Solution of Equation (5.23) is presented in Figure 5.34 for various values of A_b. With the given hydrologic data as well as sediment and abutment size information, the values of T_s and A_b are computed. The corresponding value of S is then obtained from the design chart presented in Figure 5.34. Computational efforts for obtaining the scour depth using both approaches are almost the same. However, the results obtained from both approaches may show slight differences because of variations in the form of governing nonlinear differential equations, i.e. Equation (5.16) and Equation (5.22) for the first and second approaches, respectively (See Figures A1 through A21 in Appendix). That is why a similar analysis was carried as performed for the first approach to assess the predictive ability of these approaches with respect to mean values and standard errors of estimates of the dimensionless scour depths in four different intervals of dimensionless time, i.e. $0<t/t_m \leq 0.05$, $0.05< t/t_m \leq 0.20$, $0.20< t/t_m \leq 0.50$, and $0.50< t/t_m \leq 1.0$. The results of the this analysis are shown in Figures 5.35 through 5.38.

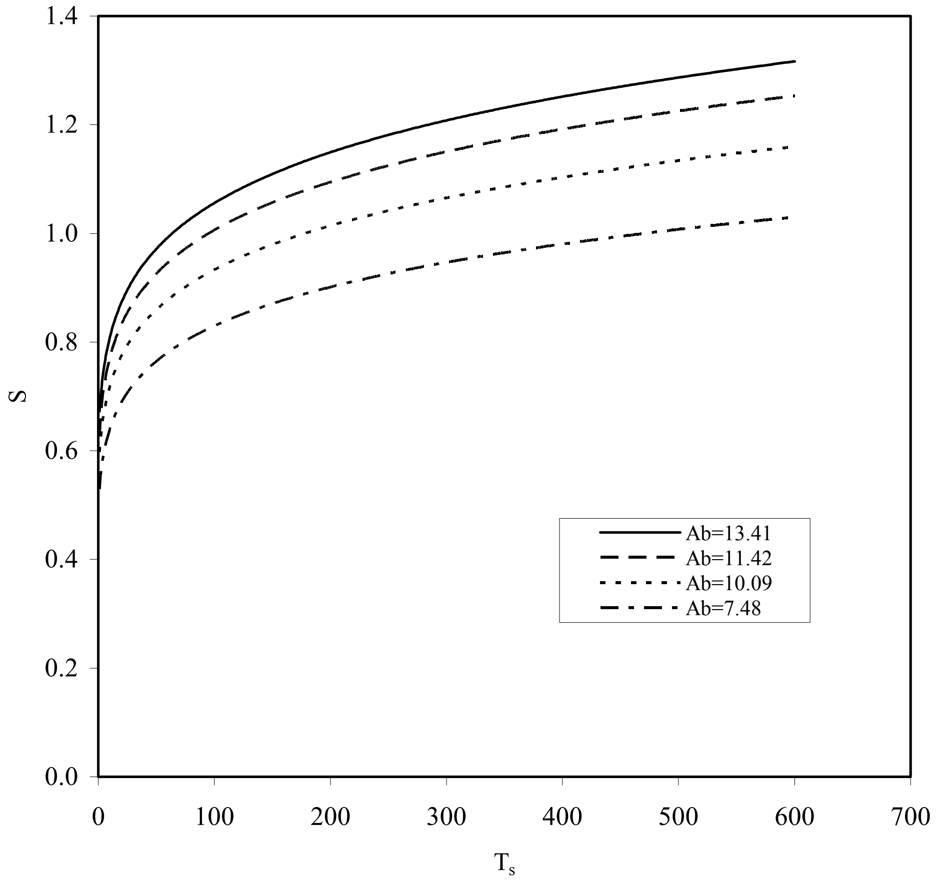

Figure 5.34. Dimensionless scour prediction chart

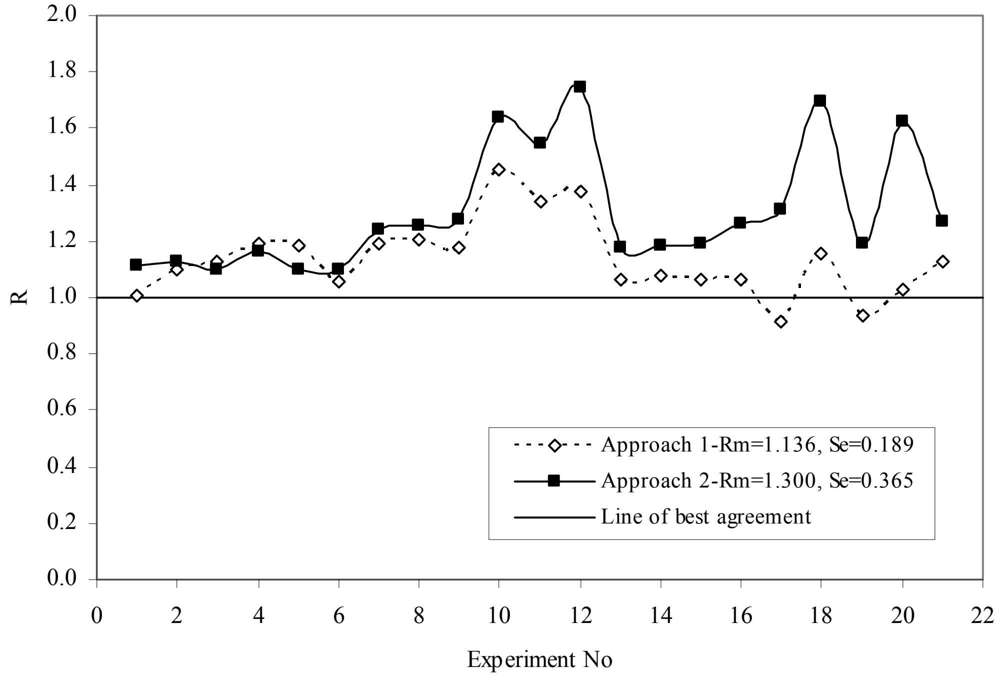

Figure 5.35. Scour prediction factors in $0<t/t_m\leq0.05$

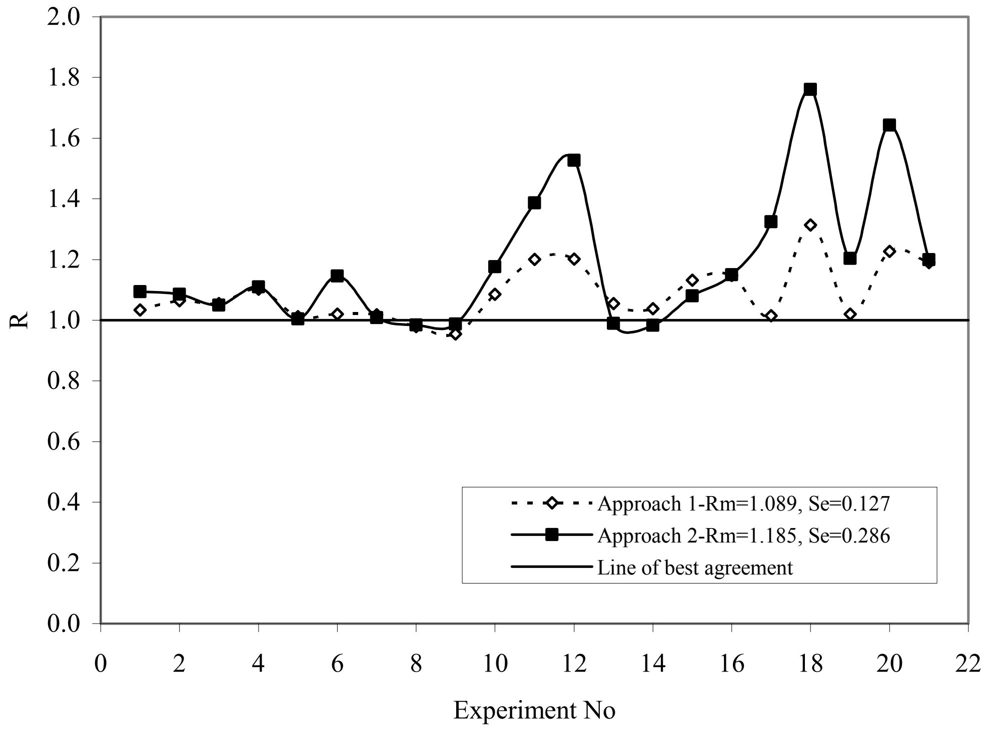

Figure 5.36. Scour prediction factors in $0.05< t/t_m\leq0.20$

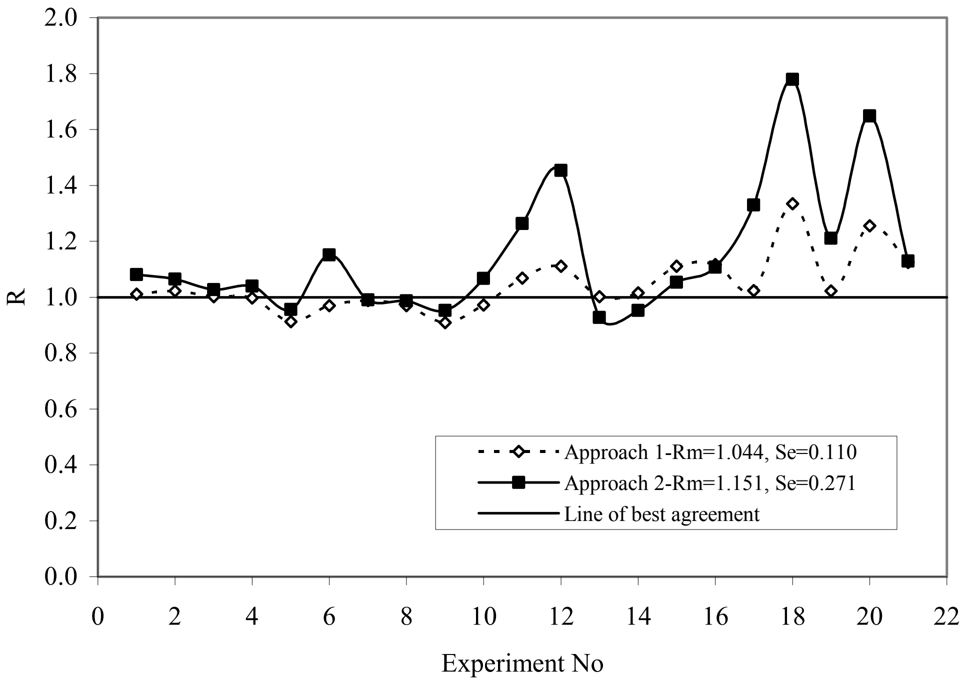

Figure 5.37. Scour prediction factors in $0.20< t/t_m \leq 0.50$

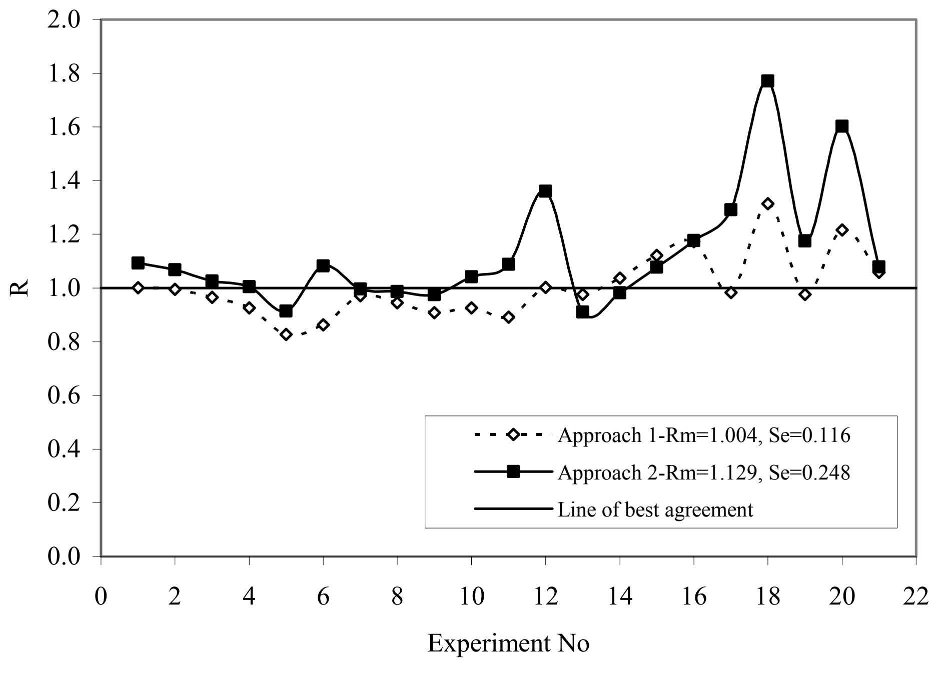

Figure 5.38. Scour prediction factors in $0.50< t/t_m \leq 1.0$

As can be seen from Figures 5.35 through 5.38, the semi-empirical model based on the first approach, on average, gives better prediction than the second approach. Therefore, the non-dimensional plots as shown in Figure 5.33 for α=2.0 can be used with confidence for practical applications.

CHAPTER 6

DISCUSSION AND CONCLUSIONS

An experimental study has been carried out to observe the temporal variation of maximum scour depth around vertical-wall and wing-wall abutments under clear water conditions. Based on the detailed interpretation and analysis of the experimental results, a semi-empirical model was developed for estimating time-dependent depth of scour at vertical-wall bridge abutments. The experiments were carried out under flow intensities ranging in $0.640 \leq u/u_c \leq 0.985$ with two different bed materials having almost uniform characteristics with median sizes 1.8 mm and 0.9 mm. The bed materials were almost uniform having geometric standard deviation of 1.40. Three different vertical-wall abutments with lengths of 12.5 cm, 10 cm, and 5 cm were tested. The relative abutment lengths ranged in $0.26 \leq y/L \leq 1.78$. With these values most of the abutments tested can be considered as of short length. Moreover, the maximum abutment size was taken as 10% of the flume width. Therefore, no contraction effects were maintained in the experiments. In the experiments, the flow Reynolds numbers are relatively beyond the lower limit of the turbulent flow, i.e. 12500. The particle Reynolds numbers based on the critical shear velocity are slightly smaller than the lower limit of the fully developed turbulent flow region according to Shields criterion, i.e. 70. That is why the effect of Reynolds number is ignored throughout the development of the proposed model.

Two different wing-wall abutments were also tested to account for the effect of abutment shape using acute angles of 60˚ and 45˚. During the course of the experiments vertical-wall abutments were observed to yield greater scour depths and wider scour holes compared to the case of wing-wall abutments because of generation of stronger separation and severe horse-shoe vortices around the upstream corner of vertical-wall abutments. Wing-wall abutments with acute angles of 45° produced smaller scouring relative to the case of 60°. Another by product of these experiments implied that the scour contours around wing-wall abutments were more rounded than those of the vertical-wall abutments.

The semi-empirical model was based on the solution of sediment continuity equation of the scour hole around the abutment. The rate of sediment transport out of the scour hole was formulated using a sediment pickup function valid for sloping beds proposed by Dey and Debnath (2001). Time-dependent geometric features of the scour hole were investigated and the shape of the scour hole was observed to remain almost unchanged with respect to time. However, its rate of change decelerated as time elapsed. It was also observed that the side angles of the scour hole, except the rear face of the abutment, was approximately equal to the angle of repose of the sediment. The volume of the scour hole was accepted to be approximated by an inverted semi-cone having a rectangular base with dimensions W and L (Equation (5.8)).

In the semi-empirical model, two different approaches were used. The first approach was based on derivation of an expression for the volume of the scour hole around the vertical-wall abutment having the aforementioned geometric characteristics. In the second approach, an empirical relation was obtained for the volume expression using the scour contours measured at different test durations. The semi-empirical method was resulted in dimensionless scour prediction equation; namely, Equation (5.17) for the first approach and Equation (5.23) for the second approach. The results of both approaches were also compared with each other and experimental results. The first approach was observed to produce better estimates. Moreover, the model yielded relatively close results with the experimental values. A prediction factor, R, is defined as the ratio of the instantaneous values of the computed scour depth to the measured scour depth in these time intervals. Since the perfect agreement corresponds to R=1.0, then the standard error of estimate, Se, of the prediction factors were computed in these time intervals. Mean prediction factor, Rm, is used to assess the prediction level in a particular time interval. The results of this analysis are shown in Figures 5.29 through 5.32. These figures imply that the proposed model gives better prediction, i.e. Rm and Se values decrease, with respect to time. Similar tendencies are also observed for the Oliveto-Hager (2002) and Coleman et al. (2003) approaches. However, the average predictive ability of the present model is higher than the other two methods. In all the intervals tested, the Coleman et al. (2003) approach yielded smaller scour depths, whereas the Oliveto-Hager (2002) method predicted slightly greater scour depths than the experimental values. Design charts based on the solution of Equation (5.17), which give the relationship between dimensionless scour depth and time for various α and m values, were derived and only one of them was given for α=2.0 in Figure 5.33. A by-product of this study is the derivation of dimensionless scour hole surface area and volume expressions, i.e. Equations (4.1) and (4.2). These equations may yield preliminary values for the approximate area of coverage of the bed around the vertical-wall abutment with an armoring countermeasure, e.g. riprap and the approximate number of layers to be used in this protection area..

Finally, some additional future studies are recommended. To this end, the validity of the proposed model may be tested using different flow, sediment, and abutment sizes than tested in this study. A similar model can also be developed for wing-wall and spill-through abutments. Effect of cumulative scour depths resulted from different independent flow conditions (storms) may be studied. Consideration of flow unsteadiness in abutment scouring may also be a topic for a future study.

REFERENCES

1. Ballio, F. and Orsi, E., (2000). Time Evolution of Scour Around Bridge Abutments. Water Engineering Research, Vol. 2, No. 4, 243-259.

2. Caner, A., Yanmaz, A. M., and Berk A., (2006). Remarks on Development of a Safety-Inspection Algoritm for River Bridges. Seventh International Congress on Advances in Civil Engineering, October 11-13, 2006 Yıldız Teknik University, Istanbul, Turkey.

3. Cardoso, A.H. and Bettess, R., (1999). Effects of Time and Channel Geometry on Scour at Bridge Abutments. Journal of Hydraulic Engineering, ASCE, Vol.125, No.4, 388-399.

4. Coleman, S.E., Lauchlan, C.S. and Melville, B.W., (2003). Clear Water Development at Bridge Abutments. Journal of Hydraulic Research, Vol. 41, No.5, 521-531.

5. Dargahi, B., (1990) Controlling Mechanism of Local Scouring. Journal of Hydraulic Engineering, Vol.116, No.10, 1197-1214.

6. Dey, S. and Debnath, K., (2001). Sediment Pick up on Streamwise Sloping Beds. Journal of Irrigation and Drainage Engineering, Vol.127, No.1, 39-43.

7. Dey, S. and Barbhuiya, A., (2005). Time Variation of Scour at Abutments. Journal of Hydraulic Engineering, Vol.131, No.1, 11-23.

8. Dongol, D.M.S., (1994) Local Scour at Bridge Abutments. Report No.554, Faculty of Engineering, University of Auckland, Auckland , New Zeland.

9. Ettema, R., Melville, B.W. and Barkdoll, B., (1998). Scale effect in Pier-Scour Experiments, Journal of Hydraulic Engineering, Vol.124, No.6, 639-642.

10. Fernandez-Luque, R. (1974). Erosion and Transport of Bed Load Sediment. Dissertation, KRIPS Repro BV, Meppel, Netherlands.

11. Franzetti S., Malavasi S., and Piccinin C., (1994). Sull'erosione alla base delle pile di ponte in acque chiare, Proceedings XXIV Convegno di Idraulica e Costruzioni Idrauliche, Napoli, Vol. II, T4 13-24. (in Italien)

12. Froechlich, D.C., (1989). Local Scour at Bridge Abutments, Proceedings of ASCE Hydraulic Engineering. New Orleans, 13-18.

13. Gill, M.A. (1972) Erosion of sand beds around spur dikes. Journal of the Hydraulics Division, ASCE, Vol.98, No.9, 1587-1602.

14. Kayatürk, Ş.Y., (2005) Scour and Scour Protection at Bridge Abutments, Thesis presented to Middle East Technical University, Ankara, Turkey, in partial fulfillment of the requirements for the degree of Doctor of Philosophy.

15. Kothyari, U.C., Garde, R.J., and Ranga Raju, K.G., (1992). Live-Bed Scour Around Cylindrical Bridge Piers. Journal of Hydraulic Research, Vol.30, No.5, 701-715.

16. Kothyari, U.C., and Ranga Raju, K.G., (2001). Scour Around Spur Dikes and Bridge Abutments, Journal of Hydraulic Research, Vol.39, No.4, 367-374.

17. Kwan, T.F., (1984) Study of Abutment Scour. Report No.328, Faculty of Engineering, University of Auckland, Auckland, New Zealand.

18. Lagasse, P.F., Zwenbergen, L.W., and Scholl, J.D., (2001). Bridge Scour and Stream Instability Countermeasures. Hydraulic Engineering Circular No.23, Report No.FHWA-NHI-01-003, U.S. Department of Transportation, Washington, D.C.

19. Lauchlan, C.S. and Melville, B.W., (2001). Riprap protection at bridge piers. Journal of Hydraulic Engineering, ASCE, Vol.127, No.5, 412-418.

20. Laursen, E.M., (1963). An analysis of Relief Bridge Scour. ASCE Journal of Hydraulic Division, Vol. 89, No. HY3, 93-118.

21. Le Feuvre, A.R., and Altınbilek, H.D., (1970). Sediment Pick Up Function, Journal of Hydraulic Division Proceedings of the American Society of Civil Engineers, Vol.96, No.10, 2051-2063.

22. Lim, S.Y., (1997). Equilibrium Clear Water Scour Around an Abutment, Journal of Hydraulic Engineering, Vol.123, No.3, 237-243.

23. Liu, H.K., Chang, F.M., and Skinner, M.M., (1961). Effect of Bridge Constriction on Scour and Backwater, Engineering Research Center, Colorado State University, Report No. CER 60 HKL 22.

24. Melville, B.W. (1997). Pier and Abutment Scour: Integrated Approach, Journal of Hydraulic Engineering, ASCE, 123(2), 125-136.

25. Melville, B.W., and Chiew, Y.M., (1999). Time Scale for Local Scour at Bridge Piers, Journal of Hydraulic Engineering, Vol.125, No.1, 59-65.

26. Melville, B.W. and Coleman, S.E., (2000). Bridge Scour, Water Resources Publications: Highlands Ranch, Colorado.

27. Mia, M.F. and Nago, H., (2003). Design Method of Time-Dependent Local Scour at Circular Bridge Pier. Journal of Hydraulic Engineering, ASCE, Vol.129, No.6, 420-427.

28. Nagakawa, H and Tsujimoto, H., (1980). Sand bed instability due to bed load motion. ASCE Journal of Hydraulics Division. Vol.106 No. HY12, 2029-2051.

29. Oliveto, G., and Hager, W. H., (2002). Temporal Evolution of Clear Water Pier and Abutment Scour, Journal of Hydraulic Engineering, Vol.128, No.9, 811-820.

30. Oliveto, G. and Hager, W.H., (2005). Further Results to Time-Dependent Local Scour at Bridge Elements. Journal of Hydraulic Engineering, ASCE, Vol. 131, No. 2, 97-105.

31. Raudkivi, A.J. and Ettema, R., (1983). Clear Water Scour at Cylindrical Piers. Journal of Hydraulic Engineering Vol.109, No.3, 338-350.

32. Rajaratnam, N. and Nwachukhu B.A., (1983). Flow Near Groin-like Structures. Journal of Hydraulic Engineering, ASCE, Vol.109, No.3, 463-480.

33. Richardson, E.V., and Davis, S.R., (1995). Evaluating Scour at Bridges. Publication No: FHWA-IP-90-017, Hydraulic Engineering Circular No.18, U.S Department of Transportation, Federal Highway Administration, Washington D.C.

34. Shirhole, A.M., and Holt, R.C., (1991). Planning for a Comprehensive Bridge Safety Program. Transportation Research Board, NRC, Washington, D.C. Vol.1, No.1290.

35. Sturm, T.W., (1999). Abutment Scour Studies For Compound Channels. U.S. Department of Transportation, Federal Highway Administration, U.S.A.

36. Tey, C.B., (1984). Local Scour at Bridge Abutments, Report No. 329, School of Engineering, University of Auckland, Auckland, New Zealand.

37. USACE (United States Army Corps of Engineers), (2002). HEC-RAS Users' Manuel Version 3.1. Davis, CA, U.S.A.

38. Van Rijn, L.C., (1984). Sediment Pick up Functions, Journal of Hydraulic Engineering, Vol.110, No.10, 1494-1503.

39. Wardhana, K., and Hadipriono, F.C., (2003). Analysis of Recent Bridge Failures in the United States. Journal of Performance of Constructed Facilities. Vol.17, 144-150.

40. Whitehouse, R. J. S., (1997). Scour at Marine Structures: A manual for engineers and scientists. Res. Rep. SR417, HR Wallingford Ltd., Wallingford, U.K.

41. Wong, W.H., (1982). Scour at Bridge Abutments, Report No.275, School of Engineering, University of Auckland, Auckland New Zealand.

42. Yanmaz, A.M., (1989). Time Dependent Analysis of Clear Water Scour Around Bridge Piers. Thesis presented to Middle East Technical University, Ankara, Turkey, in partial fulfillment of the requirements for the degree of Doctor of Philosophy.

43. Yanmaz, A.M., and Altınbilek, H.D., (1991). Study of Time Dependent Local Scour Around Bridge Piers, Journal of Hydraulic Engineering, Vol.117, No.10, 1247-1268.

44. Yanmaz, A.M., (2002). Bridge Hydraulics, METU Press Publications: Ankara, (in Turkish).

45. Yanmaz, A.M. and Çelebi, T., (2004). Reliability Model for Bridge Abutment Scour. Turkish Journal of Engineering and Environmental Sciences. Vol.28, No.1, 67-83.

46. Yanmaz, A.M., and Çiçekdağ, Ö., (2001). "Composite reliability model for local scour around cylindrical bridge piers", Canadian Journal of Civil Engineering. No. 28, 520-535.

47. Yanmaz, A.M., and Köse, Ö., (2006). Characteristic Trends of Clear Water Scouring at Bridge Abutments. Seventh International Congress on Advances in Civil Engineering, October 11-13, 2006 Yıldız Teknik University, İstanbul, Turkey.

48. Yanmaz, A.M., and Köse, Ö., (2007). Surface Characteristics of Scouring at Bridge Elements. Turkish Journal of Engineering and Environmental Sciences, No.31, 127-134

49. Yanmaz, A.M., (2006). Temporal Variation of Clear Water Scour at Cylindrical Bridge Piers. Canadian Journal of Civil Engineering, Vol.33, No.8 1098-1102.

Yanmaz, A.M., and Caner, A., (2006). Hydraulic Structure Interaction for Bridges with Special Emphasis to Effect of Type of Infrastructural Elements. Seventh International Congress on Advances in Civil Engineering, October 11-13, 2006 Yıldız Teknik University, Istanbul, Turkey.

APPENDIX

COMPARISON OF COMPUTED SCOUR DEPTHS USING APPROACHES 1 AND 2

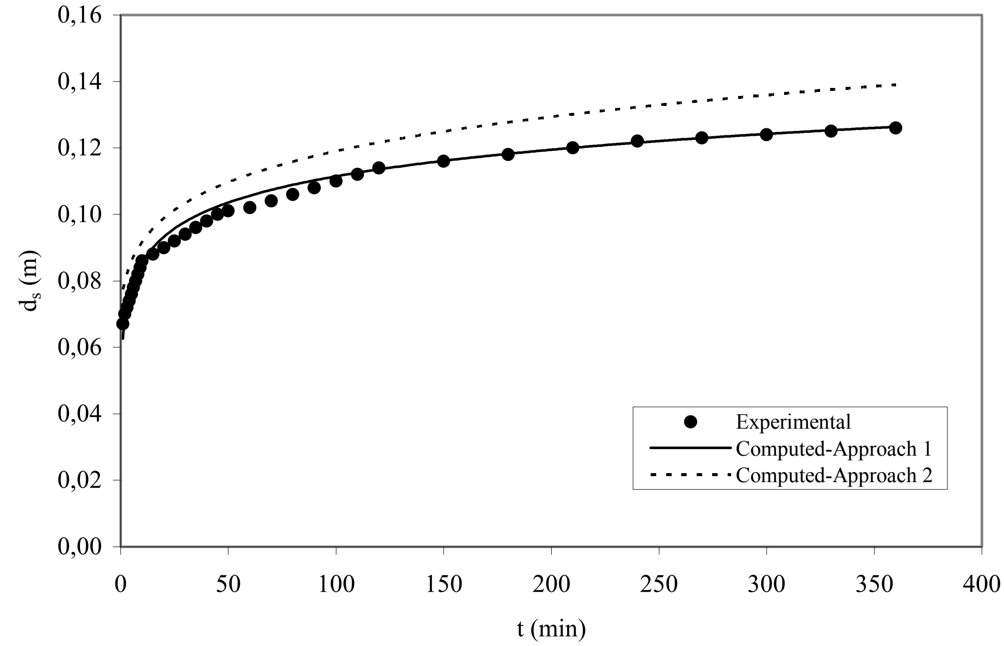

Figure A1. Comparison of Approaches 1 and 2 for Experiment 1

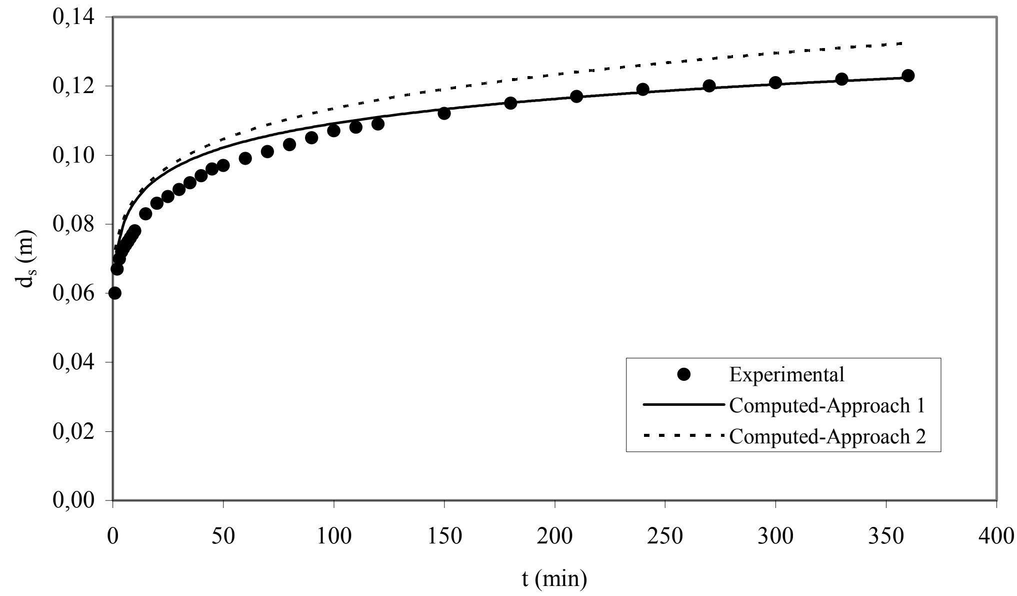

Figure A2. Comparison of Approaches 1 and 2 for Experiment 2

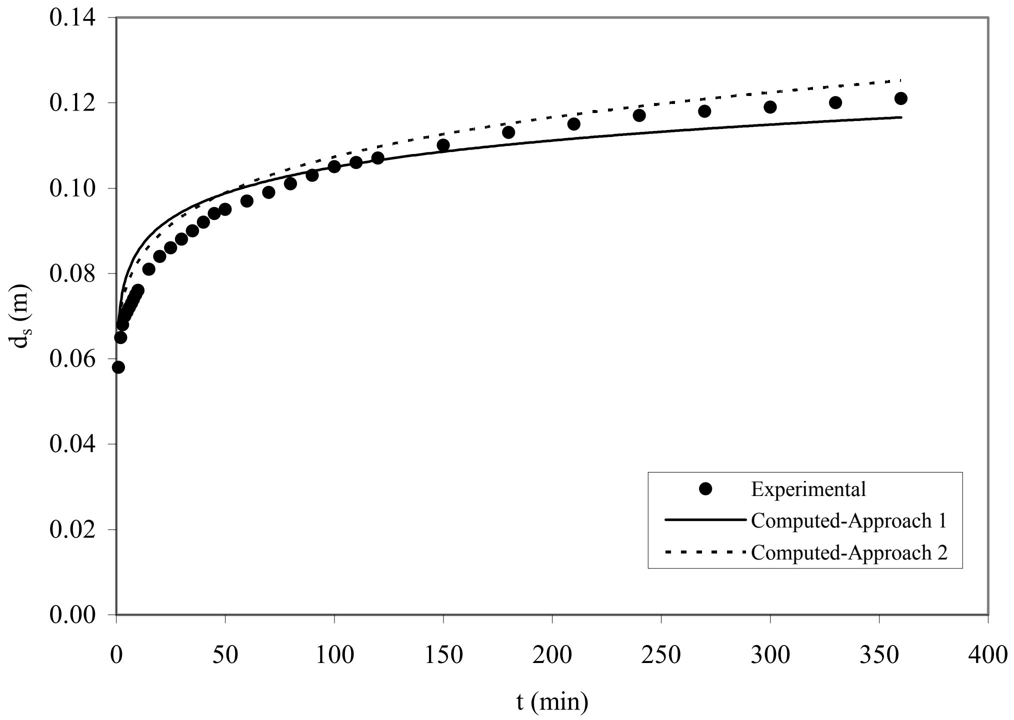

Figure A3. Comparison of Approaches 1 and 2 for Experiment 3

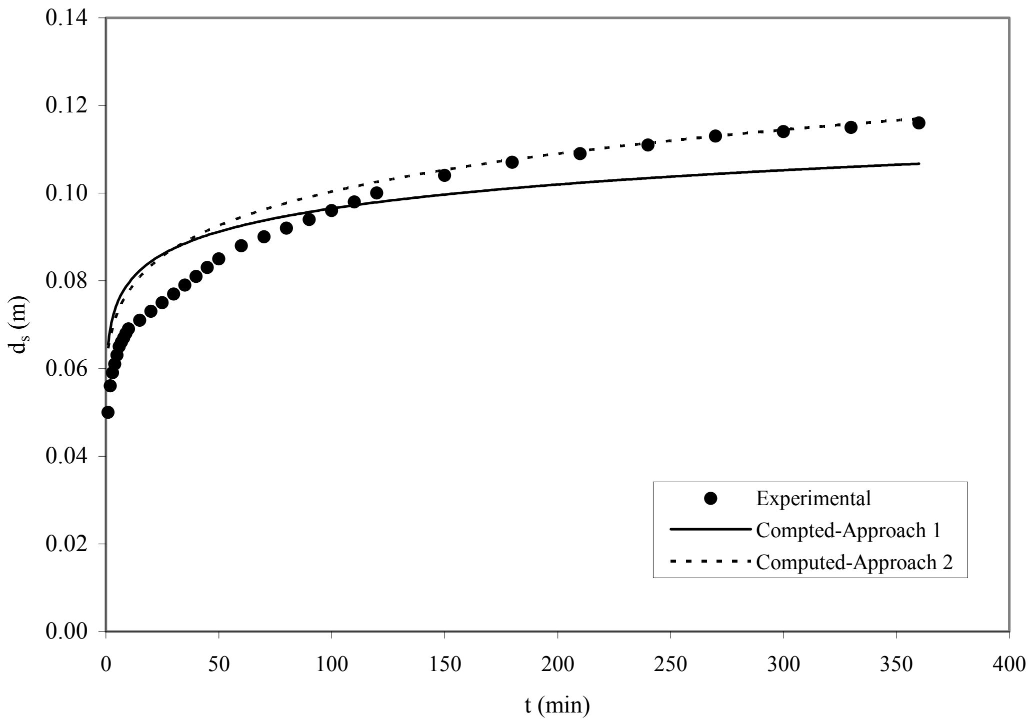

Figure A4. Comparison of Approaches 1 and 2 for Experiment 4

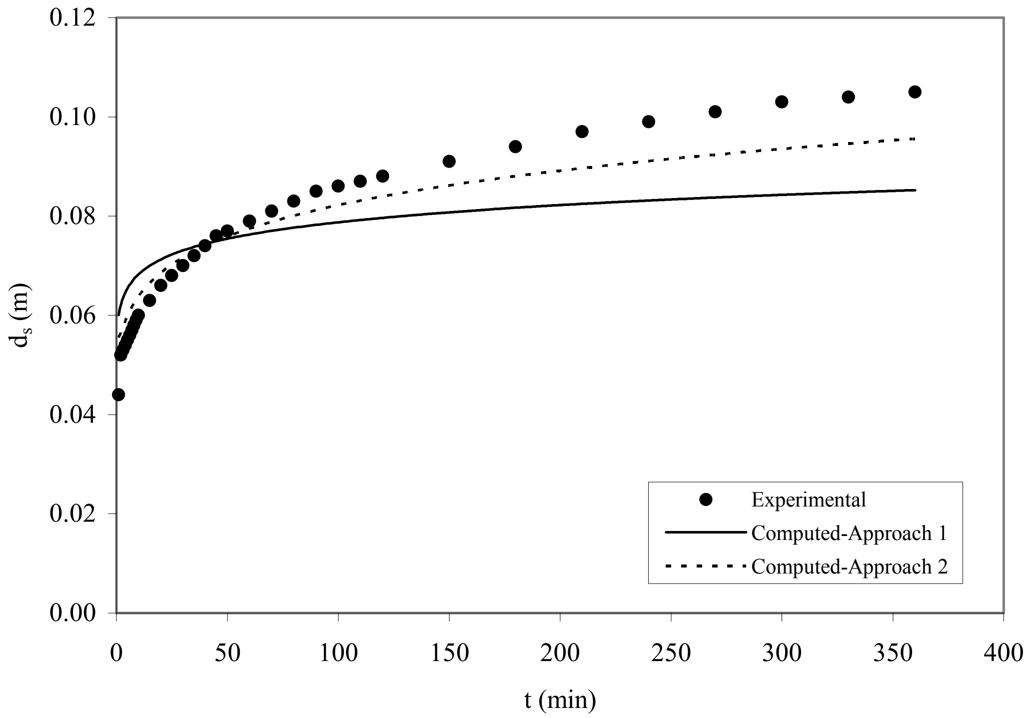

Figure A5. Comparison of Approaches 1 and 2 for Experiment 5

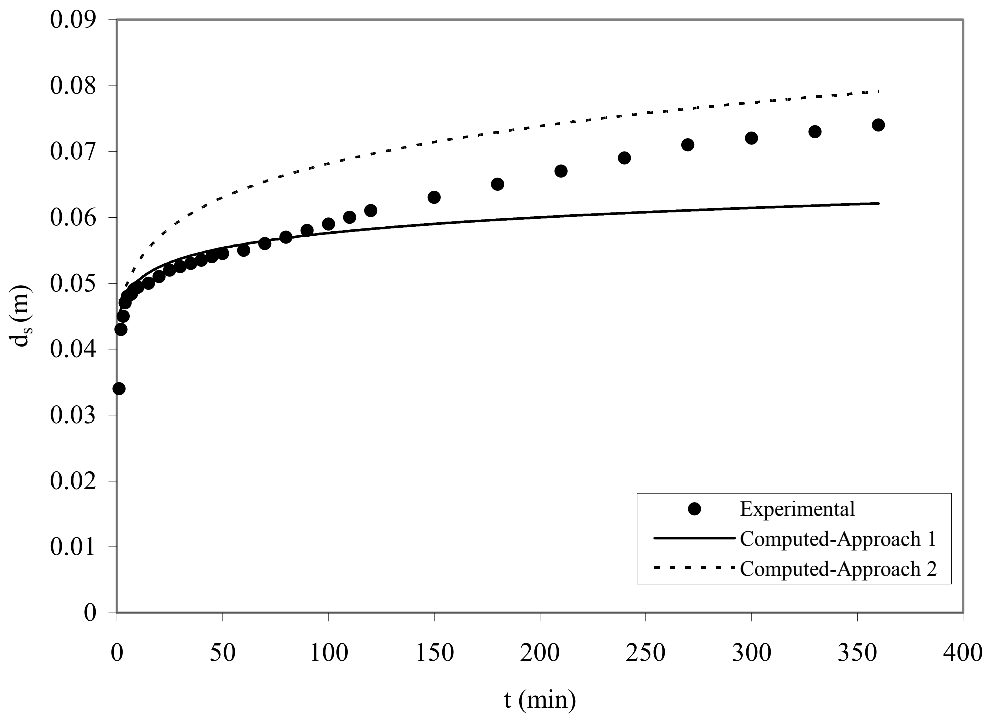

Figure A6. Comparison of Approaches 1 and 2 for Experiment 6

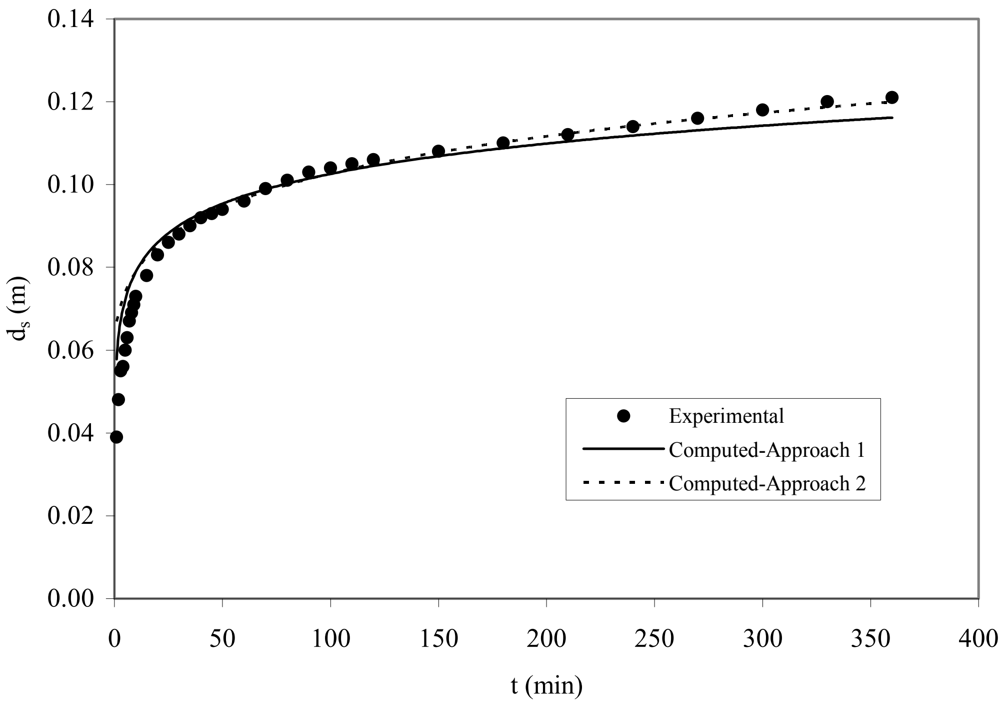

Figure A7. Comparison of Approaches 1 and 2 for Experiment 13

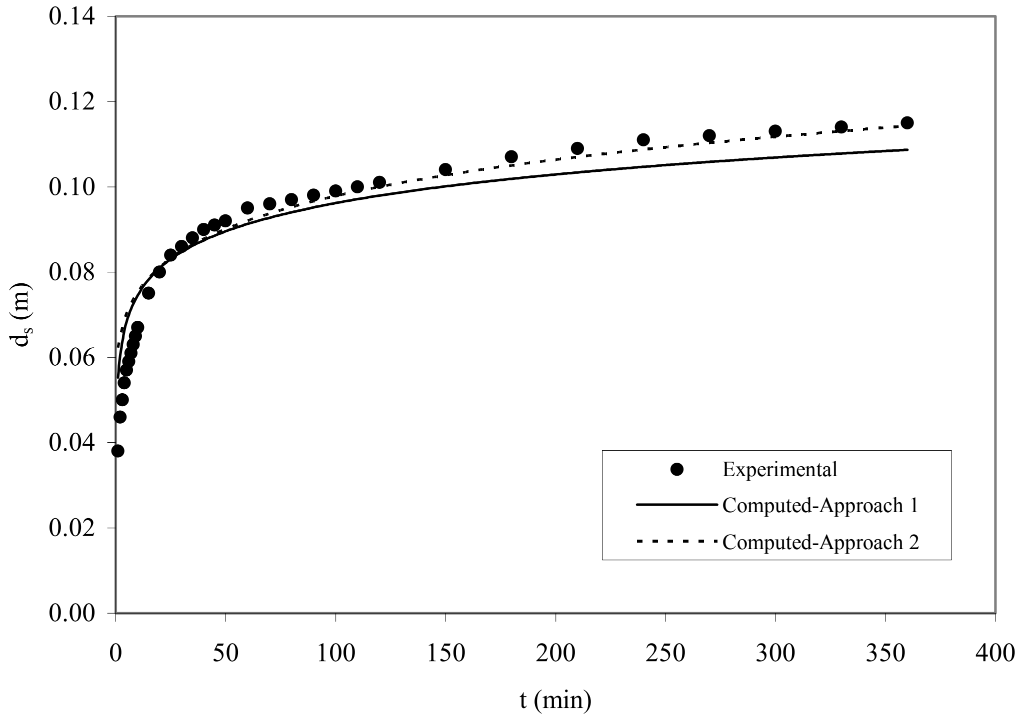

Figure A8. Comparison of Approaches 1 and 2 for Experiment 14

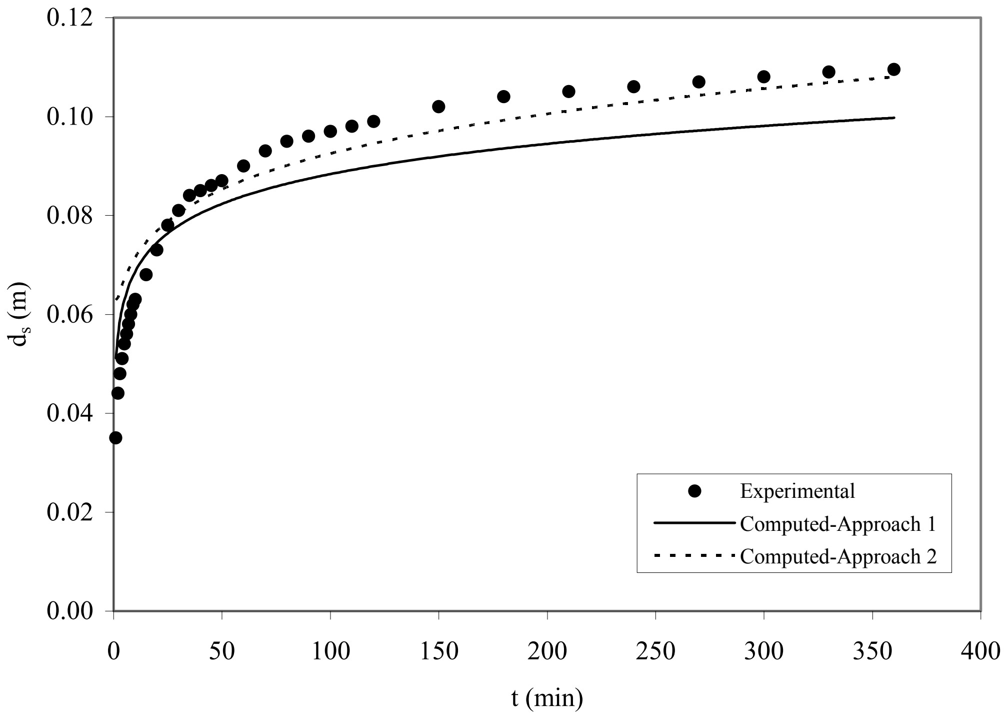

Figure A9. Comparison of Approaches 1 and 2 for Experiment 15

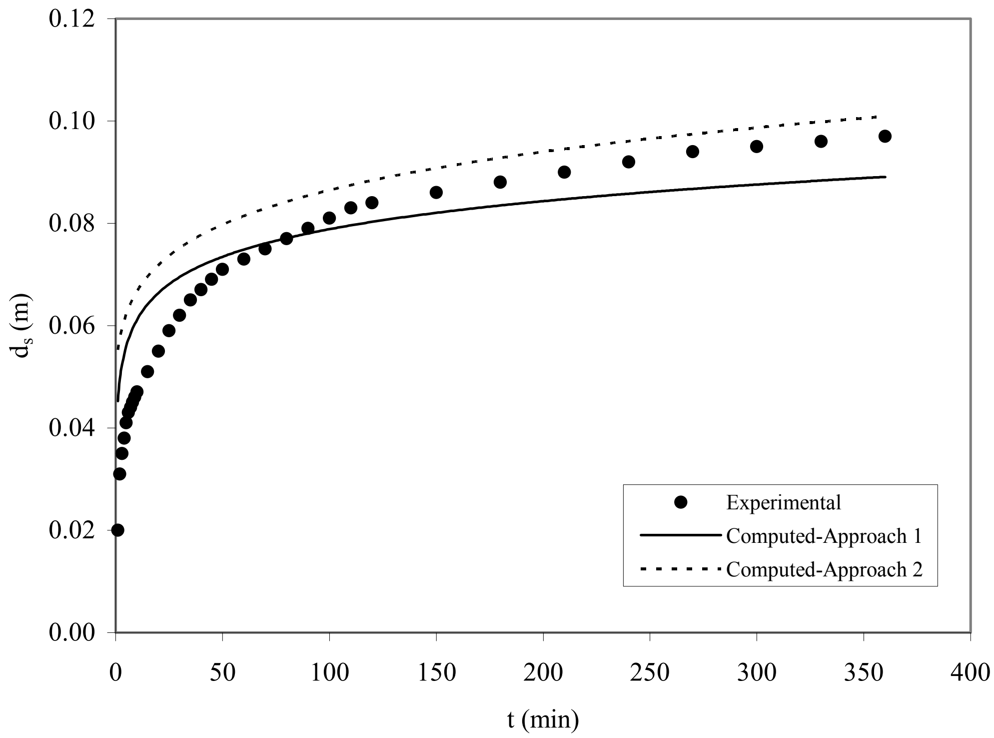

Figure A10. Comparison of Approaches 1 and 2 for Experiment 16

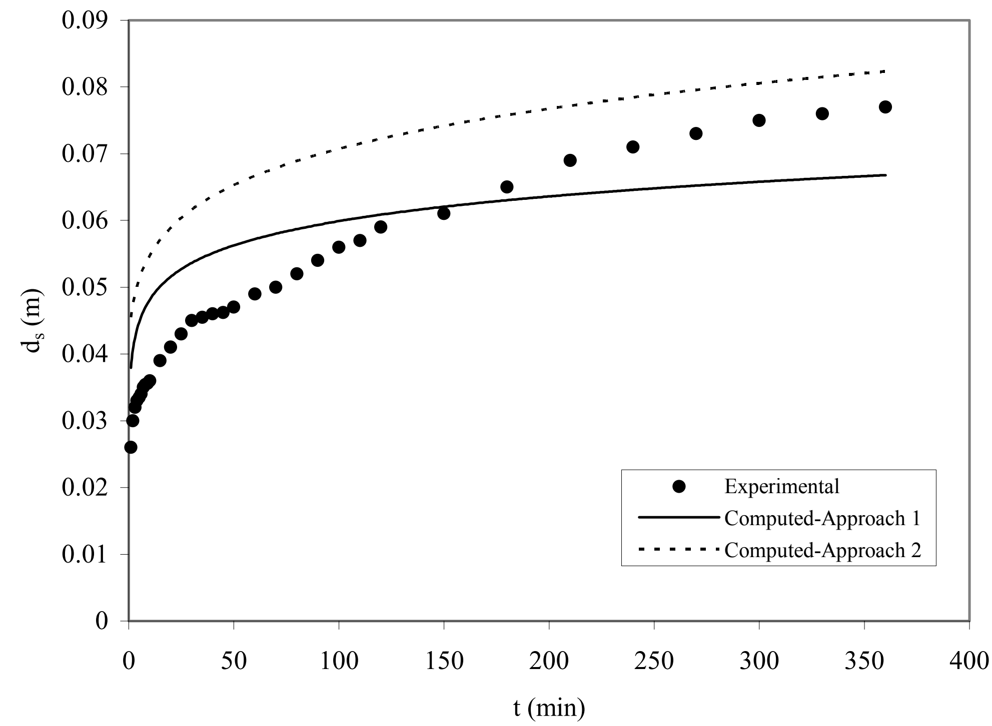

Figure A11. Comparison of Approaches 1 and 2 for Experiment 17

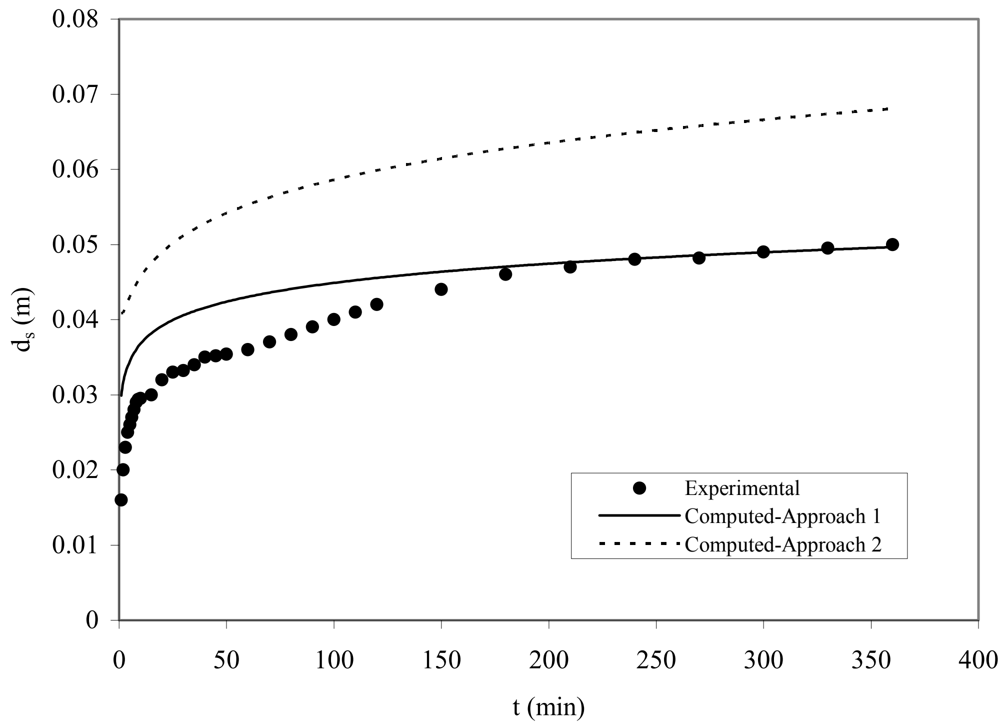

Figure A12. Comparison of Approaches 1 and 2 for Experiment 18

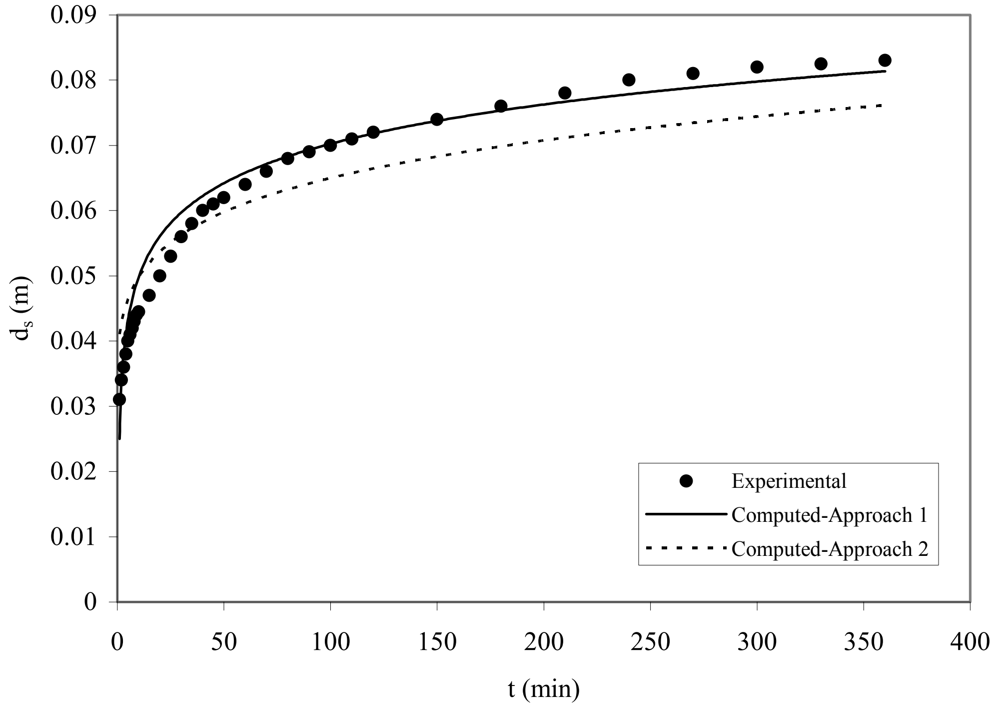

Figure A13. Comparison of Approaches 1 and 2 for Experiment 25

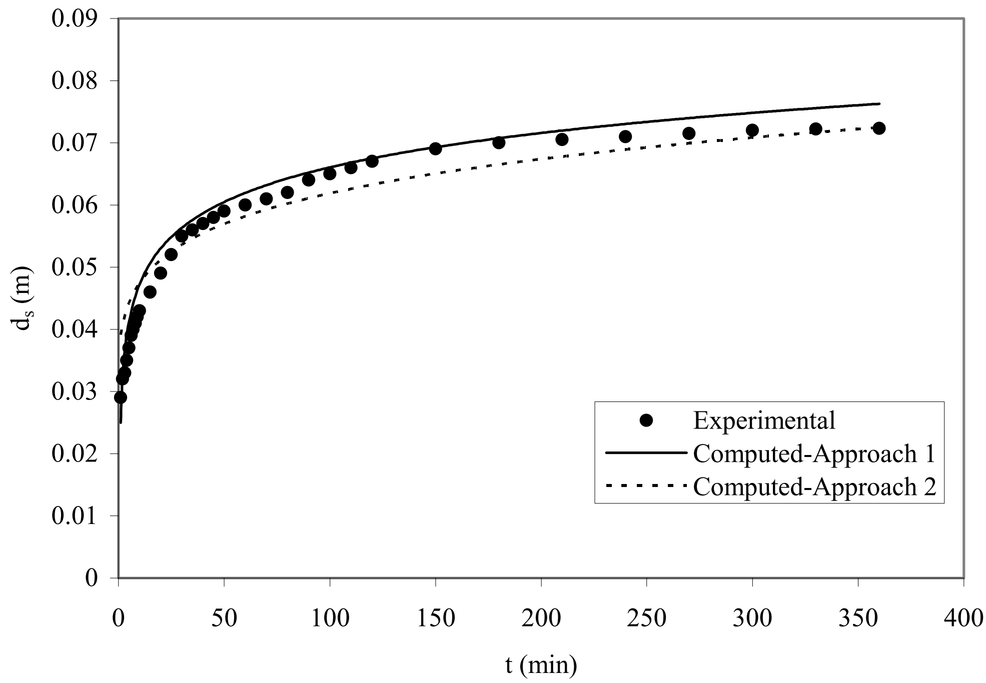

Figure A14. Comparison of Approaches 1 and 2 for Experiment 26

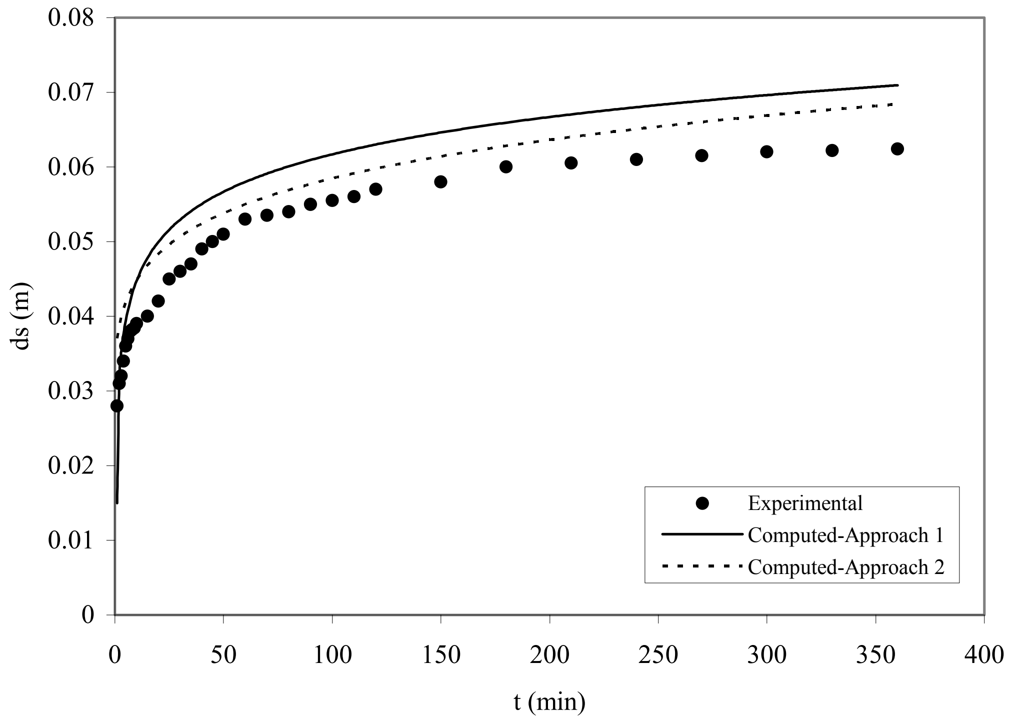

Figure A15. Comparison of Approaches 1 and 2 for Experiment 27

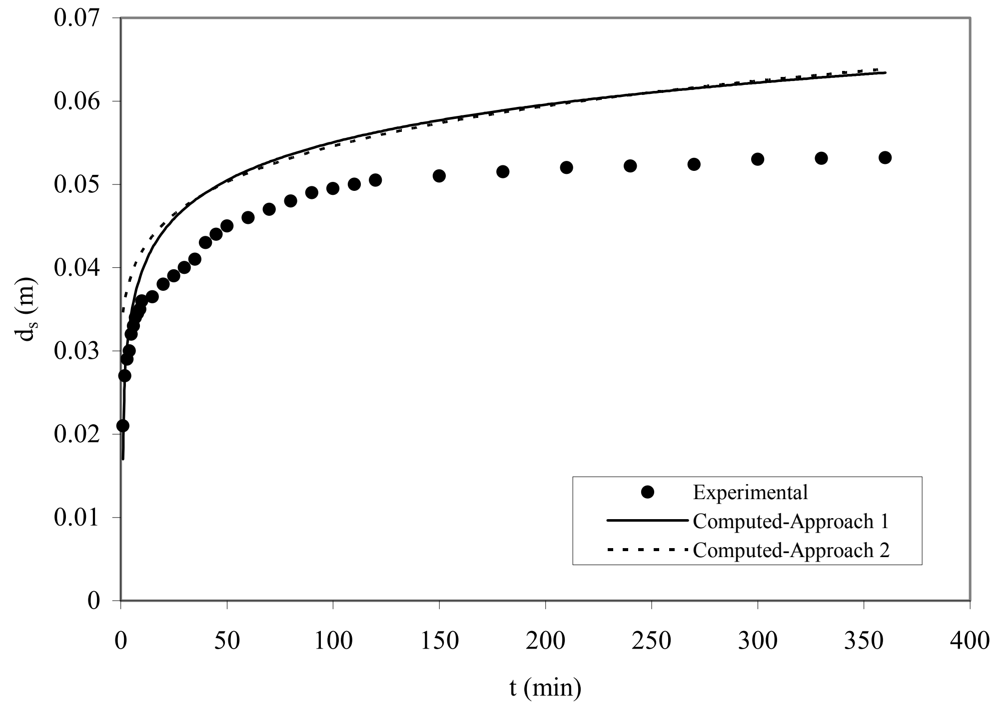

Figure A16. Comparison of Approaches 1 and 2 for Experiment 28

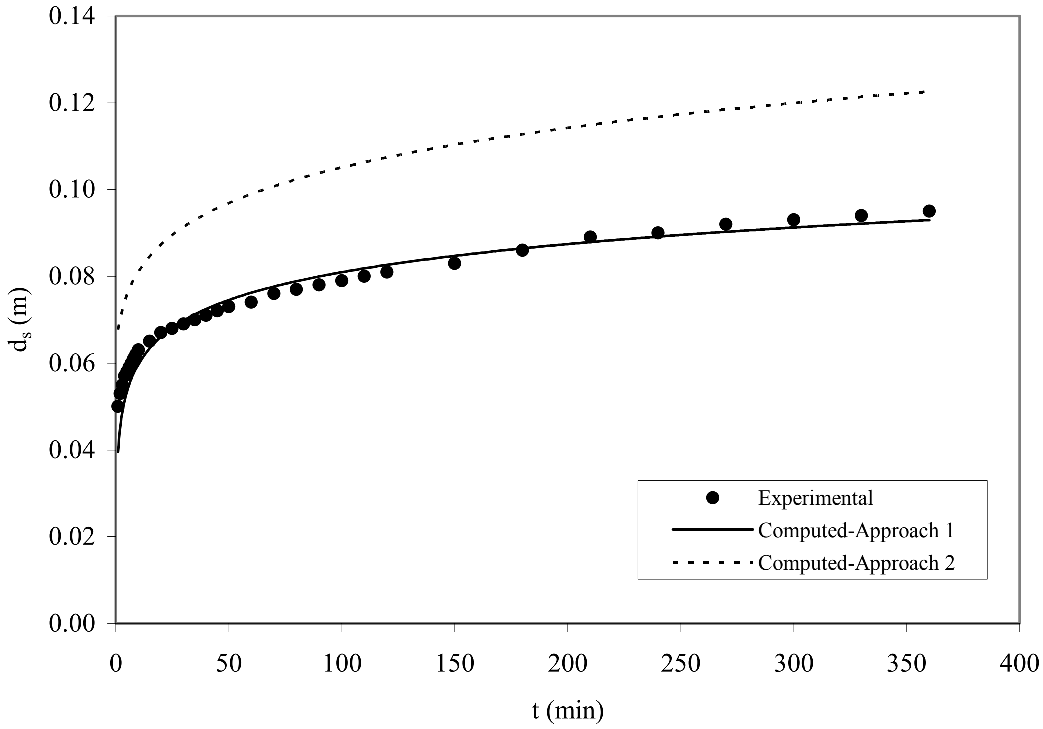

Figure A17. Comparison of Approaches 1 and 2 for Experiment 61

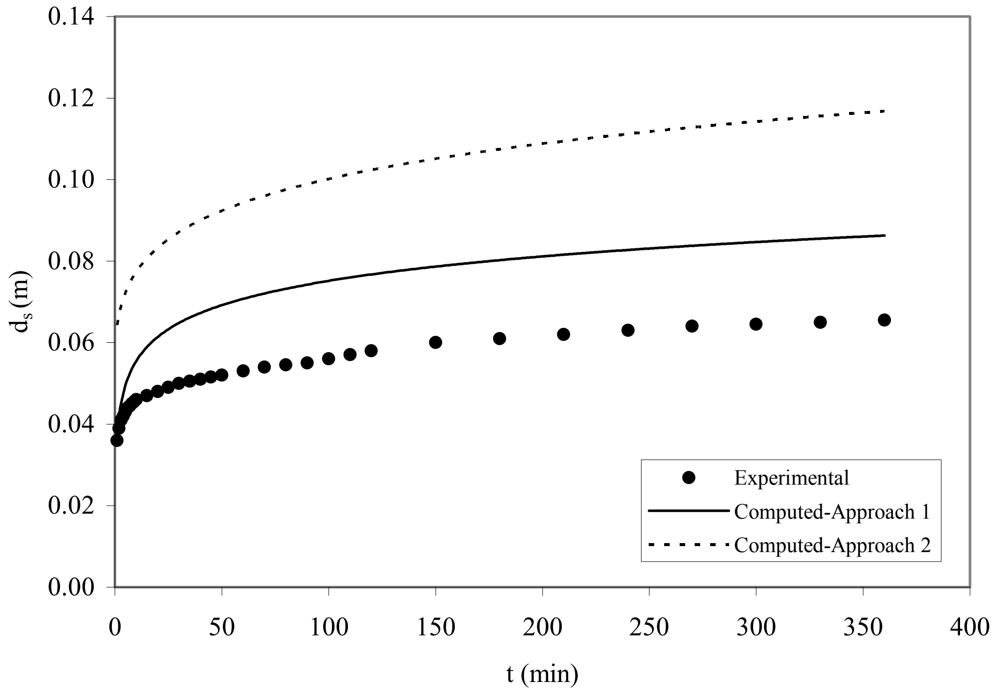

Figure A18. Comparison of Approaches 1 and 2 for Experiment 62

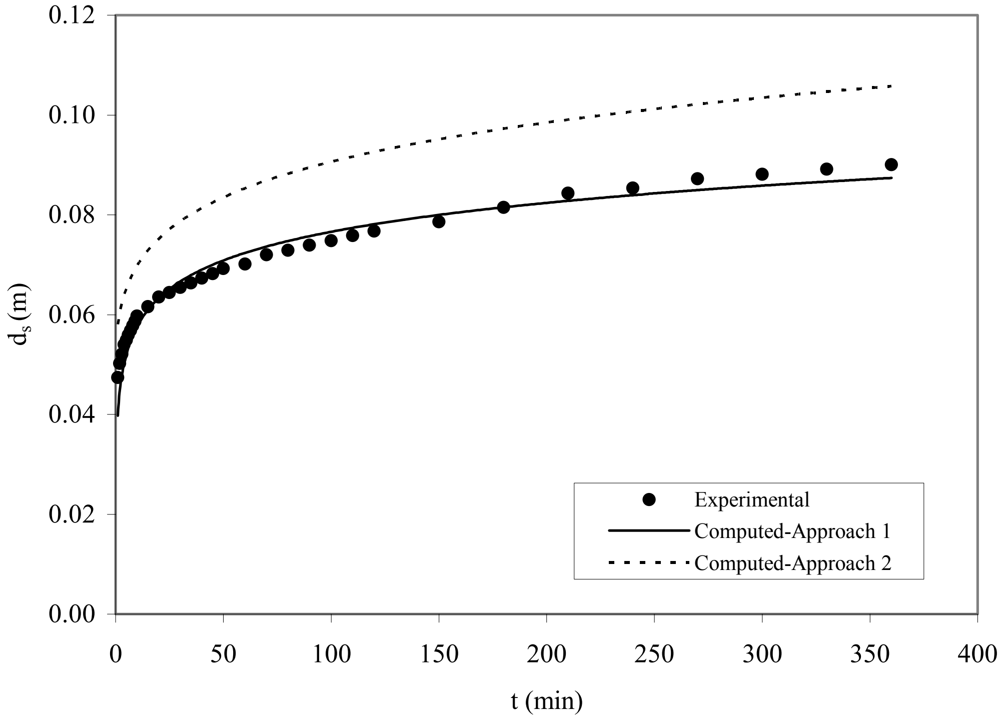

Figure A19. Comparison of Approaches 1 and 2 for Experiment 64

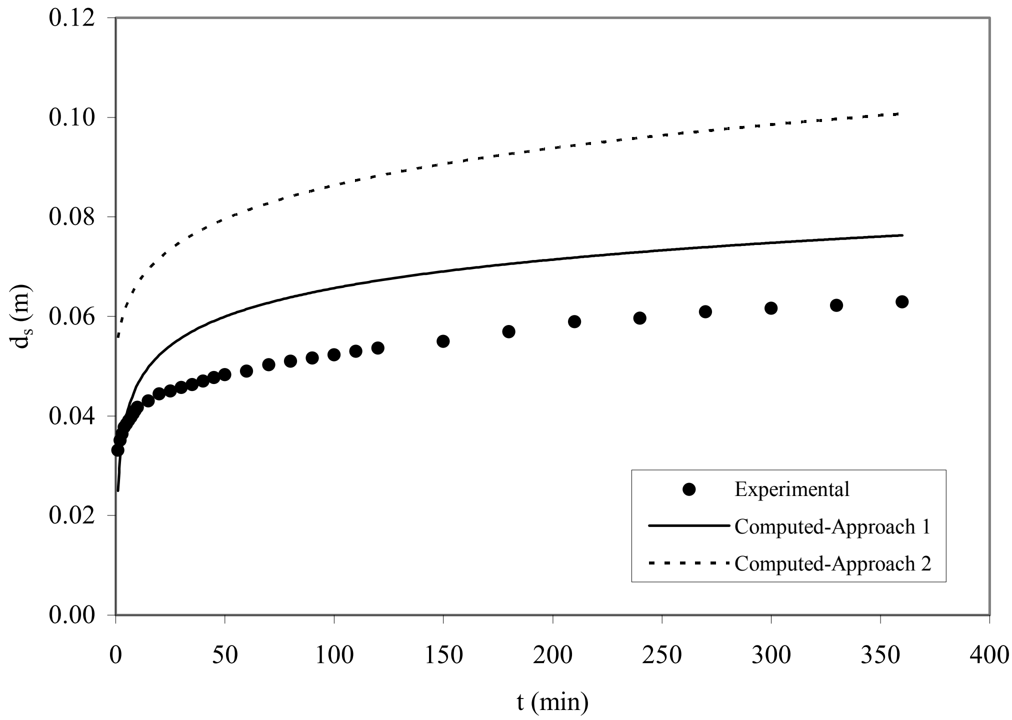

Figure A20. Comparison of Approaches 1 and 2 for Experiment 65

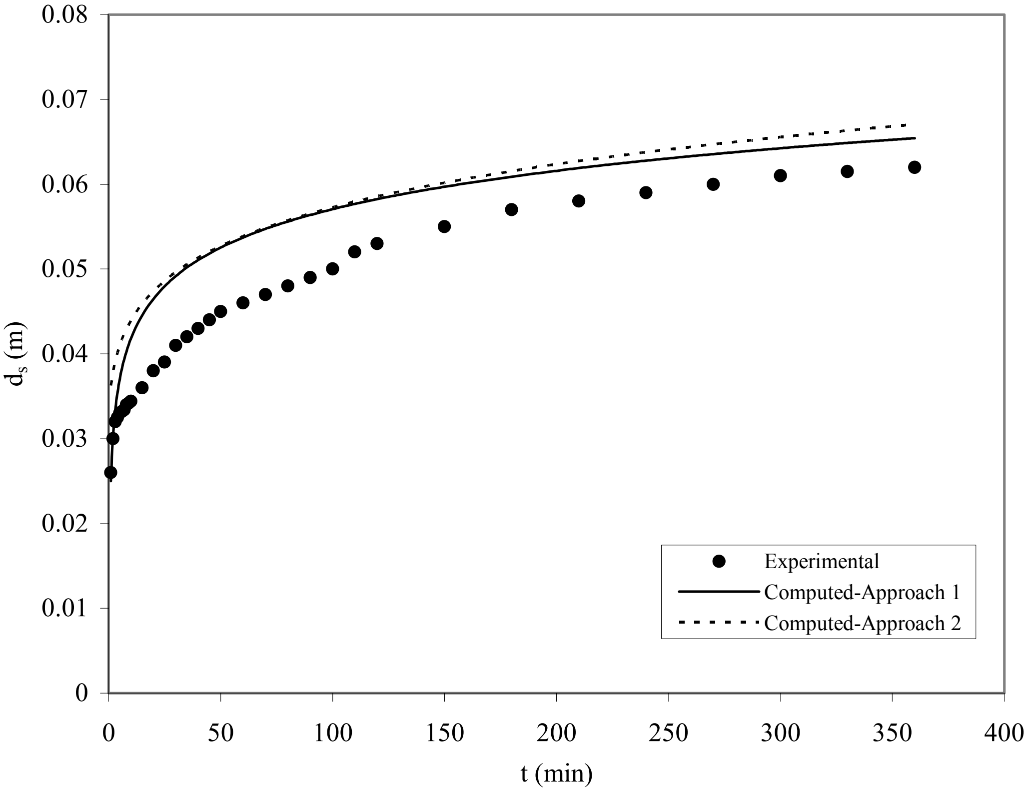

Figure A21. Comparison of Approaches 1 and 2 for Experiment 67

CURRICULUM VITAE

PERSONAL INFORMATION

Surname, Name: Köse Ömer
Nationality: Turkish (TC)
Date and Place of Birth: 8 September 1969, Aksaray
Marital Status: Married and father of two sons

EDUCATION

Degree	Institution	Year of Graduation
MS	Selçuk Unv. Civil Eng. Depth.	1999
BS	METU Civil Eng. Depth.	1994
High School	Gazi High School, Konya	1986

WORK EXPERIENCE

Year	Place	Enrollment
2001-Present	METU Department of Civil Eng.	Research Assistant
1996-2001	Nigde Univ. Aksaray Eng. Fac.	Research Assistant
1994-1996	Istanbul Municipality	Engineer
1990 July	Enka	Intern Engineer
1989 August	Tekfen	Intern Engineer

FOREIGN LANGUAGES

English

HOBBIES

Reading, travelling.